Behaviour Modelling and System Control with Human in the Loop

Stevine Obura Onyango

BEHAVIOUR MODELLING AND SYSTEM CONTROL WITH HUMAN IN THE LOOP

by

Onyango, Stevine Obura

Submitted in partial fulfillment of the requirement for the degree

DOCTORAT SIGNAL, IMAGE, AUTOMATIQUE

in the

UNIVERSITÉ PARIS-EST CRÉTEIL ET MSTIC

Co-Tutelle

TSHWANE UNIVERSITY OF TECHNOLOGY

Président du jury: Prof. Eric MONACELLI
Directeurs de thése: Prof. Boubaker DAACHI
Directeurs de thése: Prof. Yskandar HAMAM
Directeurs de thése: Prof. Karim DJOUANI
Rapporteur: Prof. Hichem ARIOUI
Rapporteur: Prof. Abdelouahab ZAATRI
Examinateur: Prof. Anna PAPPA

February 2017

DECLARATION AND COPYRIGHT

I hereby declare that the dissertation submitted for the degree Doctor of Technology: Electrical Engineering, at Tshwane University of Technology, is my own original work and has not previously been submitted to any other institution of higher education. I further declare that all the sources cited and quoted are indicated and acknowledged by means of a comprehensive list of references

Onyango S.O. Date: 24-February-2017

"We look forward to the time when the Power of Love will replace the Love of Power. Then will our world know the blessings of peace"

WILLIAM EWART GLADSTONE

ABSTRACT

Malgré le progrès en recherche et développement dans le domaine de systme autonome, de tels systèmes nécessitent l'intervention humaine pour résoudre les problèmes imprévus durant l'exécution des tâches par l'utilisateur. Il est donc nécessaire, malgré cette autonomie, de tenir compte du comportement du conducteur et il est difficile d'ignorer l'effet de l'intervention humaine dans le cadre de l'évolution continue de l'environnement et des préférences de l'utilisateur. Afin d'exécuter les opérations selon les attentes de l'operateur, il est nécessaire d'incorporer dans la commande les besoins de l'utilisateur. Dans les travaux présentés dans cette thèse un modèle comportemental de l'utilisateur est développé et intégré dans la boucle de commande afin d'adapter la commande l'utilisateur. Ceci est appliqué la commande des fauteuils électrique et assiste dans la navigation du fauteuil dans un milieu encombré. Le développement du modèle comportemental est basé sur la méthode de potentielles orientées et la détection des obstacles et le comportement du conducteur vs de ces obstacles par l'adaptation du. L'étude contribue également au développement d'un modèle dynamique du fauteuil utilisable dans des situations normales et exceptionnelles telle que le dérapage. Ce modèle est développé pour un le cas le plus courant des fauteuil avec roues arrière conductrices utilisant le formalisme Euler Lagrange avec les forces gravitationnelles et sur des surfaces inclinées. Dans la formulation de la commande, le modèle du conducteur est introduit dans la boucle de commande. L'optimalité de la performance est assurée par l'utilisation du command prédictif généralisé pour le système en temps continue. Les résultats de la simulation démontrent l'efficacité de l'approche proposée pour l'adaptation de la commande au comportement du conducteur.

ABSTRACT

Although the progressive research and development of autonomous systems is fairly evident, such systems still require human interventions to solve the unforeseen complexities, and clear the uncertainties encountered in the execution of user-tasks. Thus, in spite of the system's autonomy, it may not be possible to absolutely disregard the operator's role. Human intervention, particularly in the control of auto-mobiles, may as well be hard to ignore because of the constantly changing operational context and the evolving nature of the drivers' needs and preferences. In order to execute the autonomous operations in conformity with the operator's expectations, it may be necessary to incorporate the advancing needs and behaviour of the operator in the design. This thesis formulates an operator behaviour model, and integrates the model in the control loop to adapt the functionality of a human-machine system to the operator's behaviour. The study focuses on a powered wheelchair, and contributes to the advancement of steering performance, through background assistance by modelling, empirical estimation and incorporation of the driver's steering behaviour into the control system. The formulation of the steering behaviour model is based on two fundamentals: the general empirical knowledge of wheelchair steering, and the steering data generated from the virtual worlds of an augmented wheelchair platform. The study considers a reactive directed potential field (DPF) method in the modelling of drivers' risk detection and avoidance behaviour, and applies the ordinary least square procedure in the identification of best-fitting driver parameters. The study also contributes to the development of a dynamic model of the wheelchair, usable under normal and non-normal conditions, by taking into consideration the conventional differential drive wheelchair structure with two front castor wheels. Derivation of the dynamic model, based on the Euler Lagrange formalism, is carried out in two folds: initially by considering the gravitational forces subjected to the wheelchair

on inclined configurations with no slipping situations, and finally by incorporating slipping parameters into the model. Determination of the slipping parameters is approached from the geometric perspective, by considering the non-holonomic motions of the wheelchair in the Euclidean space. In the closed-loop model, the input-output feedback controller is proposed for the tracking of user inputs by torque compensation. The optimality of the resulting minimum-phase closed-loop system is then ensured through the performance index of the non-linear continuous-time generalised predictive control (GPC). Simulation results demonstrate the expected behaviour of the wheelchair dynamic model, the steering behaviour model and the assistive capability of the closed-loop system.

ACKNOWLEDGEMENTS

I sincerely express my gratitude and appreciation to Prof. Yskandar Hamam, who apart from being my academic study leader has also been a father and a role model. I express my special appreciation to Prof. Karim Djouani and Prof Baubaker Daachi whose scientific contributions and academic guidance were indispensable throughout the entire duration of this research. I also can't forget Dr. Nico Steyn who worked tirelessly with me, and was always available for me.

A special 'thank you' to The National Research Fund (NRF) and The South African government and People at large, to F'SATI and Electrical Engineering Department at TUT, for granting me the opportunity to conduct my research and the basic framework from which my studies were possible, I thank you.

To my brothers Kenns and Elisha, my sister Millicent, my father Benson and my mother Fellidah, and most of all to my wife Eglen, your untiring support and encouragement in all matters made a big difference. May the Almighty God bless you according to His will.

Dr. Maina Mambo, Dr Michael Ajayi and Dr. Amos Anele thank you for always lending me a patient ear whenever I posed my numerous questions.

Contents

List of Figures

List of Tables

Abbreviations

ADAS	Advance Driver Assistance Systems
APF	Artificial Potential Field
BEA	Bacterial Evolutionary Algorithm
D-H	Denavit-Hartenberg convention
DoF	Degrees of Freedom
DPF	Directed Potential Field
DTR	Distance-to-risk
EAPF	Evolutionary Artificial Potential Field
GNRON	Goals Non-reachable with Obstacles Nearby
GPC	Generalised Predictive Control
HMD	Head Mounted Display
IDM	Intelligent Driver Model
LOA	Level of Autonomy
MDP	Markov Decision Process
MOEA	Multi-Objective Evolutionary Algorithm
MPC	Model Predictive Control
NN	Neural Network
PEAPF	Parallel Evolutionary Artificial Potential Field
POMDP	Partially Observable Markov Decision Process
RHC	Receding Horizon Control
SPRT	Sequential Probability Ratio Test
TTR	Time-to-risk
VSL	Variable Speed Limit
WMS	Wheeled Mobile System

Symbols

${}^{B}(\cdot)_{A}$	$\longrightarrow$	$(\cdot)$ is a variable of (frame) A in/ w.r.t (frame) B
${}^{A}(\cdot)$	$\longrightarrow$	$(\cdot)$ is a variable in (frame) A
$(\cdot)^{T}$	$\longrightarrow$	Transpose of variable $(\cdot)$
$\dot{(\cdot)}$	$\longrightarrow$	First derivative of variable $(\cdot)$ w.r.t time
$\ddot{(\cdot)}$	$\longrightarrow$	Second derivative of variable $(\cdot)$ w.r.t time
C	$\longrightarrow$	Centre of mass
$(\cdot)_{g}$	$\longrightarrow$	Coordinate components of point C in $\{x\,y\,z\}$
$\dot{(\cdot)}_{f}$	$\longrightarrow$	Castor wheel velocity component
O	$\longrightarrow$	Mid-point of rear axle/origin of the body fixed frame
$\dot{(\cdot)}_{o}$	$\longrightarrow$	Velocity components of O as translated from C
$\dot{\dot{(\cdot)}}_{g}$	$\longrightarrow$	Component of slipping velocity
$\mathbf{v}_{O}$	$\longrightarrow$	Velocity of O as translated from the centre of front axle
$\dot{(\cdot)}_{f_o}$	$\longrightarrow$	Components of $\mathbf{v}_{O}$
$\bar{x}, \bar{y}, \bar{z}$	$\longrightarrow$	Unit basis coordinates
$\bar{\bar{x}}, \bar{\bar{y}}, \bar{\bar{z}}$	$\longrightarrow$	Cartesian components of distance l between C and O
$\{x\,y\,z\}$	$\longrightarrow$	Inertial coordinate frame
x, y, z	$\longrightarrow$	Cartesian coordinates of $\{x\,y\,z\}$
$\{X\,Y\,Z\}$	$\longrightarrow$	Body fixed frame
X, Y, Z	$\longrightarrow$	Cartesian coordinates of $\{X\,Y\,Z\}$
I	$\longrightarrow$	Inertia tensor
$I_{XX},\ I_{YY},\ I_{ZZ}$	$\longrightarrow$	Moment of inertia about X, Y and Z axis through O
I_{XZ}	$\longrightarrow$	Product inertia about X and Z axis through O
$\boldsymbol{\mathcal{I}}$	$\longrightarrow$	Composite matrix of identity matrices
V	$\longrightarrow$	Linear speed
ν	$\longrightarrow$	Linear velocity
$\boldsymbol{\nu}$	$\longrightarrow$	Velocity vector
$\nu_{0X}, \nu_{0Y}, \nu_{0Z}$	$\longrightarrow$	Components of inertial velocity of C along the instantaneous directions of X, Y and Z axis
$\mathbf{v}_{R}, \mathbf{v}_{L}$	$\longrightarrow$	Linear velocities of the right and left castor wheels

$\mathbf{v}_{R_A}, \mathbf{v}_{L_A}$	$\longrightarrow$	Components of $\mathbf{v}_R$ and $\mathbf{v}_L$ about point A
$\mathbf{v}_{R_B}, \mathbf{v}_{L_B}$	$\longrightarrow$	Component of $\mathbf{v}_R$ and $\mathbf{v}_L$ about point B
V_r	$\longrightarrow$	Reference linear speed
X	$\longrightarrow$	Distance
$\mathbf{r}$	$\longrightarrow$	Position
$\mathbf{T}$	$\longrightarrow$	Homogeneous transformation matrix
T	$\longrightarrow$	Kinetic energy w.r.t point C
$\boldsymbol{\mathcal{J}}$	$\longrightarrow$	Wheel Jacobian matrix
$\mathbf{B}_0$	$\longrightarrow$	Block diagonal matrix of wheel Jacobian matrices
$\mathbf{R}$	$\longrightarrow$	Transformation matrix of frame $\{X, Y, Z\}$ relative to $\{x, y, z\}$
b	$\longrightarrow$	Half rear axle length
$\boldsymbol{\mathcal{D}}$	$\longrightarrow$	Decoupling matrix
D_v	$\longrightarrow$	Directivity factor
$\dot{\boldsymbol{\gamma}}$	$\longrightarrow$	Rotational velocity vector of the driving wheels
$\dot{\gamma}$	$\longrightarrow$	Average rotational velocity of the driving wheels
$\dot{\gamma}_R$, $\dot{\gamma}_L$	$\longrightarrow$	Angular velocities of the right and left wheels
$\dot{\gamma}_{f_R}$, $\dot{\gamma}_{f_L}$	$\longrightarrow$	Angular velocities of the right and left castor wheels
$\dot{\mathbf{\Gamma}}$	$\longrightarrow$	Composite vector of wheel velocity vectors
N	$\longrightarrow$	Normal force at point O
$\bar{\mathbf{e}}$	$\longrightarrow$	Unit vector in the direction of motion
$\bar{\mathbf{e}}_o$	$\longrightarrow$	Unit vector in the direction of moving obstacle
$\mathbf{q}$	$\longrightarrow$	Generalised coordinates vector
q_i	$\longrightarrow$	Component of the generalised coordinate vector
$\dot{\mathbf{q}}_s$	$\longrightarrow$	Generalised velocity vector with slipping velocities
$\dot{\mathbf{q}}_\epsilon$	$\longrightarrow$	The new generalised velocity vector that includes the slipping parameters
$\mathbf{Q}$	$\longrightarrow$	External forces aiding or resisting the motion
r	$\longrightarrow$	Radius of the driving wheels
r_C	$\longrightarrow$	Radius of the castor wheels
R^2	$\longrightarrow$	Coefficient of determination

θ	$\longrightarrow$	Instantaneous angular deviation of the Z-axis from the z-axis
ψ	$\longrightarrow$	The angle between the x-axis and the line of intersection of the moving XY plane and the stationary xy plane
ϕ	$\longrightarrow$	Precession angle about the Z-axis in a counter-clockwise direction as visible in the body fixed frame (yaw angle)
ϕ_r	$\longrightarrow$	Reference angular position
$\mathcal{L}$	$\longrightarrow$	Lagrangian function
U	$\longrightarrow$	Potential energy
U_{art}	$\longrightarrow$	APF function
U_{att}	$\longrightarrow$	Attractive potential
U_{rep}	$\longrightarrow$	Repulsive potential
$\mathbf{u}$	$\longrightarrow$	Input/control vector
$\boldsymbol{\mathcal{U}}$	$\longrightarrow$	State feedback law
μ	$\longrightarrow$	Coefficient of rolling friction
$\mu_{\text{vis}},\ \mu_{\text{cmb}}$	$\longrightarrow$	Coefficients of viscous friction and Coulomb friction
M	$\longrightarrow$	Mass of the wheelchair including all its components
$\bar{\mathbf{M}}(q_i)$	$\longrightarrow$	Symmetric positive definite inertia matrix
$\mathbf{G}(q_i)$	$\longrightarrow$	Vector of gravitational forces
$\bar{\mathbf{C}}(q_i, \dot{q}_i)$	$\longrightarrow$	Matrix of centrifugal and Coriolis forces
$\mathbf{A}(q)$	$\longrightarrow$	Matrix associated with constraints of the system
$\dot{\alpha}_R$	$\longrightarrow$	Orientational velocity of the right castor wheel
$\dot{\alpha}_L$	$\longrightarrow$	Orientational velocity of the left castor wheel
$\mathcal{A}$	$\longrightarrow$	Adaptation mechanism
$a_k,\ \omega_k$	$\longrightarrow$	Linear acceleration and angular velocity respectively
$\boldsymbol{\lambda}$	$\longrightarrow$	Vector of the Lagrange multipliers
$\boldsymbol{\chi}$	$\longrightarrow$	State vector
$\boldsymbol{\mathcal{Y}}$	$\longrightarrow$	State space output vector
ρ	$\longrightarrow$	Relative degree
ρ_r	$\longrightarrow$	Local roadway curvature
$L_f h(x)$	$\longrightarrow$	Lie derivative of $h(x)$ along $\mathbf{f}_1(x)$

$L_g h(x)$	$\longrightarrow$	Lie derivative of $h(x)$ along $\mathbf{g}_1(x)$
$z = \varphi(\chi)$	$\longrightarrow$	Non-linear transformation
$\mathbf{F}(\dot{q})$	$\longrightarrow$	Vector of frictional forces
$\mathbf{E}(q)$	$\longrightarrow$	Input transformation matrix
$\tilde{\mathbf{E}}(t)$	$\longrightarrow$	Vector of errors
$\mathbf{e}$	$\longrightarrow$	Linear speed and angular position errors
$\boldsymbol{\epsilon}$	$\longrightarrow$	Vector of slipping parameters
$\boldsymbol{\tau}$	$\longrightarrow$	Vector of input torque
$\tau_{_R}, \tau_{_L}$	$\longrightarrow$	Right and left rear wheel torques
$\tau_{_r}$	$\longrightarrow$	Relaxation/reaction time
$\bar{\tau}$	$\longrightarrow$	Duration of prediction
ω	$\longrightarrow$	Angular velocity
$\omega_X,\ \omega_Y,\ \omega_Z$	$\longrightarrow$	Components of ω along the X, Y and Z axis
$\mathbf{S}(q_i)$	$\longrightarrow$	Full rank transformation matrix which transforms $\boldsymbol{\eta}$ to $\dot{\mathbf{q}}$
$s_r,\ s_h,\ s_w$	$\longrightarrow$	Slip ratio, hand stiffness and wrist stiffness
$t,\ k$	$\longrightarrow$	Time and time instant
$k_\nu,\ k_{\text{env}}$	$\longrightarrow$	Driving model parameter
$\mathbf{h}$	$\longrightarrow$	Output vector
$T_1,\ T_2$	$\longrightarrow$	Minimum and maximum prediction time respectively
$k_{(\cdot)}\ m,\ n,\ p$	$\longrightarrow$	Constants
$w,\ B,\ K\ N$	$\longrightarrow$	Constants

Dedicated to all my friends

and

most importantly

my best friend and wife Eglen,

my daughter Fellidah,

my son Jesse,

and

my sister Millicent.

Chapter 1

INTRODUCTION

The recent robotic advancements and autonomous controls are quite evident in many areas of application. However, these have not relieved the human fully from the operator role. Human still intervenes to clear the complexities and environmental uncertainties that machines encounter during the operation. As a result, operator support and assistive systems, like autopilots in aircraft and advance driver assistance systems (ADAS) in auto-mobiles, have been developed to optimise the operator interventions through warnings and use of automated systems in the control and management of service machines. In auto-mobiles for instance, the driver assistance systems constantly interact with the driver to ensure a faultless operation of the vehicle. Indeed, the correct operation of such systems depends not only on the automated assistive system, but also on the handling behaviour of the human operator.

It may be known in general, that different operators will exhibit diverse handling behaviours and preferences, when operating similar systems under similar conditions. Besides, human operators appreciate the assistance not only because the assistive system can perform the intended task, but also, based on the way the support system executes the assistance. This complicates the ability to realise the assistance that the operator appreciates, without synthesising the operator's handling behaviour into the control system. Although the adaptability of assistive systems to the operator's handling behaviour may not be very necessary in some applications, the operator-specific assistive systems become very essential in applications where the service machine forms an integral component of the user's life, like in the use wheelchairs.

One way of realising the operator-specific assistance is through modelling and incorporating the handling behaviour of the operator in the control system. The modelling

of handling behaviours entails the formulation of structures, and specifications of processes, that simulates the control actions of the operator. It involves the definition of initial conditions and operational limits of the operator and machine, with parallel consideration of the prevailing operational context and presumed assumptions. This, however, does not guarantee the possibility of finding a formulation that absolutely replicates the contextual handling behaviour of a human operator. As a result, it is almost inevitable, that some elements of human control are necessary to realise proper operation of such assistive systems.

The operator handling/behaviour models, have been formulated in different fields for various reasons, including design and accident analysis. The modelling of handling behaviour for design reasons is concerned with the development and assessment of different machine procedures and interfaces; while the modelling for accident analysis regards the causes of events that result in the human behaviours, for the sake of investigations. Coincidentally, most behaviour models have supported the design and development of dynamic and assistive systems, regardless of the modelling reason. In motor-vehicle safety assessment for instance, the driver models formulated to assist in the understanding and planning of solutions to traffic bottlenecks (Ahmed, 1999), have also aided the design and development of ADAS (Panou et al., 2007).

In order to design and evaluate the assistive system that takes into consideration the operator's handling behaviour, it may be necessary that the appropriate machine model and control architecture are available. Balanced equations derived from the Newton's laws and the virtual work concept, are generally used to express a machine's behaviour. Indeed, different procedures consisting of D'Alembert's, Lagrange's and Hamilton's can be used to formulate the basic laws of dynamics by considering the states of physical variables and functional components of a dynamic system. In particular, this study focuses on the standard powered wheelchair, and contributes to

the advancement of steering performance through background assistance. It involves modelling, empirical estimation, and incorporation of a wheelchair model and the driver's steering behaviour model into the control system.

1.1 Background and motivation of the study

Wheelchair prevalence could be linked to the role they play in alleviating mobility restrictions over short distances. According to the South African profile report of persons with disability (Statistics South Africa & Lehohla, 2014), 2.3% ($\approx$ 1.2 million) of the total South African population ($\approx$ 52 million) depend on the wheelchair. Moreover, the percentage of people in need of wheelchairs could be much higher in other underdeveloped countries because diseases responsible for mobility impairments like cerebral palsy can be associated with lower socio-economic status (Sundrum et al., 2005). While this may seem to represent a marginal portion of the population, it may not be possible to over emphasise the important sense of independence and self-esteem, that users with debilitating impairments experience with wheelchairs. It may be noted in the absence of wheelchairs and other mobility aids, that ambulatory impairments may result in extreme emotional loss, neglect, stress and even isolation (Finlayson & van Denend, 2003).

Normally, manual or powered wheelchairs can be used by individuals with physical lower limb impairments. However, the manual wheelchairs present difficult physical demands for users with both physical and cognitive impairments. On the other hand, powered wheelchairs eliminate the physical demands, but necessitate special control skills that some potential users do not possess (Simpson et al., 2008). In order to accommodate such users, the contemporary wheelchair research is focused towards user-suited interfaces and autonomous control.

Several robotic functionalities with computers and sensors have been considered in the design of autonomous wheelchairs in order to provide the user with a variety of hands-free navigation capabilities. Nonetheless, the studies and developments that regard wheelchair control for the sake of driver assistance and rehabilitation are still limited in spite of the current advancements. According to Fehr et al. (2000), about 10% of the users still encounter considerable difficulties in their daily use, and upto 40% find the steering task close to impossible. Besides, Fehr et al. (2000) observe that some potential users with multiple sclerosis and high-level spinal cord injuries, have spent extremely long training and rehabilitation durations with insignificant success. In the absence of caretakers, such individuals may not be able to use the wheelchair. Encompassing this user group necessitates assistive improvements in the control and management of wheelchair systems.

In order to empower debilitated individuals with the full independence and self-esteem that the stronger users experience, it is important that the high-level decision making tasks and control process are granted to the user, and not the autonomous wheelchair controller. This means, that the user may still need to perform the ordinary steering manoeuvres with necessary assistance and a suitable interface. Assisting a driver who is in active control, may require the system to determine, in the appropriate way, the assistive adjustment as well as the extent to which the adjustment is provided. The control system therefore needs to be aware of the intention and steering preferences of the driver. It is considered that this could be realised by taking the driver's steering behaviour into consideration in the design of the wheelchair's control system. This is regarded as control with the user-in-the-loop.

According to Panou et al. (2007), drivers are known to adjust their speed in order to establish the equilibrium between the environmental situation and the acceptable subjective risk. This compensatory mechanism is proposed, to adapt the steering

control of the wheelchair to the driver's handling behaviour. It is presumed that the approach reduces the driver's workload in fine control, and provides steering assistance regardless of the impairment condition. Besides, the assistance could remedy the effects of functional deterioration and fatigue and improve the comfort and safety of the driver.

Validating the assistive system necessitates the formulation of a wheelchair model and proper implementation of a control architecture. It is important that the actual behaviour of the wheelchair is represented as much as possible by the model. In literature, the modelling of differential drive wheelchairs is carried out from both kinematics and dynamic perspectives. The kinematic models present ideal formulations that relate the wheel rates of the wheelchair to the body-fixed frame velocities, by considering the geometric properties. However, kinematic models do not account for the effects of mass, inertia and acceleration, and are therefore used with anticipation that the controller will be robust enough to account for the unconsidered dynamical properties (Tarokh & McDermott, 2005; Tian et al., 2009; Zhang et al., 2009).

Dynamic modelling on the other hand, incorporates both kinematic and dynamic properties of the system. For this reason, dynamic modelling is one of the common modelling approaches in the literature. Most dynamic models, however, presume two dimensional configurations with pure rolling constraints, and rarely account for the combined effects of wheel slip, frictional resistance and gravitational disturbance (Oubbati et al., 2005; Kozłowski & Pazderski, 2004). As a result, such models may not be comprehensive enough to reflect the actual outdoors behaviour of the wheelchair. It is suggested, that one solution to wheelchair automation and performance improvement is through better and realistic system modelling.

1.2 Problem statement

A large percentage of the wheelchair user community can steer with confidence in adequate environments. However, the steering accuracy varies with the kind of impairment, the extent of disability and the inherent monotony of wheelchair steering (Fehr et al., 2000). Extreme cases of the steering inaccuracies have caused collision accidents in typical residential settings (Fehr et al., 2000; Cooper et al., 1996; Rodgers et al., 1994). Besides, the available wheelchair control techniques have not addressed the progressive deterioration in the steering capability of users with degenerative conditions (Ando & Ueda, 2000). Accordingly, this thesis intends not only to address the above steering inaccuracy problem, but also seeks to ensure that the desired accuracy and the ensuing steering assistance is adapted to the driver's steering behaviour, and benefits the whole user community regardless of the disability condition. It is considered that this could be achieved through better modelling and system control. There is need, therefore, that an appropriate control architecture and a realistic model of the wheelchair and the driver's steering behaviour is available. Thus, the following sub-problems are observed:

1.2.1 Sub-problem 1

Wheelchair driving or driver models are considerably few in the literature. Besides, the available models, suffer lack of individuality, focusing mostly on common user attributes, and assume that all drivers respond to navigation situations by similar general patterns (Diehm et al., 2013). Such driver models employ the general parameters that barely correspond to measurements obtained from extreme drivers, and hardly take into consideration the contextual nature of human response to stimuli.

It is therefore important that a wheelchair steering model, capable of addressing the specific steering behaviour of the driver, is formulated.

1.2.2 Sub-problem 2

The disability condition of the wheelchair user-community requires assistive systems that take into consideration the favourable indoor as well as the unstructured outdoor steering situations. The available wheelchair models, however, fail to take into consideration the aggregated effects of extreme dynamic steering situations on the wheelchair (Zhu et al., 2006; Tian et al., 2009; Zhang et al., 2009). This therefore necessitates the formulation of a comprehensive wheelchair model that presumes the unstructured and structured dynamic conditions, and takes the effects of gravitational forces, wheel-slip and rolling friction on the usable-traction into consideration.

1.2.3 Sub-problem 3

The existing steering assistance solutions provide discrete levels of shared control; with full computer control at the autonomous level, and full driver control at the operator level (Rofer & Lankenau, 1999; Levine et al., 1999). The driver is tasked with the responsibility of choosing the appropriate control level, and the intended destination in the case of full autonomous control. It is considered, that choosing the destination and control mode may constitute a cognitively challenging responsibility to some users. Moreover, a particular path to the destination may be preferred; if the wheelchair is steered autonomously to the goal without necessarily following the preferred path, the driver may fail to appreciate the assistance. It is therefore important that the control and decision making tasks are granted the driver, while the steering assistance is executed by the steering behaviour model in the control

loop. In this regard, a pertinent control architecture is required to accomplish the steering assistance.

1.3 Research Objectives

The primary objective of this study is to advance the state of the art in wheelchair steering, by synthesising the driver's handling behaviour into the control system, so as to provide a driver-specific background steering assistance. This involves integrating the wheelchair dynamic model and the driving behaviour model of the user in the control system, to adapt the control of the wheelchair to the driver's steering behaviour.

The following objectives are therefore considered:

- To formulate and verify a versatile empirical driving model of a powered wheelchair user, based on the observable actions of the driver, with particular consideration of the steering signals and the prevailing environmental situation.
- To identify the steering behaviour of the driver in terms of the driving model's parameters, using the steering data generated from the virtual worlds of an augmented wheelchair platform.
- To formulate and validate a dynamic model of a differential drive powered wheelchair, that takes into consideration the effects of rolling friction and gravitational potential of the wheelchair, on both inclined and non-inclined surfaces.
- To implement a control system that incorporates the wheelchair model and the driving behaviour model in the control loop, in order to adapt the steering of the wheelchair to the driver's behaviour and realise the intended steering support.

1.4 Methodology

Human-in-the-loop control is increasingly becoming one of the acceptable concepts of realising the provisional demands of semi-autonomous controllers that occasionally necessitate human intervention (Rothrock & Narayanan, 2011; Chiang et al., 2010; Tsui et al., 2011; Stoelen et al., 2010; Smith, 2003). Human-in-the-loop approach to system control is adopted and implemented in this study using the classical feedback control technique (Isidori, 1995; DeFigueiredo & Chen, 1993). The idea is executed by synthesising the wheelchair model and the discrete reactive model of the driver's steering behaviour in the control system. The assistive control with human-in-the-loop is effected in three stages.

At the first stage, the formulation of a dynamic model of the wheelchair is carried out. The conventional differential drive structure of the wheelchair with two front castor wheels is considered (DeSantis, 2009; Mohareri et al., 2012). Its dynamic model derivation is based on the Euler Lagrange formalism (Uicker, 1969; Kahn & Roth, 1971), and is carried out in two folds. Initially, both kinetic and gravitational energy is considered in the Lagrangian function to account for the wheelchair's dynamic properties on both inclined and non-inclined configurations without slipping situations. The slipping parameters are then formulated and incorporated into the model. The determination of the slipping parameters is approached from the geometric perspective, by considering the non-holonomic motions of the wheelchair in the Euclidean space. Because of its non-holonomic nature, the model constitutes the class of uncertain non-linear systems.

The study also involves the development of a steering behaviour model for wheelchair drivers. The formulation is based on the reactive potential field approach (Khatib, 1985; Koren & Borenstein, 1991; Jaradat et al., 2011), that has been considered

by numerous experimentally validated models in the literature (Jaradat et al., 2011). The formulation and identification of the time-series empirical driver model is carried out on account of two fundamental sources of information comprising the general observation of wheelchair steering and the generated microscopic steering data. In particular, the directed potential field method is considered in the formulation of the driver's risk detection and risk avoidance behaviours (Schneider & Wildermuth, 2005; Taychouri et al., 2007). The advantage of the proposed directed potential field method is that: apart from using the distance representation and taking the risks dissemination into account, it also allocates variable repulsive potential on the relative direction of the risk from the wheelchair. In the identification of the driver-specific steering behaviours, the ordinary least square procedure is considered in the computation of best-fitting driving model parameters.

At the final stage, the closed-loop model utilising the partial-state feedback controller is proposed in the tracking of user inputs by torque compensation (Codourey, 1998). The control of similar non-linear systems by feedback linearisation can either be full-state or partial-state. The full-state (or input-state) feedback linearisation involves complete linearisation of the system's states with respect to control inputs by coordinate transformation and static state feedback, while the partial-state or the input-output feedback linearisation procedure linearises dynamics of the systems between the input and the output. In real-life however, the exact conditions for the full-state linearisation are only satisfied by few non-linear systems (Isidori, 1995; Hunt et al., 1983; Su, 1982). Because the proposed dynamic wheelchair model does not satisfy the full-state feedback linearisation conditions (Isidori, 1995), the partial-state feedback linearisation technique is considered. Nevertheless, the system is minimum-phase with stable internal dynamics. The optimality of the resulting closed-loop system is ensured through the performance index of the non-linear continuous-time generalised predictive controller (GPC).

1.5 Outline of the main contributions

The main contributions of this work can be summarised as follows:

- The identified driver-specific parameters of the driving behaviour model constitutes the equilibrium between the subjective risk level of the driver and the prevailing environmental situation. The formulation and implementation of a driving behaviour model using driver-specific parameters, to adapt the wheelchair's velocity to the driver's behaviour to achieve the background steering assistance with minimum corrective adjustments on the steering signals, entail the main contributions of this thesis. Besides, the proposed assistive system employs the driver-specific parameters in the driving model to ensure both fine steering manoeuvres and automatic risk and collision avoidance behaviours.

- The study also contributes to the development of a wheelchair driving behaviour model that is simple and linear in the parameters, with a capacity to allocate directed reactive resources against sensor detectable risks. These attributes make the driving model implementable on-line as real-time intelligent co-driver, on board the wheelchair, that predicts and provides local corrective solutions to possible steering errors in accordance with the driver's preference and current situation.

- The development of a dynamic model of a differential drive wheelchair and derivation of slipping parameters also constitutes a contribution of the study. The dynamic model takes into account the effects of rolling friction, slipping parameter and gravitational potential of the wheelchair, on both inclined and non-inclined surfaces, and therefore presents a more realistic representation of the wheelchair.

- The study incorporates the driving behaviour model, the wheelchair model and a feedback controller in a closed-loop system, to adapt the control of the wheelchair to the driver's behaviour to realise the intended background steering assistance.

1.6 Delineations and Limitations

This study is based on the following assumptions:

- In order to formulate the wheelchair dynamic model, it is considered that the wheelchair, including its components, is built from rigid bodies, and therefore possess no flexible links.
- It is presumed that the symmetric structure of wheelchair remains unchanged during use, implying that the centre of mass will always remain along the longitudinal axis of the wheelchair's motion.
- In the modelling of slipping parameters, it is considered that the front castor wheels are relatively far away from the centre of mass compared to the hind wheels, and therefore experience no longitudinal slip because of the reduced force effect. The castor wheels velocity is thus presumed to represent the wheelchair's absolute velocity.
- In the driving behaviour modelling, explicit knowledge of the driver's subsequent intentions is presumed to be available.

1.7 Publications

1. Onyango S.O., Hamam Y., Djouani K., Daachi B., & Steyn N. (2016). A Driving Behaviour Model of Electrical Wheelchair Users. Computational Intelligence and Neuroscience, 2016(2016), 20. http://doi.org/10.1155/2016/7189267

2. Onyango S.O., Hamam Y., Djouani K., & Daachi B. (2016). Modeling a powered wheelchair with slipping and gravitational disturbances on inclined and non-inclined surfaces. SIMULATION, 92(4), 337355. http://doi.org/10.1177/0037549716638427

3. Onyango S.O., Hamam Y., Djouani K., & Daachi B. (2015). Identification of wheelchair user steering behaviour within indoor environments. In 2015 IEEE International Conference on Robotics and Biomimetics (ROBIO),. Zhuhai China: IEEE. http://ieeexplore.ieee.org/xpls/abs_all.jsp?arnumber=7419114&tag=1

1.8 Thesis Chapter Overview

Chapter 1 presents the general introduction as well as the background and motivation for the study. Chapter 2 reviews the previous and current insights about the practises and methodologies used in the modelling and control of systems with human-in-the-loop. This includes the current advancements in the modelling of the differential drive system, particularly, wheeled mobile robots and wheelchair systems. An overview of the existing user handling models is provided. Because of the structural similarities between cars and wheelchairs, the driving model developments for the two systems is also elaborated. Chapter 2 further includes a few methodologies used in the control of

non-linear systems. In Chapter 3, the proposed dynamic model of a differential drive wheelchair system is introduced. It presents the employed formulation and validation procedure of the wheelchair model as well as the derivation and incorporation of slipping parameters into the dynamic model. Chapter 4 presents the proposed wheelchair driving model. This also encompasses the formulation, parameter identification, and validation of the driver model. The closed-loop system with human-in-the-loop is presented in Chapter 5, while Chapter 6 provides the conclusion, and outlines a few opportunities for further research.

Chapter 2

CONTROL WITH HUMAN-IN-THE-LOOP METHODOLOGIES: A SURVEY

2.1 Introduction

This chapter presents the relevant previous and contemporary advancements in the control of dynamical systems with human-in-the-loop. It entails the existing modelling and identification contributions on both dynamical systems and operator behaviours. The chapter elaborates the control methodologies employed to manage the integration of the dynamic wheelchair and the driving behaviour models in the control loop. This includes the concept of time, kinematic structure and virtual work in system modelling, and analysis of microscopic user-data for system identification, which constitute the fundamental design requirements taken into consideration to evaluate the desirable operational behaviour of a system. Since the literature in this field is quite elaborate, a limited scope of the survey is necessitated. As a result, the chapter is limited to the modelling and control aspects that relate to wheeled-mobile system (WMS).

2.2 Background

A WMS is a mechanism with actuated and possibly non-actuated rolling wheels, mounted to provide both support and relative motion (Muir, 1988). The system not only consists of the main body and wheels, herein referred to as the moving platform, but also the surface upon which the platform moves. The application of WMSs is

quite ancient in the transportation sector, and more evident in the modern world, with continuing research and developments in the transportation, defence, medical and manufacturing sectors. The common structural configurations of the wheeled platforms include the differential drive with two non-steered driving wheels and one or more caster wheels for stability, the tricycle with two non-steered and one steered wheels, the synchro-structure, the steered Ackermann and the omnidirectional drive structure (Katevas, 2001). The differential drive structure produces a straight line motion when all its drive wheels are turned at the same rate in the same direction, and an in-place rotation with zero turning radius, given equal and opposite turning velocities. Owing to the simple configuration and easier odometry, the differential drive structures find diverse application in common user and robotic systems. This chapter focuses on the differential drive structure with two front or rear caster wheels as applied in the powered wheelchair (Ding & Cooper, 2005; DeSantis, 2009).

Based on the type and assembly of the driving wheels, holonomic and non-holonomic constraints may be imposed on the platform's motion. In consequence, the motion a WMS and the implied complexity in its controllability is highly dependent on the structural configuration. The holonomic constraints relate the time and positional variables of a kinematic system. In the presence of holonomic constraints, the final state of a kinematic link, is only dependent upon the initial states of other connected links. This means that given the initial states, it is possible to compute both translational and rotational positions of the link from the linear and rotational positions of the adjacent links. Besides, all velocity constraints can be integrated into positional constraints. As a result, all degrees of freedom (DoFs) related to a spacial kinematic system with holonomic constraints are easily controllable on planar surfaces with simple motion planning tasks (Mariappan et al., 2009). The omnidirectional holonomic wheels are numerous in the literature of mobile robotics. However, their main drawback entails the complexity of the wheeling system that necessitates

high energy besides the periodic maintenance required by the actuators (Xu, 2005; El-Shenawy, 2010). Because of this, the holonomic wheels are rarely implemented in common daily applications. The configurations with non-holonomic constraints on the other hand, introduce a continuous closed-circuit of constraining parameters, that governs the transformations of the system from one state to the other (Bryant, 2006). Accordingly, the velocity constraints are non-integrable, indicating that the final state of the system depend on the transitional trajectory values within the parameter space. The strength of the non-holonomic structures, nonetheless, lies in the construction simplicity, with fewer controllable axis required to ensure the necessary mobility. This makes them reliable, efficient, flexible and prevalent. Besides, the usage of multiple disk shaped wheels improves the robustness and stability of systems with non-holonomic constraints in the presence of irregular terrains. However, non-holonomic systems are strongly non-linear, and require exhaustive non-linear analysis (Astolfi, 1996; Koon & Marsden, 1997). Thus, designing a good control system is generally a considerable challenge.

2.3 Modelling of WMSs

The majority of the literature concerns the kinematic and dynamic modelling. The kinematics of a WMS refers to the study of the system's motion that results from the geometry of constraints of the wheels' rotational motion (Muir, 1988). In kinematic modelling, the preceding requirement regards the allocation of numerous coordinate frames within the system and the environment, to facilitate the formulation of parameters and variables of the kinematic model. The kinematic modelling parameters, include the angles and distances between the various coordinate systems, while the variables include the relative positions, velocities and accelerations of the body and

the wheels. Dynamic modelling on the other hand, determines the relationship between the actuator forces and the resulting motion of the WMS. The parameters involved in dynamic modelling include the angles and distances between different coordinate systems, mass and inertia components, and frictional coefficients; while the variables include the positions, velocities and accelerations of the wheels and the body.

Notably, two approaches are available in the literature of kinematic and dynamic modelling of WMSs: the non-generic vector approach, based on geometric interpretation of global relationships between the centroid velocity and the joints' rates (Kelly & Seegmiller, 2010; Byung-Ju Yi & Whee Kuk Kim, 2000); and the generic transformation approach that involves an outline of the system's kinematic structure, with coordinate frames that may be assigned according to Sheth-Uicker's convention (Sheth & Uicker, 1971; Muir, 1988; Holmberg & Khatib, 2000). In the transformation approach, the wheel Jacobian and joints transformation matrices are formulated to express the displacement relationships between the different links of a WMS.

2.3.1 Special kinematic characteristics of a WMS

The following special characteristics of a WMS also provide a distinction between the internal kinematics; that relates the different links of a mechanism, and the external kinematics; that provides a relationship between a mechanism and its environment (Schaal et al., 2003; Ambike & Schmiedeler, 2006).

1. Each wheel is in contact with the body and the surface of travel, forming as many parallel closed-chains as the number of wheels. As a result, WMSs necessitates parallel computation of both kinematic and dynamic models. Unlike the mobile systems, most stationary mechanisms (with exception of manipulators

whose end effectors are in contact with fixed objects) have open-chains with links that are serially connected by joints without closed-circuits. In consequence, the stationary mechanisms only require serial kinematic and dynamic modelling. According to Muir (1988), a mechanical structure that amounts to a closed-chain system can be represented by Figure 2.1. The structure, comprising the main body, N open-chains, and the environment not only models WMSs, but also a variety of robotic mechanisms. Analogous to a WMS, the main body represents the body of the WMS, the N open-chains represent the N wheels, while the environment represents the surface of travel.

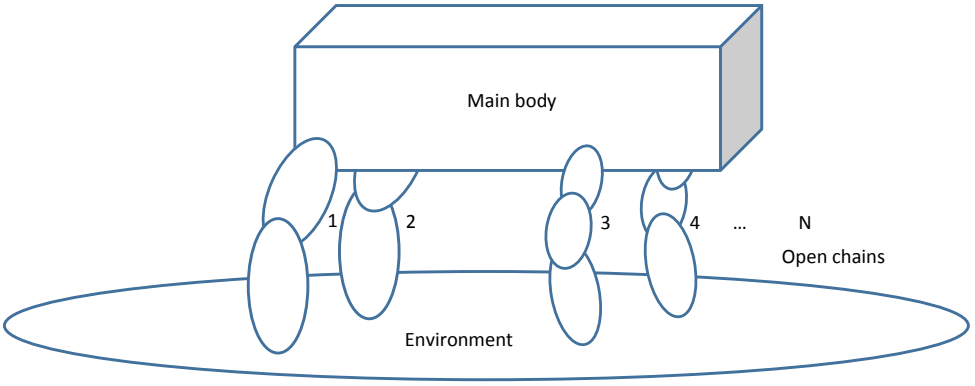

FIGURE 2.1: A simple closed chain mechanism

2. A higher-pair pseudo joint, that enables rotational and translational motions with respect to the point of contact exists, between each wheel and the surface of travel. According to (Katevas, 2001), a pair is a joint between two bodies that keeps them not only in contact, but also in relative motion. A lower pair involves a surface contact, while a higher pair involves a point or a line contact. Most stationary robotic mechanisms employ the lower-pair revolute, prismatic, helical, cylindrical, spherical or planar joints.

3. Unlike the open-chain mechanisms, where all joints must be actuated and sensed, it may be unnecessary to actuate and sense all the DoFs of the wheels to provide adequate control. Indeed, it is more favourable to compute the motion of non-actuated wheel because it is less likely to be affected by slippage.

4. Friction is important at the point of contact between the wheel and the surface of travel. The dry friction between the wheel and the surface of travel plays a very important role in ensuring the motion of the adjoining bodies. The friction in the wheel bearings is, however, undesirable because it results in excessive dissipation of energy.

2.3.2 Kinematic modelling of a differential drive system

By formulating the constraints that the joints impose on the adjacent links, the kinematic models provide the basis for both dynamic modelling and model-based control. In WMSs, the computed constraints include positional, velocity and acceleration constraints of the body and the wheels, relative to the inertial coordinate system. This necessitates the simplifying assumption that the WMS is only built from rigid bodies, the transformation matrix and the wheel Jacobian matrix to describe and relate the translational and rotational motions associated with the joints. The relationship between the joints' velocities may be computed by differentiating the corresponding positional relationships.

2.3.2.1 Coordinate system assignment

The conventional kinematic modelling procedure begins by assigning various coordinate frames to the various joints of a mechanism. Two conventions are commonly

applied in the assignment of coordinate frames: the Denavit-Hartenberg convention (Niku, 2001), and the Sheth-Uicker convention (Sheth & Uicker, 1971). The Denavit-Hartenberg, also known as D-H convention, presents two displacements and two rotations characteristic parameters for attaching the coordinate frames to the links of a spacial kinematic chain. The convention entails a 4×4 homogeneous transformation matrix, that, apart from describing the size, the shape and the associated transformations of the link, also relates the successive coordinate frames on the kinematic chain. Given the base effector's coordinate vector, the transformation matrices may be cascaded from the base link to the end effector to determine the position and orientation of the end effector of a stationary robotic manipulator. This convention attaches one coordinate frame to every joint of the kinematic chain. In spite of its popularity, the D-H convention does not present an obvious joint ordering criteria, and therefore leads to ambiguous transformation matrices, especially in systems with multiple closed-chains like WMS where one link, the environment, associates more than two joints (Katevas, 2001). Sheth-Uicher convention solves this problem by assigning one coordinate frame at the end of each link, implying that each joint will have two coordinate axis (Muir, 1988). In a WMS, the links include the surface of travel and the body, while the joints connecting the two links are the wheels and the center of mass of the WMS. The latter joint is not physical, but rather a relationship between the body and the surface of motion.

In order to formulate the kinematic model, a stationary or inertial coordinate frame may be assigned on the surface of travel to provide an absolute reference for the system's motion. The motion of a coordinate frame fixed at a point in the body relative to the inertial coordinate frame, herein referred to as body-fixed coordinate frame, may be interpreted as the WMS's motion. It is noted, that although the choice of position of origin and orientation of coordinate frames is not unique, it is preferred that positions and orientations which produce the appropriate formulation of a kinematic

model is considered. Depending on the number of wheels, the coordinate frames may be assigned at the point of contact between the surface of travel and the wheel. Each wheel and the main body can then be modelled as a planer pair with two or more DoFs, contingent on the associated kinematic constraints.

2.3.2.2 The homogeneous transformation matrix

Spacial kinematics may be regarded as a way of representing the rigid body's pose and displacement (translational and/or rotational motions) within a space. The 4×4 homogeneous transformation matrix consolidates both positional vector and rotational displacement matrix in a compact matrix notation. The matrix is used in kinematic modelling to transform a point's coordinate to its corresponding coordinate in another coordinate frame, such that, given the position of origin of frame A with respect to frame B, denoted by ${}^{B}\mathbf{r}_{A} = \begin{bmatrix} {}^{B}\mathbf{r}_{A}^{x} & {}^{B}\mathbf{r}_{A}^{y} & {}^{B}\mathbf{r}_{A}^{z} \end{bmatrix}^{\mathrm{T}}$, and the corresponding orientation, computed using the rotation matrix of direction cosines, ${}^{B}\mathbf{R}_{A}$, in Equation (2.3), any position vector ${}^{A}\mathbf{r}$ in frame A can be transformed into position vector ${}^{B}\mathbf{r}$ in frame B by expression (2.1), or expression (2.2) in matrix form.

$$ {}^{B}\mathbf{r} = {}^{B}\,\mathbf{R}_{A}\ {}^{A}\mathbf{r} + {}^{B}\,\mathbf{r}_{A} \tag{2.1} $$

$$ \begin{bmatrix} {}^{B}\mathbf{r} \\ 1 \end{bmatrix} = \begin{bmatrix} {}^{B}\mathbf{R}_{A} & {}^{B}\mathbf{r}_{A} \\ 0^{T} & 1 \end{bmatrix} \begin{bmatrix} {}^{A}\mathbf{r} \\ 1 \end{bmatrix} \tag{2.2} $$

where

$$ {}^{B}\mathbf{R}_{A} = \begin{bmatrix} (\bar{x}_{A} \cdot \bar{x}_{B}) & (\bar{y}_{A} \cdot \bar{x}_{B}) & (\bar{z}_{A} \cdot \bar{x}_{B}) \\ (\bar{x}_{A} \cdot \bar{y}_{B}) & (\bar{y}_{A} \cdot \bar{y}_{B}) & (\bar{z}_{A} \cdot \bar{y}_{B}) \\ (\bar{x}_{A} \cdot \bar{z}_{B}) & (\bar{y}_{A} \cdot \bar{z}_{B}) & (\bar{z}_{A} \cdot \bar{z}_{B}) \end{bmatrix}, \tag{2.3} $$

with $(\bar{x}_A \;\; \bar{y}_A \;\; \bar{z}_A)$ and $(\bar{x}_B \;\; \bar{y}_B \;\; \bar{z}_B)$ representing the unit basis vectors of the frames A and B respectively. The component, ${}^{B}\mathbf{T}_A = \begin{bmatrix} {}^{B}\mathbf{R}_A & {}^{B}\mathbf{r}_A \\ 0^T & 1 \end{bmatrix}$ in Equation (2.2) and (2.4), is the 4×4 homogeneous transformation matrix, consisting of four sub-matrices namely: the rotation matrix, the position vector, the perspective transformation and the scaling. Any transformation matrix ${}^{C}\mathbf{T}_A = {}^{C}\mathbf{T}_B \; {}^{B}\mathbf{T}_A$, may be computed with a strict consideration of the transformation order.

$$ {}^{B}\mathbf{T}_A = \left[\begin{array}{c:c} {}^{B}\mathbf{R}_{A(3\times3)} & {}^{B}\mathbf{r}_{A(3\times1)} \\ \hdashline 0^{T}{}_{(1\times3)} & 1_{(1\times1)} \end{array}\right] = \left[\begin{array}{c:c} \text{rotation matrix} & \text{position vector} \\ \hdashline \text{perspective vector} & \text{scalar} \end{array}\right] \tag{2.4} $$

In WMSs, the relative change in position and orientation of the body with respect to the surface of motion result from the wheels' rotational motion. The wheel Jacobian matrix is used in kinematic modelling to relate the rotational motion of the wheels to the body's motion. The analysis of Jacobian matrix has been considered the main tool for evaluating the kinematic performance of robotic manipulators (Tarokh & McDermott, 2005; Galicki, 2016; Kanzawa et al., 2016). Several guidelines, including manipulability, condition number, isotropy and global conditioning index for kinematic performance, have been proposed (Merlet, 2007). An isotropic Jacobian matrix is emphasised because it establishes a linear map between the joints' and the body's velocities, ensuring that each actuator is providing a proportional effort in the body's direction of motion (Zaw, 2003; Singh & Santhakumar, 2016). According to Muir (1988) and Ostrovskaya (2000), derivation of wheel Jacobian matrix is based directly on the velocity transformation matrices.

2.3.2.3 Forward and Inverse Kinematic Solutions

The forward and inverse kinematic solutions can be obtained by parallel computation of the wheels kinematic equations of motion. The forward kinematic solution computes the body's velocity from the sensed positions and velocities of the wheels, while the inverse kinematic solution determines the actuated velocity of the wheels from the body's velocity. For instance, given the wheel Jacobian matrices, $\boldsymbol{\mathcal{J}}_i|_{i=1\cdots w}$, and the wheel velocity vectors, $\dot{\boldsymbol{\gamma}}_i$, where w is the number of wheels, the body velocity, $\boldsymbol{\nu}$, may be computed according to Equation (2.5). It is important that all the equations in (2.5) are solved in parallel, to characterise the motion of the WMS.

$$\boldsymbol{\nu} = \boldsymbol{\mathcal{J}}_i \dot{\mathbf{q}}_i$$

$$\begin{bmatrix} \boldsymbol{\mathcal{I}}_1 \\ \boldsymbol{\mathcal{I}}_2 \\ \vdots \\ \boldsymbol{\mathcal{I}}_N \end{bmatrix} \boldsymbol{\nu} = \begin{bmatrix} \boldsymbol{\mathcal{J}}_1 & 0 & \cdots & 0 \\ 0 & \boldsymbol{\mathcal{J}}_2 & \cdots & 0 \\ \vdots & \vdots & . & 0 \\ 0 & 0 & \cdots & \boldsymbol{\mathcal{J}}_N \end{bmatrix} \begin{bmatrix} \dot{\boldsymbol{\gamma}}_1 \\ \dot{\boldsymbol{\gamma}}_2 \\ \vdots \\ \dot{\boldsymbol{\gamma}}_N \end{bmatrix} \tag{2.5}$$

or

$$\mathbf{A}_0 \boldsymbol{\nu} = \mathbf{B}_0 \dot{\boldsymbol{\Gamma}}$$

where $\boldsymbol{\mathcal{I}}_i|_{1\cdots w}$ are the identity matrices, $\mathbf{B}_0$ is a block diagonal matrix of the wheels Jacobian matrices and $\dot{\boldsymbol{\Gamma}}$ is composite velocity vector of the wheels. Equation (2.5) contains a set of algebraic linear equations whose numerical solutions may be computed by classical control techniques. The actuated inverse solution may then be computed by finding the velocity solution for the actuated wheels, while the sensed forward solution is computed from the wheels' positions and velocities. Since WMSs contain multiple closed-chains, it may be unnecessary to actuate and sense all wheels in order to compute a kinematic model. However, in case of some non-actuated and non-sensed wheel-variables, the Muir (1988)'s procedure for separating the actuated

and the non-actuated, as well as the sensed and the non-sensed variables may be considered together with the least-square method to compute both inverse and forward solutions.

2.3.2.4 The kinematic model of a differential drive system: An example

Differential drive WMSs commonly employ the conventional disk-shaped wheels. The disk-shaped wheels posses only two DoFs, consisting of the translational motion in the direction of orientation and the rotational motion about the point of contact on the surface of travel. In reality, an area rather than a point of contact exists between the wheel and the surface of contact. The rotation about this area, otherwise referred to as the rotational DoF, is therefore slippage. However, because of its formulation difficulties, the lateral slip is rarely taken into consideration in most kinematic models.

Differential drive systems entail a specific drive mechanism for each of the parallel driving wheels. The transformation from the wheels rotational velocity ($\dot{\gamma}_R\ \dot{\gamma}_L$) to the translational velocity ($V\ \omega$) of the centre of the drive wheels axle is expressed by Equation (2.6), and the sensed forward kinematic solution is computed by expression (2.7).

$$\begin{bmatrix} V \\ \omega \end{bmatrix} = \begin{bmatrix} \frac{r}{2} & \frac{r}{2} \\ \frac{r}{2b} & \frac{-r}{2b} \end{bmatrix} \begin{bmatrix} \dot{\gamma}_R \\ \dot{\gamma}_L \end{bmatrix} \tag{2.6}$$

$$\dot{q} = \begin{bmatrix} \dot{x} \\ \dot{y} \\ \dot{\theta} \end{bmatrix} = \begin{bmatrix} \cos\theta & 0 \\ \sin\theta & 0 \\ 0 & 1 \end{bmatrix} \begin{bmatrix} V \\ \omega \end{bmatrix} = \begin{bmatrix} \frac{r\cos\theta}{2} & \frac{r\cos\theta}{2} \\ \frac{r\sin\theta}{2} & \frac{r\sin\theta}{2} \\ \frac{r}{2b} & \frac{-r}{2b} \end{bmatrix} \begin{bmatrix} \dot{\gamma}_R \\ \dot{\gamma}_L \end{bmatrix} \tag{2.7}$$

Because the Jacobian matrix of the disk-shaped wheels in Equation (2.7), is not square, the conventional disk-shaped wheels are referred to as degenerate. Thus, in spite of the ability to compute the WMS's body velocity from the wheels rotational

velocities, the inverse kinematic solution can only be computed if the system possess the capability of executing the desired motion.

2.3.3 Dynamic Modelling of differential drive systems

Unlike kinematic models, dynamic formulations relate the acceleration properties of motion, like mass, inertia, force and torque, between different joints and links of a mechanism. Depending on the accuracy of the dynamic formulation, the resulting simulation should be true to the actual behaviour of the modelled system. Although, the stated accuracy may be difficult to reach in actual sense, it is well known, that the accuracy of electrical and mechanical models, employing both kinematic and dynamic formulations, could extend the model's capabilities and improve performance. A kinematic model on its own may only provide acceptable execution of simple tasks at low speed and small loads. However, with the acceleration properties taken into account, the dynamic model may provide satisfactory performance for accurate tasks like pick and place and path following in robotic manipulators and WMSs respectively.

The Newton's laws and the concept of virtual work generally form the basis upon which all dynamic formulations of classical mechanics rely. However, the dynamic laws can be formulated in several other ways. Some of the important formulations include the D'Alembert's principle, the Lagrange's equations and Hamilton equations (Wells, 1967; Miller, 2004). The dynamic equations of motion applying to a wide variety of rigid-body mechanisms are mainly based on the Newtonian and Euler-Lagrange formulations (Hahn, 2003). These dynamic modelling procedures observe a mechanism, consisting of joints and rigid links, as a massless structure upon which forces and torques are exerted. The point of exertion corresponds to the origin of the assigned coordinate frame, and the exerted force and torque interact by disseminating to other points. Both the Newton's and Euler-Lagrange's procedures compute the

mechanism's motion resulting from the applied time dependant forces and torques, relative to the inertial coordinate frame, based on the D'Alembert's principle. Other dynamic methodologies include the Gauss Method (Schiehlen, 1997), Gibbs-Appell Method (Korayem & Shafei, 2009) and Kane Method (Kane et al., 2012; Jazar, 2011).

2.3.3.1 The Newton-Euler formulation

The Newton-Euler formulation treats each link of a multi-body mechanism in turn, utilising the Newton's law and the Euler's equation directly on the links connected by joints kinematic constraints (Dasgupta & Choudhury, 1999). The propagation properties of the forces and torques within the individual links are expressed by kinematic parameters of the link Jacobian matrix, while the propagation between the joints and links are expressed by coupling parameters of dry friction in the joint coupling matrix. Because the inertial and gravitational forces and torques are distributed within the link, they are directly expressed relative to a common frame, normally, the centre of mass coordinate frame; while, the actuator and constraint forces applied at specific points are propagated using the Jacobian matrix and the joint coupling matrix, to the common frame of reference (Muir, 1988). The equations of motion are then computed by summing up, within the common frame of reference, the independently modelled forces and torques that act on the link.

The forces and torques include the actuation, inertial, gravitational and frictional forces. The inertial forces and torques consist of three components: the self inertial, whose elements are proportional to the translational and rotational accelerations; the Coriolis, whose elements are proportional to the square of rotational velocities along similar rotational axes; and the centripetal, whose elements are proportional to the products of rotational velocities along non-similar axes of rotation. The gravitational

force acting on the rigid-body is expressed along the z-axis aligned parallel but opposite the gravitational field while the actuator forces are modelled directly from the driving actuator's dynamics.

2.3.3.2 The Euler-Lagrange dynamics

The Lagrangian formalism on the other hand offers a general point of view of a rigid-body mechanism. It reduces the formulation of system dynamics to a procedure that assumes identical steps without regards to the number of links and system constraints, and the assigned type and motion of the coordinate frames. Besides, the formalism allows a wide variety of coordinate frames to be used, and automatically eliminates system constraints from the equations of motion that result directly from the generalised coordinates (Wells, 1967)

The Euler-Lagrange's approach is centred on the definition of energy functions in terms of the generalised variables of a suitable coordinate frame. The energy functions include scaler quantities like kinetic energy, potential energy and virtual work. However, for most systems the Lagrangian function, $\mathcal{L}$, from which the equations of motion automatically results is simply considered as the difference between kinetic energy, T, and potential energy, U. The Euler-Lagrange's method thus necessitates the assignment of body-fixed and inertial coordinate frames, to represent both T and U in the recommended forms, $T = T\left(q_i, \dot{q}_i, t\right)$ and $U = U\left(q_i, t\right)$. The n coordinates $q_{i,j}\big|_{i=1\cdots n}$, in the generalised coordinate vector $\mathbf{q} = [q_1 \cdots q_n]^T$, describe the configuration or position of the system in an n dimension configuration space, while $(q_i, \dot{q}_i, t)$ specifies the state of the system. The kinetic energy T assumes the form of Equation (2.8), where $\bar{\mathbf{M}}(q_i)$ satisfies $\bar{\mathbf{M}}(q_i)^T > 0$, such that $\bar{\mathbf{M}}(q_i) \in \mathcal{R}^{n\times n}$ is the generalised inertia matrix.

$$T = \frac{1}{2}\dot{\mathbf{q}}\bar{\mathbf{M}}(q_i)\dot{\mathbf{q}} \tag{2.8}$$

Given a set of initial conditions, the Lagrangian function $\mathcal{L}$, is employed in the formulation in Equation (2.9) to ascertain the unique solution of the n second-order differential equations of motion; where $\mathbf{A}(q_i)^T$ is the transpose of matrix $\mathbf{A}(q_i)$ associated with the system's constraints, m is the number of non-holonomic constraints, $\boldsymbol{\lambda}$ is a vector of the Lagrange multipliers, and Q_i are the external forces aiding or resisting the motion.

$$\frac{d}{dt}\left(\frac{\partial \mathcal{L}}{\partial \dot{q}_i}\right) - \left(\frac{\partial \mathcal{L}}{\partial q_i}\right) - \sum_{j=1}^{m} \mathbf{A}_{ij}(q_i)^T \lambda_j = \mathbf{Q}_i \tag{2.9}$$

2.3.3.3 Newton-Euler versus Euler-Lagrange

A number of researchers believe that the Newton-Euler procedure possess important advantages that makes it the most suitable method for modelling multi-link and multi-DoFs mechanical structures. One of the advantages is its recursive structure that greatly simplifies the formulation, especially where the links are attached in a convenient way (Hollerbach, 1980). The other advantages include the applicability to closed-chain, lower-pair and higher-pair mechanisms with wide structural characteristics as well as its capability to model expansive physical force and torque phenomena. Besides, its advocates believed that it produces the best algorithm with a customised symbolic code (Khalil & Kleinfinger, 1987). This is regarded as necessary in the investigation of systems with both numerous links and DoFs, because changes in the system's topology only affect the link's indexation, without altering the structure of the algorithm (Chen & Yang, 1998).

On the other hand, the opponents of the Euler-Lagrange procedure consider that the numerical handling of Euler-Lagrange models become more and more expensive with the increasing number of links and internal DoFs compared to the Newton-Euler formulations. The proponents, however, argue that it is also possible to couple the

procedure with a customised symbolic code and compute a model using the Euler-Lagrange formulation in a recursive manner, and that both algorithms are equally efficient and possess equivalent computational time, with proper choice of the Lagrangian formulation (Silver, 1982; Hollerbach, 1980). Besides, the formalism reveals easily the structural properties of the system that are instrumental for controller design, and automatically eliminates the system constraints (Ortega et al., 2013).

The formulation of choice between the Newton-Euler and Euler-Lagrange is therefore an interesting debate. In fact, a clear conclusion as to which is the most superior method is still non-existent (Silver, 1982). The main objective is the formulation speed, the accuracy of the derived model and how well the intended goal is attained. It is therefore presumed that the formulation of choice is a matter of personal preference. It is considered in this study that in the absence of a customised symbolic code, when investigating only one kinematic mechanism, the increasing complexity of the system under consideration coupled with the recursive nature of the Newton-Euler's formulation necessitates extra modelling insight with much bookkeeping, to formulate an accurate model. Besides, the manual elimination of joints constraints in the derivation of closed-chain equations, presents considerable difficulties with the Newton-Euler's method (Kane & Levinson, 1983). The Euler-Lagrange formalism is therefore adopted in this thesis.

In the literature, a general strategy to dynamic formulation of equations of motion of parallel manipulators is proposed by Khalil & Ibrahim (2007), taking the inverse dynamics computational advantage of the Newton-Euler's approach into consideration. Contrary to Kane & Levinson (1983)'s opinion, Dasgupta & Choudhury (1999) believe that the application of Newton-Euler's approach is more economical in the formulation of equations of motion of parallel or hybrid manipulators, than serial manipulators, because it only necessitates the consideration of equilibrium equations of

motion of the individual links that contribute to the systems motion. The problem of dynamic modelling and identification of passenger vehicles using the inverse dynamic model of Newton-Euler formalism is presented in (Venture et al., 2006), while Luh et al. (1980) and Featherstone (1987) presented a fast computational algorithms that solve the forward and inverse torque dynamics of a manipulator based on the Newton-Euler procedure. The algorithm proposed by Luh et al. (1980) entails two recursions based on the joints motion. The first computes the kinematics of the body, while the second utilises the body kinematics to formulate the joint torques by transforming the end-effector forces back to the base. The use of the Newton-Euler's recursive formulation is also proposed by Khalil (2011) to facilitate a faster modelling process with reduced number of operations; while De Luca & Ferrajoli (2009) proposed a modified recursive method to compute the residual vector dynamic expressions, and evaluate a passivity-based trajectory tracking control law. The modified recursive Newton-Euler method of De Luca & Ferrajoli (2009) automatically generates the Coriolis and centrifugal matrices that satisfy the skew-symmetric property.

The use of Newton-Euler method in the modelling of WMSs is also prevalent (Wu et al., 2000; Korayem & Ghariblu, 2003; Kozłowski & Pazderski, 2004). In (Muir, 1988), a kinematic and dynamic methodology for modelling robotic systems with closed-chains, friction, and pulse-width modulation, as well those with higher-pair, non-actuated and non-sensed joints, is identified and developed. The applicability of the kinematic-based and dynamic-based methodologies to WMSs are also demonstrated.

The Euler-Lagrange procedure is also widely used in the computation of equations of motion of robotic manipulators and multi-agent systems (Chen, 2001; Subudhi & Morris, 2002; Mei et al., 2011). Other research articles that utilise the Euler-Lagrange approach in the modelling of flexible links include (Sunada & Dubowsky,

1983; Book, 1984). In the modelling of mobile systems, the procedure has been applied to formulate constrained dynamic equations of motion of wheeled robots and vehicles. In particular, D'Andrea-Novel et al. (1991) considered both Lagrange formulation and differential geometry to derive the model of a three-wheel mobile robot with non-holonomic constraints; while Emam et al. (2007); Onyango et al. (2009a,b, 2011, 2016) considered the formulation to derive the model of a wheelchair with non-holonomic constraints.

2.4 Operator behaviour modelling

The presence of human at the centre of operation of machines and other dynamic systems is the main root and motivation of design ideas in system control. Lately, for the same reason, unmanned systems have began to find application in areas like military aviation and guided transport. However, these systems have not eliminated the remote or physical human assessment performed by the operator, who remains fully responsible for the overall operation. Thus, careful consideration of the operator becomes an important issue in the design and development of dynamic systems. Presently, the consideration is evolving from that of a manual human controller, to a supervisor that monitors the operations. This necessitates the evaluation of physical and mental processes that guide the operator's behaviour in system control. One area that clearly necessitates a careful consideration of the human-in-control is the automotive transport where numerous operating conditions and human behaviours are involved. A specific example in this area is the automatic gearbox system found in particular vehicles, which dynamically adapts to the drivers' different driving behaviours. Although quite elemental from the cognitive point of view, these in-vehicle systems are generally essential in vehicle control. Additionally, a driver behaviour

model could be useful in the regulation of transport safety, if considered when setting-out the rules and standards to govern vehicle control and traffic management.

2.4.1 Existing driver behaviour models

The history of driver behaviour modelling is long-standing with a great variety of models that tackle different aspects of the driving task. However, most of the available driver models pertain particularly to motor-vehicles, and very few target the behavioural aspects of a wheelchair driver on the steering task. The analysis and formulation of the driving task necessitates consideration of dynamic interactions that occur between the driver, the vehicle and the environment, because every state of the vehicle can be linked to these interactions. However, some driver specific factors like disposition and experience, that provide significant contributory influence in the driving behaviour, may also need be taken into account. Michon (1985) classifies the driver models as either taxonomic models, consisting of those that do not take into consideration the interaction between the model's components, or functional models, that accounts for the interaction. Differently, Plöchl & Edelmann (2007) consider the classification in terms of the model's application, but observe that the driver models can also be classified as either descriptive, i.e. those that provide descriptions, classifications and schemes; or mathematical, i.e. those that utilise the identification, control, fuzzy logic, stochastic, neural networks theories and hybrid approaches.

It is agreeable because of the numerous classifications, that most of the available models will overlap the classes. This implies that unique driver model may not exist, but those customised to satisfy certain specific demands of the driver. Scores of driver model are therefore available in the literature within these and (probably) more classifications. This section surveys the available driver behaviour models according to the following classification (Engström & Hollnagel, 2007).

2.4.1.1 The control theoretic models

These models consider driving as a control task that focuses on minimising the error between the actual and the target state, using the feedback and feedforward control theories. The control theoretic driver models concentrate on the vehicle to establish that a defined trajectory is followed at a defined speed. Although very useful in lateral and longitudinal control in defined environments (MacAdam, 2003; Guo et al., 2004), these models rarely capture the higher level driving aspects in decision making like learned patterns. One of the earliest driver model expressed in Equation (2.10) was presented by Kondo & Ajimine (1968) based on a two wheeled vehicle that runs at a constant speed along a straight line with side wind disturbances.

$$\triangle\, y_p(t) \approx y(t) + L\psi(t) = y(t) + T_p V \psi(t) \approx y(t + T_p) \tag{2.10}$$

The model attempts to diminish the lateral predicted deviation $\triangle y_p$ at some distance

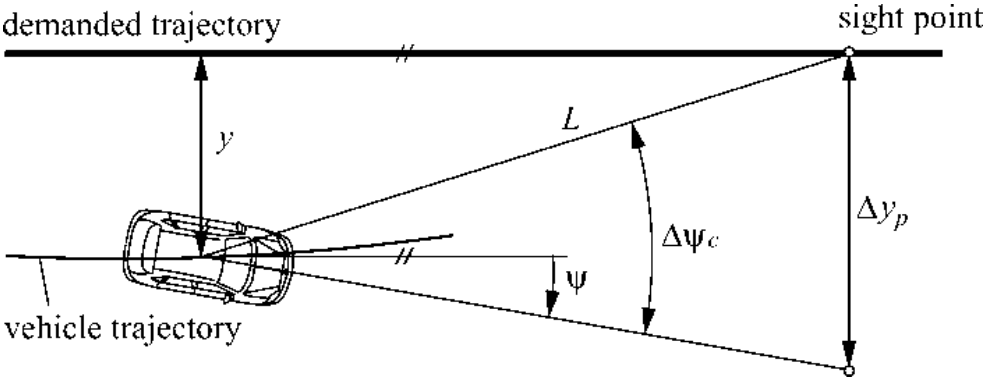

FIGURE 2.2: A pictorial description of the driver model presented by Kondo & Ajimine (1968)

L ahead of the vehicle according to Figure 2.2. In Equation (2.10), T_p is the preview time given by L/V, where V is the speed of the vehicle, while $\psi(t)$ is the yaw angle and $y(t)$ is deviation. Until recently, several improvements have been made on this model to consider the visual angle between the longitudinal axis and the sight point

$\triangle\psi_c$, and to provide compensation on the lateral deviation $\triangle y$, with regards to a reference position, yaw angle error $\triangle\psi$, and local roadway curvature ρ_r, (Allen et al., 1987; Mitschke, 1993; Apel & Mitschke, 1997; McRuer et al., 1977).

The Donges (1978)'s two level driver steering behaviour model has also received significant attention in this category. The model consist of a guidance level, that entails perception and response in the anticipatory open-loop control mode, by optimising a quadratic criterion that uses the angle of the steering wheel and a desired path curvature. The second stabilisation level provides compensations towards the occurring deviations in a closed-loop mode. An extension of the model is proposed by Plochl & Lugner (2000) who introduced a third level to account for local deviations. A further improvement on the Donges (1978)'s model can be found in (Edelmann et al., 2007).

2.4.1.2 The information processing models

Information processing models attempt to represent human cognition including perception, decision making and response selection, as a logical sequence of computational steps. These models have made great influence in the understanding of multiple task sharing, where different components of the driving task interact to accomplish the global driving task. An example of the information processing model is the concept of mental work-load intoduced by de Waard (1996). Other information processing models entail the dual task studies performed to evaluate the extent of interference between the tasks (Wickens, 2002). It has not been possible, however, to incorporate the information processing models into a more general driver behaviour model (Salvucci, 2001). According to Engström & Hollnagel (2007), the information processing models of driver behaviour consider human beings as passive receivers of information, making it hard to account for the drivers' capability in the active traffic situations management like self-pacing.

2.4.1.3 The motivational models

Motivational models attempt to formulate the risk regulating behaviour of the driver in dynamic situations. Unlike the information processing models, the motivational models emphasise the drivers' self-paced driving nature in the endeavour to understand their dynamical adaptation to varying driving conditions. Motivational models mainly differ in the criteria suggested to regulate the adaptation. While some may utilise qualitative criteria like task difficulty or risk level, the quantitative models that regard the subjectively chosen safety margin may also be considered in this category. Concerning the adaptation regulation criteria, the Wilde (1982)'s theory of risk-homoeostasis, for instance, presumes that drivers aim to stay within a constant range of accepted risk, while the Summala (1988)'s theory of zero-risk supposes that the drivers attempt to keep the perceived subjective risk at zero-level. In a similar perspective, Fuller (2005), considers task difficulty rather than risk range, as the primary factor that influence the drivers' adaptation. Ordinarily, motivational models have been reprimanded for being too general with respect to the internal mechanisms, to an extent that it is extremely difficult to produce testable suppositions. The artificial neural network methodology has been considered quite often in the realisation of motivational models because it emulates the adaptive behaviour of human in system control, and can be used to represent the interactions of the model's internal mechanisms. In the literature, Kraiss & Kuttelwesch (1991) examined the possibility of using the neural network approach to model a driving support system to assist in the overtaking task. The model's decision parameters that include the vehicle's speed and distance to collision, are used to select the appropriate angle of the steering wheel and position of the accelerator or brake pedal. The authors experimentally show that human driving can be identified from the relationship between inputs and outputs of the trained network. In (MacAdam et al., 1998), the use of neural networks to

examine the headway driving data obtained during normal highway driving, and to represent the longitudinal control behaviour is demonstrated. The article considers pattern recognition methods in the identification of headway keeping behaviours and relative distribution displayed by participant drivers. Human factors and accident causation relationships are investigated in (Kageyama & Owada, 1996) and extended in (Kuriyagawa et al., 2002) to represent the age and experience effects. The use of genetic algorithms to represent the emergency situations encountered during driving is also considered by Nagai et al. (1997).

The application of system identification using steering data is also considerably common. Pilutti & Galip Ulsoy (1999) used a back-box model with autoregressive exogenous structure (ARX), to identify the driver model's parameters, while Chen & Ulsoy (2001) proposed the same formulation for both driver model and driver model uncertainties, using the actual driving data from a fixed-base driving simulator. The Chen & Ulsoy (2001)'s model employed the auto-regression moving average with exogenous inputs (ARMAX) to improve on accuracy, based on the consideration that ARMAX can yield residuals closer to white noise with fewer parameters given the same model order. The system identification approach is also considered by Diehm et al. (2013). The authors, however, do not take into account exogenous inputs in their affine autoregressive system, but instead derive a multi-step model output error criterion, and present an algorithm to identify the parameters of the subsystem using measurable motion data. Although, the consideration of black-box method of system identification is straight forward and common with availability of data, it is believed in this thesis that it is possible to find sufficient information to relate the driver's actions to the perceivable contextual environment.

2.4.1.4 Hierarchical models

Hierarchical models constitute the formulation approaches where sub-tasks are arranged in the order of rank. A popular example is Michon (1985)'s hierarchical representation, in which the entire driving task is subdivided into three hierarchically coupled and ordered levels of demand consisting of strategic, tactical and control level, with each demand level encompassing the driver, the vehicle and the environment. At the strategic level, the global goal is perceived and a general plan of the journey is established. The driver for instance considers the available routes and evaluates the resulting costs. Although the involvement of the strategic level in the actual steering control is limited, it helps in making decisions regarding the lower levels of demand and the amount of risk the user is willing to tolerate. At the tactical level, safety is the primary consideration. The driver continuously adjusts the instantaneous goal and driving speed in order to avoid the prevailing risk conditions. The driver's knowledge regarding both the vehicle and the environment plays a very important role at this level in solving the problems at hand. Finally, the fine controls and instantaneous decisions, including user preference, are executed at the control level with little conscious effort in view of stabilisation. The other well known hierarchical model is the Rasmussen (1986)'s model that divides the operative behaviour of the driving performance into three levels: knowledge based, rule based and skill based behaviours. The driver applies the knowledge based behaviours in less familiar and difficult environments, while the rule based behaviours that pertains to the implementation of learned rule, apply when interacting with other drivers. Lastly, the skill based behaviours relate to the automatic operation performed in accustomed situations, without conscious cognitive processing. Hierarchical models provide detailed description of the dynamical processes between the different levels, however, they commonly fail to express the actual execution of these interactions.

A hierarchical driver model of two lane highway traffic that takes into consideration the Michon (1985)'s decision levels is outlined with control sub-systems in (Cheng & Fujioka, 1997), and a similar consideration is proposed by Song et al. (2000) to take the human drivers' overtaking and car following behaviours into consideration.

2.4.2 Driver behaviour models for path and speed planning

The majority of the driver models require a desired path or speed to track. In most cases, these are specified directly. However in certain cases, the path generation task may be constituted theoretically as a separate component of the driver model, or independently formulated as the driver model. Numerous proposals, regarding path generation, have been made that utilise variables like time, acceleration, velocity, lateral position, rpm e.t.c, as the optimisation principles that represent the drivers' intuitive preferences (Prokop, 2001). For instance, a driver model that predicts the reference path when negotiating a bend is proposed by Lauffenburger et al. (2003), using lines and polar curves to describe the reference trajectory, by taking the road and driver's profile as well as vehicle characteristics into consideration. In the improved model (Lauffenburger et al., 2005), the authors propose a variable curve negotiating speed that depends on the tolerated lateral acceleration and the instantaneous curvature of the generated trajectory. Kageyama & Pacejka (1992) also consider mental influence as part of the environmental risks aiding the driver's directional decision. Kageyama & Pacejka (1992)'s model regards the driver's risk feeling from the forward view as an important information for course decisions, and presumes that drivers generally prefer courses with minimal risk levels. The formulation uses exponential functions to describe the risk levels based on fuzzy logics. An adaptive lateral preview model of the driver is also proposed in (Ungoren & Peng, 2005). The model, based on the adaptive predictive control framework, uses preview information, weight adjustments

and internal model identification, to simulate various driving styles and determine the optimal steering action of the driver. In (Eboli et al., 2016) the use of speed and acceleration is considered to determine the drivers behaviour.

One of the recent formulations presented to maximise the safety and mobility in a connected vehicle environment is the variable speed limit (VSL) control algorithms in Equation (2.11) proposed by Khondaker & Kattan (2015), where the variables $X_i(t)$, $V_i(t)$ and $a_i(t)$ represent the longitudinal position, speed and acceleration at time t of the i^{th} vehicle in the network, and T_m is the simulation time step size in seconds.

$$\begin{aligned} V_i(t+1) &= V_i(t) + a_i(t)T_m \\ X_i(t+1) &= X_i(t) + V_i(t)T_m + \frac{1}{2}a_i(t)T_m^2 \end{aligned} \tag{2.11}$$

The driver's acceleration and deceleration behaviours adopted from the intelligent driver model (IDM) (Treiber et al., 2000) are utilised to investigate the control algorithm based on the model predictive control methodology. The model also uses a changeover algorithm (from free-flow to car-following, and vice versa) and the traffic flow prediction model to optimise and calculate the total travel time, time to collision to measure the instantaneous safety, and fuel consumption to compute the environmental impact. Other on-road motion and path planning models may be found in the review articles (Katrakazas et al., 2015; Plöchl & Edelmann, 2007) and in (Xiu & Chen, 2010; Pauwelussen, 2015; Wang et al., 2014; Guo et al., 2013; Bornard et al., 2016; Seppelt & Lee, 2015).

2.4.3 The context around the use of wheelchairs

A wheelchair that provides the most beneficial service may be determined based on the available mobility needs and the ways in which it satisfies or used to satisfy the

user's needs. These normally take into consideration the probable usage duration and the environment in which the wheelchair is anticipated to be used. The environment plays an important design role in dictating the needed physical and control parameters like foldability, size and manoeuvrability. Pathological factors such as impaired mobility, user recovery and cognitive function, as well as socio-demographic factor like the need to upgrade and the extent of involvement of the user in the in the procurement/design process constitute the circumstances that contribute to the variability in the use of wheelchairs over time. Taking the user's perspective into consideration by predicting the potential short-term or long-term mobility needs of the user may be helpful to supplement wheelchair appreciation and minimise cases of abandonment. The desired optimal purpose of the wheelchair may thus be a function of the interface between the driver and his environment, or where assistive technology is involved, between the driver, the wheelchair and the environment. A steering behaviour model that takes into consideration the driver's and the driving context is not only important in supplementing wheelchair appreciation but also necessary in the design to ensure easier control.

2.4.4 Existing wheelchair driver and steering models

Extensive information regarding the modelling and control of powered wheelchairs exists, however, studies that takes into consideration the driver's behaviour for assistance and rehabilitation are still limited. In fact, apart from (Emam et al., 2010; Hüntemann et al., 2008; Demeester et al., 2006, 2003a; Vanacker et al., 2006; Onyango et al., 2015), more behaviour model related to wheelchair drivers could not be located. Studies in the vast area of behaviour modelling have been approached mainly from the field of automotives, aviation simulators and robotic intelligence (Cacciabue & Carsten, 2010; Boril et al., 2012). Majority of the wheelchair driver models available

in the literature are concerned with detecting the intended direction of travel rather than adaptating the wheelchair to the driver's steering behaviour. The common examples include the intelligent decision making agents by Yong Tao et al. (2009) and Taha et al. (2008) for driver intention detection in uncertain local environments based on partially observable Markov decision process (POMDP); and by Taha et al. (2007) for global intention recognition for autonomous wheelchair navigation. A multi-hypothesis approach that predicts the driver's intention and provides collaborative control, by adjusting the steering signal to avoid the observable risks during navigation is also considered in (Carlson & Demiris, 2008, 2012). The use of Bayesian networks to recognise wheelchair driver's intention and estimate the uncertainty on the driver's intent is also common (Demeester et al., 2006; Hüntemann et al., 2008; Vanhooydonck et al., 2010; Demeester et al., 2003b). The proposed Bayesian network approaches formulate the driver's intended direction of travel on-line during navigation and takes into consideration the involved uncertainty. However, they are computationally intensive, and rarely incorporate the adaptable driver's steering preferences.

Besides the intention detection models, Vanacker et al. (2006) consider a filtering approach that presumes an experienced reference driver to eliminate the driver's handicap, while Parikh et al. (2004, 2007); Qinan Li et al. (2011); Urdiales et al. (2013); Levine et al. (1999); Montesano et al. (2010) propose task oriented models that generate autonomous behaviours at different levels. The task oriented models allocate the driver more or less control depending on the contextual need at one extreme level, and enable the wheelchair to perform autonomous tasks without the driver's input at another extreme level. However, the resulting behaviour in both autonomous and semi-autonomous do not account for the driver's steering preferences.

A reactive steering behaviour model, usable in wheelchair adaptation, is proposed

by Emam et al. (2010). The model is derived in terms of two force components: the driving force component, $\mathbf{F}_d$, and the environmental or obstacle component, $\mathbf{F}_k$, expressed in Equation (2.12) and (2.13) respectively. The model is however non-linear and does not represent in a simple way the directed influence of risks. In addition, it is not tested on steering data.

$$\mathbf{F}_d = \frac{K}{\tau_r}\left[V_{\max}\left(1 - \frac{\mathrm{X_{saf}}}{\mathrm{X_{obst}}}\right)\bar{\mathbf{e}} - \nu_{\mathrm{act}}\right] \tag{2.12}$$

$$\mathbf{F}_k = k_o \exp\left(-\frac{\mathrm{X_{obst}}}{B}\right)\bar{\mathbf{e}}_o \, D_v \tag{2.13}$$

In the equations; K is the weight constant, τ_r is the driver's relaxation or reaction time, $V_{\max}$ is the maximum limit of the wheelchair's speed, $\mathrm{X_{saf}}$ is the safe distance, $\bar{\mathbf{e}}$ is a unit vector in the direction of motion and $\mathrm{X_{obst}}$ is the actual wheelchair distance from the obstacle. Additionally, B is a constant that represents the range of the repulsive force, $\bar{\mathbf{e}}_o$ is a unit vector in the direction of the moving obstacle while D_v is the directivity factor.

2.5 System control with human-in-the-loop

System control entails management of a plant's behaviour using a device or a collection of devices under some intelligent directions. This may involve making decision based not only on the knowledge of the plant's dynamical capability, but also the operator and the operational environment. As used in this context, the device may take the human, the human-machine or purely the machine form. Previous research in this domain derives from the interaction of humans with stationary and mobile robots, i.e. proximate and remote interactions respectively, during teleoperation or supervisory controls. The control of a dynamical system with a human-in-the-loop

has been referred to as mixed-initiative interaction or shared control by some researchers, because the human-in-the-loop and the (classical) controller act on the same dynamical system (Goodrich & Schultz, 2007). Some of the studies that have considered the human-in-the-loop control to reduce cognitive burden on the operator include (Chrpa et al., 2015; Stanciu & Oh, 2007).

2.5.1 Shared control in general applications

Human-machine interactions exist inherently in all machines designed to provide human beings with services. In the literature, the factors that affect the interaction between human and machines have been suggested based on different levels of autonomy (Sheridan & Verplank, 1978; Riley, 1989; Parasuraman et al., 2000; Goodrich & Schultz, 2007). For example, the continuum level of autonomy (LOA) scale, suggested by Goodrich & Schultz (2007), supposes that the interaction between human and machines ranges between teleoperation; where direct human control is involved, and dynamic autonomy; where peer-to-peer collaboration is effected. However, other studies have regarded human-machine interactions based on machine (or human) learning, training, and adaptation to human (or machine) behaviour. An example is the conceptual framework presented by Hoc (2010) from a cognitive point of view, to study the cooperation between humans and machines in highly dynamic applications. Evaluating the interaction between human and machines to design technologies that produce desirable behaviours, therefore, becomes an essential component in the development of systems that intend to incorporate supportive controls.

The majority of the studies related to shared control have regarded user interfaces, human interventions at planning levels, and work flow models, to enhance the interaction at the supervisory side of the LOA scale (Murphy, 2004; Tzafestas & Tzafestas, 2001; Morris et al., 2003; Bruemmer et al., 2005). Others on the other hand, have

suggested various discrete levels of autonomy that include teleoperative, safe, shared and autonomous modes with manual switch (Mano et al., 2009; Bruemmer et al., 2005). In (Beard, 2005), for instance, the system's static and dynamic safe regions are defined using control Lyapunov functions according to the proposed attractive and repulsive behaviours. The human inputs are used to control the system only within a safe partitioned region. However, outside the specified region, the user inputs are snapped to the closest applying control input. This architecture employs a behaviour based strategy that ensures smooth transition as well as flexibility and stability. A similar approach with certain autopilot modes, is considered by Matni (2008) to broaden reachability abstractions of shared control in the pilot-autopilot interaction during the landing of an aircraft. For further reference, the available technologies supporting shared and cooperative control may be referred in (Krüger et al., 2009).

A human-in-the-loop control architecture where a modelled operator is integrated in the control loop is presented by Feng et al. (2016). The responsibility of the human-in-the-loop is to account for the human imperfections and machine uncertainties that arise during interactions. One example is the approach employed in (Corno et al., 2015) using a second order sliding mode controller to design a bicycle control system that helps cyclists to regulate their heart rates, and maintain a desired constant effort throughout the entire trip. The approach involves modelling the cyclist, the bicycle and heart rate dynamics, identification of the models and validation of the control system using experimental data.

A notable challenge with the human-in-the-loop control architecture concerns the choice and realisation of the human operator's decision levels. Several artificial intelligence, probabilistic and possiblistic tools have been considered in formulation of operator behaviour. In (Berg-Yuen et al., 2012) for instance, the authors model

the operator as a Markov decision process (MDP), and formulate a receding horizon control problem to assist in the determination of an optimal control sequence over a finite horizon, based on probability ratio test (SPRT) estimation. Feng et al. (2016) also used the MDP in the operator modelling to enable synthesis of control protocols for autonomous systems. A partially observable Markov decision process (POMDP) has been considered by Lam & Sastry (2014) to manage feedbacks during the interactions between human and machines, while the use of the neural networks in the implementation of human-in-the-loop controls is considered by (Zhang & Nakamura, 2006; Looney & Tacker, 1990). Similarly, the application of fuzzy logic and regression tree methodologies in the formulation of implicit frameworks for human-machine interaction that are sensitive to human anxiety is also observed (Rani et al., 2007).

The use of classical control approaches are not very popular. One of the few available examples, is the Lee & Lee (1992)'s design methodology. The authors modelled and incorporated both human dynamics and force feedback into the control loop, and used a PID controller to realise a shared teleoperator control, also, Gabay & Merhav (1977) presented an identification method that establishes the parameters, time delay and order of an on-line parametric model of the human operator in a closed-loop tracking task.

2.5.2 Application in motor-vehicle and wheelchair control

The notable areas of application of the shared control research in motor-vehicle include lane-keeping, car-following and roadway departure avoidance. Although the fundamental objective in these areas is supportive control, the shared control in motor-vehicle applications is also aimed at ensuring that the application is not only usable to skilful drivers, but also to the inexperienced and novice. In (Enache et al., 2010), a practical realisation of a lane departure avoidance system is presented. The

steering assistance system, formalised as an input-output hybrid automation, controls the driver's interaction only when the steering column torque is insufficient and the vehicle is at risk of departing from the driving lane. Gray et al. (2013) combine threat, stability assessment and control of a passenger vehicle into an optimisation problem using a non-linear model predictive control (MPC), and estimates of the observed nominal behaviour of the driver. The use of probability weighted ARX model in the formulation and identification of driver behaviour is considered in (Okuda et al., 2014) to assist in the corporative cruising of multiple cars. The presented methodology, as depicted in Figure 2.3, involves the identification of each driver's highway car-following skills using MPC to account for the drivers individual driving differences. It is observed that the conventional driver assistance systems are more conservative, focusing, solely, on the average driver. As a result, the logical consequence of the resulting behaviour could be unpredictable and may lead to a non-desired outcome if a series of cars with such assistive systems exist in the same traffic. In consequence, the authors adopt a personalised and cooperative driver assistance system.

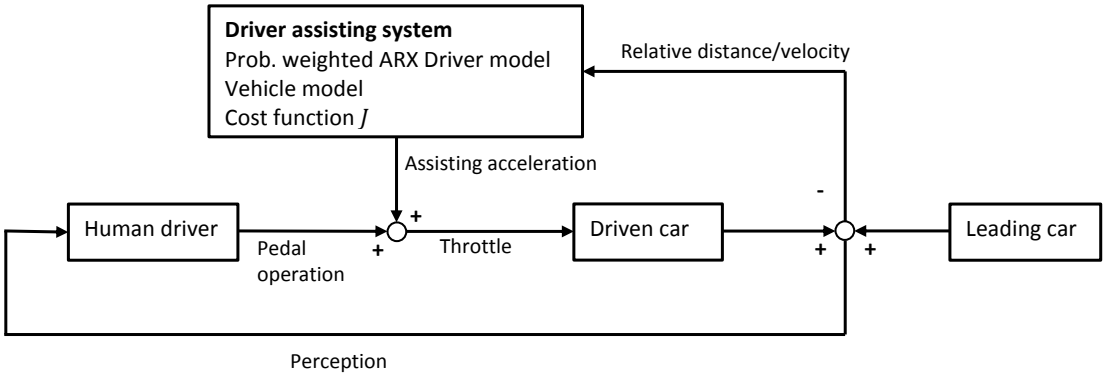

FIGURE 2.3: Okuda et al. (2014)'s predictive driver assisting system in a single car

Ideally, the known and structured motor-vehicle's operational environment, consisting of distinct driving lane, overtaking rules and speed limits rarely exist for the wheelchair. Thus, the numerous collaborative as well as the available shared control systems for motor-vehicles may not make sense in wheelchair control. The literature of smart wheelchairs, with wheelchair accustomed autonomous and semi-autonomous systems is, however, vast. For a detailed review, a survey of the older smart wheelchair may be referred in (Simpson, 2005), while some of the recent smart wheelchairs developments with anti-collision features and way-finding modules can be found in (How et al., 2013; Viswanathan et al., 2011; Wang et al., 2011).

Wheelchair systems with collaborative or shared control are presented in (Zeng et al., 2008, 2009). The collaborative system consist of a graphical user interface, where the user selects a preferred path and destination, and controls the speed as the intelligent system guides the wheelchair along the software guide-paths. The system also provides an intuitive path editor that allows the user to modify the guide paths and avoid obstacles at will. Besides, an elastic path controller that seeks to maintain the original path is unified with a proportional and derivative controller to enable the wheelchair return to the original path in the absence of the user's conscious effort after a guide path modification. Yu et al. (2003) presented a bi-level control system that provides a natural user interface for a personal mobility aid system with an admittance-based controller at the first level, and a shared adaptive controller based on the user's metric performance at the second level in order to allocates control between the user and computer.

A shared control strategy based on a reactive algorithm is implemented by Urdiales et al. (2010) to enable constant cooperative adaptation between the wheelchair and the driver. The control strategy entails evaluating and weighing the driver's and wheelchair's local performance to generate, in a reactive way, a combined signal that

represents the most efficient response to a situation. The system consists of a three layer control strategy, where at the lowest level, the safeguard layer remains 'always active' to prevents imminent collisions by stopping the wheelchair in a dangerous situation. The middle reactive layer, where the shared control is implemented, is based on the Khatib (1985)'s potential fields approach. It formulates the goals as attractors and obstacles as repellers in order to create a vector field that drives the wheelchair towards the intended destination, with emphasis on the steering safety, smoothness and directness. This layer employs two behaviours to avoid the traditional potential field problems when doors or walls are detected. The topmost deliberative layer that is meant for users with cognitive impairments plans a safe path to the destination and decomposes the generated path into a series of way-points. The driver and wheelchair signals are merged to a shared velocity $\nu_{_S}$ based on a weighting criteria that takes into consideration the current and the recent past user $\nu_{_H}$, and wheelchair $\nu_{_R}$, velocity efficiencies according to Equation (2.14).

$$\nu_{_S} = (1 - k_{_H}) \cdot \eta_{_R} \cdot \nu_{_R} + k_{_H} \cdot \eta_{_H} \cdot \nu_{_H} \tag{2.14}$$

where $\eta_{_R}$ and $\eta_{_H}$ are the wheelchairs and the users efficiencies respectively, while $k_{_H}$ (considered as equal to 0.5) is a factor that may be used to allow global increase/decrease of the user's contribution in case of the caretaker's advise. The efficiency η is calculated as an average of the smoothness η_{sm}, directness η_{dir} and safety η_{sf} efficiencies. In their subsequent study (Peinado et al., 2011), the authors considered estimating the efficiencies by predicting the performance based on similar driving situations from the driving database of the previous users.

A shared control architecture is also implemented by Carlson & Demiris (2012), where the system attempts to recognise the intended direction of the user based on the angular direction of the joystick. The architecture involves an autonomous controller

that executes an ordinary obstacle avoidance algorithm in the determination of a safe path to the intended goal. The user's signals are incorporated with the autonomous controller's signal if enough confidence exist that the user is seeking the pointed sub-goal. Similarly, the Shared Control by Qinan Li et al. (2011) combines the user's joystick signals with the reactive controller's signals to enhance safety and comfort according to Figure 2.4. For further information, other articles that implement the

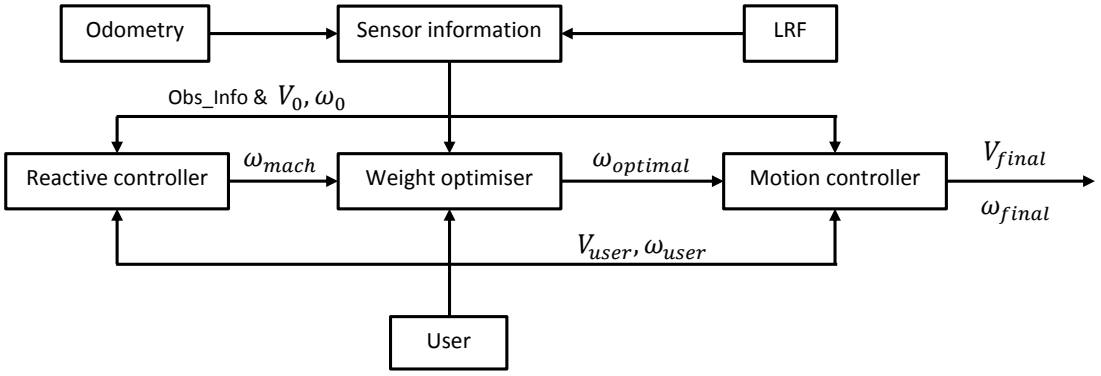

FIGURE 2.4: The Qinan Li et al. (2011)'s architecture of the dynamic shared control

shared control architectures in wheelchair systems include (Mitchell et al., 2014)

2.5.3 Control theoretical tools

It is generally difficult to single-out a specific control theoretical tool that works better than others. In fact, the choice of a model-based control tool is often derived from the nature of the system's dynamics or structure of the available model. A brief discussion of the previous studies regarding the theoretical as well as analytical tools employed to implement the control of wheelchair with human-in-the-loop is presented. The methods consist of the input-output feedback linearisation considered in the closed-loop system implementation, and the non-linear continuous time GPC whose

performance index is used to ascertain the optimality of the resulting minimum-phase closed-loop system.

2.5.3.1 Model predictive control

Model predictive control (MPC), that is also referred to as receding horizon control (RHC) has been applied quite often in the control of industrial processes, especially where the plant's dynamics are complex and hard to formulate. The advantages of the MPC method that plays a significant role in the realisation of control with human-in-the-loop include the ability to impose constraints, like saturation limits, on the inputs and system states. Besides, MPC computes optimal solutions of the control problem by taking the input constraints and the system's measured states into consideration at each time instant. One of the earliest considerations of the MPC method, is the application by MacAdam (1980) in driver steering, to predict finite successive points of the future path and generate the appropriate steering command. Succeeding studies have demonstrated that varying the parameters like preview time and weights of the cost function can be utilised in the realisation of various control behaviours. As a result, the MPC or RHC method has been used widely in the formulation of control behavious with human-in-the-loop (Ungoren & Peng, 2005; Treiber et al., 2000; Gray et al., 2013; Okuda et al., 2014). A review of the MPC literature, focusing majorly on the control formulation as well as stability and optimality conditions of constrained linear and nonlinear systems is presented by Mayne et al. (2000). The authors use Lyapunov theory to prove the stability techniques that involve terminal constraints and special terminal cost. The use of MPC is also considered in by Prokop (2001) to relate the perception, preferences and experience of the driver in various traffic situations. The study considers a minimisation cost function that involves various goals and driving styles to represent the driver's accelerating, decelerating and steering

behaviours. The authors considered as fundamental, the idea that human beings use their expert knowledge and sensory perception to predict the future behaviour of a system over the next few seconds. The modelled behaviours of the driver include the minimisation of lateral and longitudinal acceleration, the driver's braking effort, path following errors as well as forward velocity changes. The use of PID control loops is also considered to realise both feedback and feedforward control in the driver model. Keen & Cole (2012) proposes a linear MPC based steering controller using a formal system identification procedure, with the lane change steering data from 14 drivers of an instrumented test vehicle, to reduce the steering angle prediction error. The procedure emphasises the avoidance of identification bias, resulting from the operation of the closed-loop driver-vehicle system. Other applications of the MPC based control include Van-Overloop et al. (2015); Kleinman & Perkins (1974); McRuer & Krendel (1962).

The use of MPC however contrasts the classical optimal control methods, whose feedback laws rely on the accurate model of the system's dynamics. In addition, considerably complex on-line and off-line computations may be required where predictive control of a non-linear model is involved. The latter can exclude practical implementation of the controller where higher bandwidth control is necessitated, yet the processor power is limited. The computational burden could be avoided by reducing the non-linear problem into a linear set. This may involve breaking down the operating space into various regions with linear behaviour that can be solved by different independent linear controllers. See (Murray-Smith & Johansen, 1997; Ge & Song, 2008; Costa et al., 2014). The issue of state space decomposition and switching different controller is particularly critical where system disturbances are involved. However a simpler non-linear continuous-time GPC that regards the local model approach and involves successive linearisation based on the current position of

the system in the operating space as defined by the states and inputs is considered (Demirciolu & Gawthrop, 1991; Johansen et al., 1998; Siller-Alcalá, 1998).

2.5.3.2 Feedback linearisation

The classical feedback linearisation method that necessitates an accurate model of the system's dynamics is also considered in the closed-loop model, to track the user inputs by torque compensation (Jaulin, 2015). Feedback linearisation can either be input-state or full-state. The input-state feedback completely linearises the input-state non-linearities after coordinate transformation and static state feedback. A linear controller can then be chosen and used to control the linearised system. The use of input-state feedback linearisation is however restricted by the fact that the exact linearising compensators can sometimes be difficult to design. Besides, a wide range of systems exist whose non-linearities cannot be entirely compensated, thus limiting the application of the linearisation procedure. As a result, several reality systems may fall outside the input-state feedback linearisable category.

For such systems, the input-output feedback linearisation procedure can be considered. The procedure linearises the entire system dynamics between the input and the output. However, the state equation may only be partly linearised (Isidori, 1995, 1999). Some non-linear residual dynamics, referred to as internal or zero dynamic, may result from the input-output transformation. These dynamics are not dependant on the inputs of the system, and are therefore not controllable. In fact, the main challenge with the input-output feedback linearisation is realised when the internal dynamics cannot stabilise. A system is referred to as non-minimum phase system when this is the case. See examples (Sun et al., 2016; Fiorentini & Serrani, 2012). A non-minimum phase system can be controlled by neglecting the internal dynamics in a way that the resulting system is input-state linearisable (Sun et al., 2016), or

the internal dynamics may be stabilised concurrently with the system's input-output behaviour (Yang et al., 2012; Serrani, 2013). The non-minimum phase condition is, however, disregarded because the selected outputs of the closed-loop wheelchair model in this thesis produces no zero dynamics. The structural procedure of feedback linearisation control may be represented as in Figure 2.5.

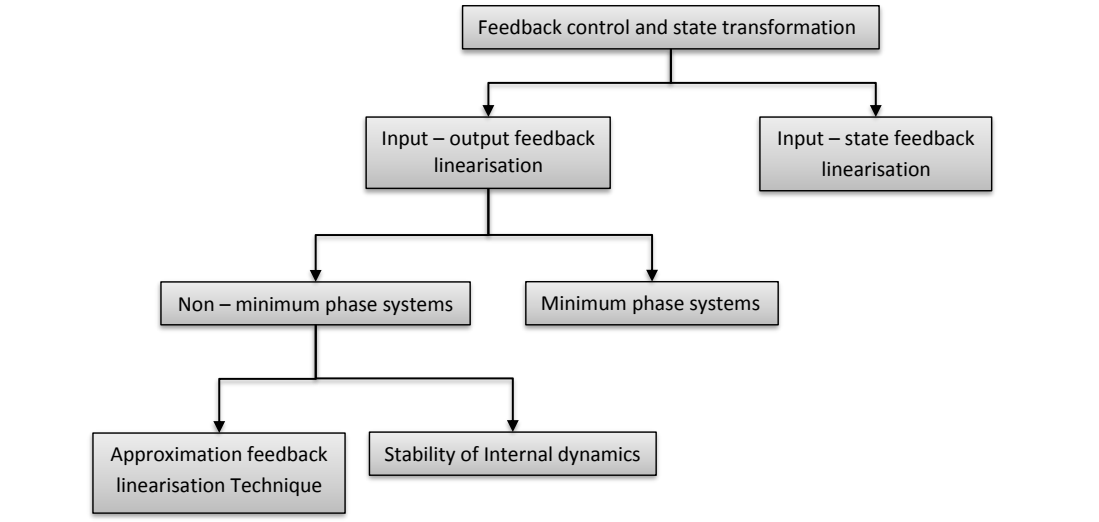

FIGURE 2.5: The structural procedure of feedback control

Notwithstanding the considered control theoretical tool, a significant need for proper operation of the system regards the coordination between the machine and the human operator. To accomplish a desired trajectory tracking, the operator should be capable of effective manipulation of the system's motion, irrespective of topology, dynamic or kinematic characteristics of the system. The control of wheelchair with human-in-the-loop is therefore emphasised to accomplish the assistive mobility objective, by adapting the wheelchair to the driver's behaviour.

2.6 Feedback linearisation procedure

The input-output feedback linearisation procedure results in a system with a global linear relationship between the input and output variables. The procedure achieves exact linearisation by inverting the system dynamics through a non-linear coordinate change and application of a feedback law. Suppose the standard state-space representation of a MIMO non-linear system expressed in Equation (2.15) is considered, the following input-output feedback linearisation steps can be used to achieve a linearised system

$$\begin{aligned} \dot{\boldsymbol{\chi}} &= \mathbf{f}(\chi_i) + \mathbf{g}(\chi_i)\mathbf{u} \\ \boldsymbol{\mathcal{Y}} &= \mathbf{h}(\chi_i) \end{aligned} \tag{2.15}$$

where $\boldsymbol{\chi} \in \mathcal{R}^n$, $\boldsymbol{\mathcal{Y}} \in \mathcal{R}^p$ and $\mathbf{u} \in \mathcal{R}^m$ are the states-space, outputs and control inputs respectively; functions $\mathbf{f}$ and $\mathbf{g}$ describe the system dynamics, while $\mathbf{h}$ is the output function; and the parameters n, m and p represent the dimensions of the states vector, inputs vector, and outputs vector respectively.

1. If the system has a relative degree ρ, the state feedback law $\mathbf{u}(\chi_i)$ in Equation (2.16), where $\boldsymbol{\mathcal{D}}(\chi_i)$ is the decoupling matrix expressed with vectors $\boldsymbol{\mathcal{Z}}$ and $\boldsymbol{\mathcal{U}}$ in Equations (2.17) and (2.18) is applied to compensate the non-linearity of the system.

$$\mathbf{u}(\chi_i) = \boldsymbol{\mathcal{D}}(\chi_i)^{-1}\left[\boldsymbol{\mathcal{U}} - \boldsymbol{\mathcal{Z}}\right] \tag{2.16}$$

$$\boldsymbol{\mathcal{D}}(\chi_i) = \begin{bmatrix} L_{g1}L_f^{\rho_1-1}h_1(\chi_i) & \cdots & L_{gm}L_f^{\rho_1-1}h_1(\chi_i) \\ \vdots & \ddots & \vdots \\ L_{g1}L_f^{\rho_m-1}h_m(\chi_i) & \cdots & L_{gm}L_f^{\rho_m-1}h_m(\chi_i) \end{bmatrix} \quad \boldsymbol{\mathcal{Z}} = \begin{bmatrix} L_f^{\rho_1}h_1(\chi_i) \\ \vdots \\ L_f^{\rho_m}h_m(\chi_i) \end{bmatrix} \tag{2.17}$$

$$\boldsymbol{\mathcal{U}} = \begin{bmatrix} -\mathbf{K_1} & 0 & \cdots & 0 \\ 0 & -\mathbf{K_2} & \cdots & 0 \\ \vdots & \vdots & \ddots & \vdots \\ 0 & 0 & \cdots & -\mathbf{K_m} \end{bmatrix} \begin{bmatrix} \begin{pmatrix} h_1(\chi_i) \\ \vdots \\ L_f^{r_1-1}h_1(\chi_i) \end{pmatrix} \\ \vdots \\ \begin{pmatrix} h_m(\chi_i) \\ \vdots \\ L_f^{r_m-1}h_m(\chi_i) \end{pmatrix} \end{bmatrix} \tag{2.18}$$

The elements of the vectors $\mathbf{K}_i$, in Equation (2.18) are chosen to ensure that the polynomial in Equation (2.19) is Hurwitz stable for all outputs.

$$s^{\rho_i} + K_{i(\rho_i-1)}s^{\rho_i-1} + K_{i(\rho_i-2)}s^{\rho_i-2} + \cdots + K_{i1}s + K_{i0} = 0 \tag{2.19}$$

2. A non-linear transformation $\boldsymbol{z} = \boldsymbol{\varphi}(\chi_i) = \begin{bmatrix}\boldsymbol{\xi}^T & \boldsymbol{\psi}^T\end{bmatrix}^T$ is then applied; where $\boldsymbol{\xi} = \begin{bmatrix}y, & \dot{y}, & \cdots, & y^{(\rho-1)}\end{bmatrix}^T$, while $\boldsymbol{\psi}$, of length $n-\rho$, is chosen to ensure that the function $\boldsymbol{\varphi}(\chi_i)$ is a diffeomorphism. Equation (2.15) can now be written in the following form (Isidori, 1995, 1999):

$$y^{(\rho)} = \boldsymbol{\mathcal{U}} \qquad y(0) = y_0 \tag{2.20}$$

$$\dot{\psi} = \mathcal{Q}\left(y, y^{(1)}, \cdots, y^{(\rho-1)}, \psi\right) \qquad \psi(0) = \psi_0 \tag{2.21}$$

where $\mathcal{Q}$ denotes a non-linear function of ψ, y and $y^{(i)}$, that defines $\dot{\psi}$, with (i) being the i^{th} time derivative. Equation (2.21) expresses the internal or zero dynamics of the system, which is generally independent of the control input u.

The linearisation decouples the internal internal dynamics from the input-output behaviour of the non-linear system in Equation (2.15). Thus $\boldsymbol{\psi}$ has no effect on the output y. Equations (2.20) and (2.21) can now be rewritten as follows, as a function

of the transformed coordinates:

$$\begin{aligned} \dot{\xi}_i &= \xi_{i+1}\,\big|_{i=1,\ 2,\ \cdots,\ (\rho-1)} \\ \dot{\xi}_\rho &= \boldsymbol{\mathcal{U}} \\ \dot{\psi} &= \mathcal{Q}\,(\psi, \xi) \\ \text{with}\ \ \xi_1(0) = y_0 \ \ &\text{and} \ \ \psi(0) = \psi_0 \end{aligned} \tag{2.22}$$

At this point, the system's input-output behaviour is globally linearised, and simple proportional controller $\boldsymbol{\mathcal{U}}$ in Equation (2.18) can be used to control its outputs. This, however, does not control the internal dynamics which can still be unstable.

2.6.1 Zero Dynamics

Suppose that the equilibrium point of the system in Equation (2.15) is at the origin, $\chi = 0$, then it follows that the first ρ coordinates of the transformed system in Equation (2.22) are equal to zero i.e. $\xi_i = 0\,|_{i=1,\ 2,\ \cdots,\ \rho}$. Besides, when $\chi = 0$, the value of ψ can be made zero because ψ can be arbitrarily fixed, implying that the point $(\xi, \psi) = (0, 0)$ denotes the equilibrium point of the transformed system, with $L_f^r h(0) = 0$ and $Q(0, 0) = 0$. The problem of zeroing the system outputs would therefore involve finding all the pairs (χ, u) of the initial states χ_i and u for all t in the region of $t = 0$, such that the corresponding output $y(t)$, which is zero at $t = 0$ remains at zero in the region of $t = 0$. One obvious solution to this problem is the pair $(0, 0)$, however it is necessary to compute all the pairs that satisfy this property.

Since $y(\chi_i) = 0$ in the region of $t = 0$, the time derivative $\dot{y}(\chi_i) = \ddot{y}(\chi_i) = \cdots = y^{r-1}(\chi_i) = 0$, resulting in both ξ and $\dot{\xi}$ equal to zero. If the lie derivatives of the transformed system are denoted by $c(\xi,\ \psi) = L_f^r h(\chi_i)$ and $d(\xi,\ \psi) = L_f^{r-1} L_g h(\chi_i)$, then the new input $\boldsymbol{\mathcal{U}} = 0$ and the input vector of the original system u must satisfy

the Equation (2.23), where the solution of ψ^* is computed from $\dot{\psi}^* = Q\,(0,\ \psi^*)$.

$$u = -\frac{c\,(0,\ \psi^*)}{d\,(0,\ \psi^*)} \tag{2.23}$$

The function, $\dot{\psi}^* = Q\,(0,\ \psi^*)$, defines the zero dynamics of the non-linear system (2.15). The zero dynamics correspond to the system's internal dynamics whenever the output $y = h(\chi_i)$ is restricted to remain at zero by the input u. The concept zero dynamics of non-linear systems corresponds to the concept of zeros of linear systems.

2.7 Conclusions

The chapter intended to outline a conceptual modelling and control framework for dynamic systems with human in the control loop. A survey of the literature regarding the modelling and control methodologies employed in such systems is elaborated. A special attention is given to WMS in terms of the modelling procedures, operator behaviours and control methodologies applied to incorporate the handling behaviours of the operator in the overall design. In particular, the motor-vehicle and wheelchair frameworks have been considered. The existing modelling procedures and methodologies applied to WMS are presented, with a brief observation of the advantages and drawbacks of the popular modelling methodologies. A classification of the available driver behaviour models, driver adaptation criteria and shared control methodologies proposed in the literature are reviewed. The presented control theoretical tools include the model predictive control and feedback control. It is observed that dynamic modelling presents a better representation of the system's behaviour, and that the existing driver-in-the-loop control system often fail to account for the driver's specific behaviour.

Chapter 3

MODELLING A POWERED WHEELCHAIR WITH SLIPPING AND GRAVITATIONAL DISTURBANCES

3.1 Introduction

The locomotive support that wheelchairs provide to people with ambulatory impairments, necessitates control systems that take into consideration not only the favourable indoor driving situations, but also the unstructured conditions that users experience in outdoor environments. Designing such a control system necessitates the formulation of a comprehensive wheelchair model. Most dynamic models in the literature, however presume the non-inclined indoor planer surfaces, and therefore fail to take the combined effects of both gravitational forces and rolling friction on the usable-traction into consideration. Wheel-slip situations are also commonly neglected. This chapter contributes to wheelchair modelling by formulating a dynamic model that considers the effects of rolling friction and gravitational potential on the wheelchair's road-load force, on both inclined and non-inclined surfaces. The dynamic model is derived through the Euler Lagrange procedure, and wheel-slip is geometrically determined by an approach that reduces the conventional number of slip-detection encoders.

3.2 Background and Motivation

Although most wheelchair drivers are able to comfortably move a joystick and make a fine movement correction when driving, others are only able to click on switches. A number of potential users, on the other hand, are incapable of driving and controlling a powered wheelchair with such interfacing devices, and can only rely upon caretakers to access the environment. The usage and potential users of electric-powered wheelchairs are determined to a large extent by the functionality of their embedded controllers. It is therefore necessary for a model based controller, that the wheelchair model is comprehensive enough to reflect real situations. The modelling of differential drive wheelchairs and other wheeled-mobile systems has previously been studied from the ideal perspective, where only the kinematic properties are taken into consideration, without regard to the dynamic attributes (Tarokh & McDermott, 2005; Zhu et al., 2006; Morales, 2006; Tian et al., 2009; Zhang et al., 2009). Such models fail to account for the effects of the system's mass, inertia and acceleration, and do not consider the contributions of both conservative and non-conservative forces on the system's motion. However, the outdoor wheelchair usage generally demands driving on paths with diverse ground surface characteristics. The slippery and hilly configurations encountered in such situations could complicate the controllability of a wheelchair, and lead to a severe accident with injuries to the user, if not taken into consideration during design (Wretstrand et al., 2004; Weiss et al., 2006). Furthermore, the rolling friction between the wheels and the road surface could be used to realise an optimised transfer of torque to the wheels during acceleration, if properly regarded. This could improve the controllability and lessen the slipping situations during motion. These considerations are therefore very important in the formulation of a wheelchair model.

A few researchers have considered the effects of such dynamic conditions. Fierro &

Lewis (1997) and Oubbati et al. (2005) for instance, presented the dynamic models of wheeled robotic systems with constrained motion on non-inclined planer surfaces. Although the models took into consideration the contributions of mass and inertia, they neither regarded the effects of rolling friction, nor considered the influence of gravitational forces experienced by the system during normal use. Frictional effects have been taken into consideration in various studies (Kozłowski & Pazderski, 2004; Chen & Huang, 2006; Stonier et al., 2007), while slipping situations in the dynamic model have been accounted for by (Williams et al., 2002; Olson et al., 2003; Sidek & Sarkar, 2008). Although such dynamic models are numerous, they are commonly based on the various structures of wheeled-mobile systems considered in section 2.2, and may therefore not reflect the behaviour of the conventional differential drive wheelchair with front castor wheels.

There are relatively few dynamic models in the literature formulated to specifically describe the motion of a wheelchair, and a few that only take into consideration the influence of mass and inertia have been reported (Katsura & Ohnishi, 2004; Nguyen et al., 2007; De La Cruz et al., 2011). These presentations restrict the motion of a wheelchair to horizontal work-planes and therefore disregard the influence of gravitational potential. Emam et al. (2007) presented a wheelchair dynamic model for non-normal driving conditions involving wheel-slip situations. Although the model takes the rolling friction and wheel-slip effects into account, it also constrains the wheelchair's motion to non-inclined planer surfaces.

A dynamic model that takes the rolling friction as well as the up-hill and down-hill gravitational forces into consideration has been reported (Onyango et al., 2009a,b, 2011). However, the authors did not consider the estimation of slipping parameters. The most recent study (to the best of our knowledge) in this respect has been presented by Chénier et al. (2011, 2015). The study proposed a good dynamic model for

manual wheelchair propulsion, usable by a new kind of motorised roller ergometer to simulate the behaviour of a wheelchair on both straight and curvilinear level ground paths. However, two observations could be made with regards to this model. First, like most dynamic models, it is based on horizontal level grounds. The influence of gravitational potential is therefore assumed to be constant. Second, the model is formulated based on the no-slip condition, which means the rolling friction model does not take slip velocity into account. These are acceptable modelling assumptions for the proposed application. However, the effects of gravitational potential and slipping situations could be significant during the actual outdoor usage. Such conditions therefore need to be taken into consideration during modelling. We could not find a wheelchair model that takes all of the aforementioned dynamic situations into account. This chapter (also see Onyango et al., 2016) therefore contributes to wheelchair modelling by considering the combined effects of extreme dynamic situations accessible to a wheelchair during both indoor and outdoor usage. This involves estimating the slipping parameters of a conventional differential drive wheelchair, by taking the wheelchair's rolling friction and the varying gravitational potential on both inclined and non-inclined surfaces into consideration during modelling.

The rest of the chapter is organised as follows: The dynamic modelling with gravitational forces is presented in Section 3.3, taking the ideal non-holonomic constraints of the wheelchair into account. This is followed by estimation and incorporation of slipping parameters into the dynamic model in Section 3.4. The simulation results to validate the dynamic model are discussed in Section 3.5, with some concluding remarks in Section 3.6.

3.3 Dynamic model with gravitational forces

3.3.1 Description of the wheelchair and frames of reference

A differential drive wheelchair of the type shown in Figure 3.1 is considered for modelling. The procedure employs Sheth-Uicher convention in the assignment of co-ordinate frames at the two links, the body and the surface of travel; and considers the centre of mass, as the joint that links the two. Point O, located at distance b from the rear wheels along the Y-axis is the mid-point of rear axle, and is also presumed to be the origin of the body fixed frame $\{X\,Y\,Z\}$, while point C is the centre of mass. The generalised coordinates of the centre of mass, stated with respect to the inertial coordinate frame $\{x\,y\,z\}$ are given by $\mathbf{q} \in \mathcal{R}^{n\times 1} = [x_g, y_g, z_g, \phi]^T$, while the Cartesian components of the distance l between C and O are $\bar{\bar{x}}, \bar{\bar{y}}$ and $\bar{\bar{z}}$, (not shown in Figure 3.1). Furthermore, the angular positions of the right and left motorised wheels are γ_R and γ_L respectively. The procedure describes a two and a half dimensional wheelchair model that assume constant angular velocities ω_X and ω_Y. This consideration is based

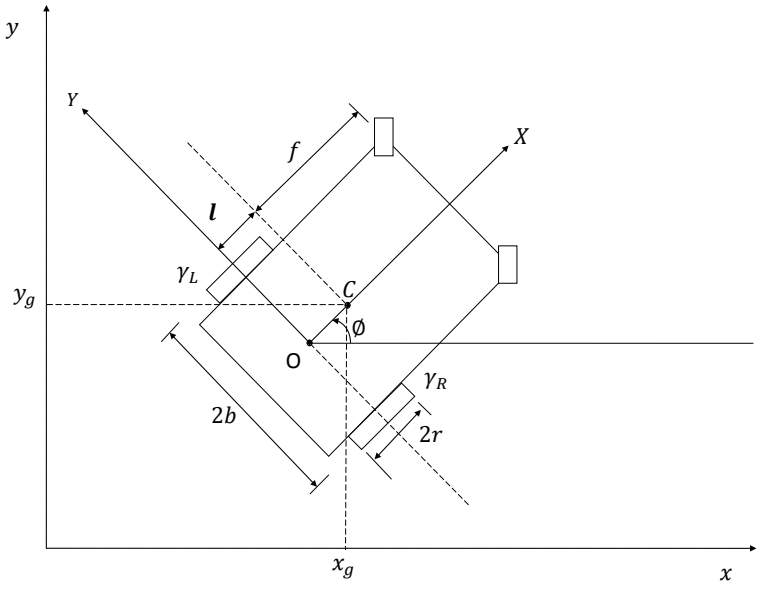

FIGURE 3.1: A differential drive wheelchair model.

on the idea that a driver (through a conventional joystick) only has control of $\dot{X}$ and ω_Z otherwise denoted as V and $\dot{\phi}$ respectively. The angular velocities ω_X and ω_Y are determined by the road surface, and since they lack a dedicated control actuator, these derivatives may introduce the undesired zero dynamics in the control system. Accordingly, the unstructured environment considered in the dynamic model only entails the effects of path inclination and slipping situations (surface characteristics).

The structure consists of two active rear wheels of radius r, and two passive front castor wheels of radius $r_{_C}$. These are driven by applying the torques $\tau_{_R}$ and $\tau_{_L}$ on the right and left rear wheel respectively. It may be necessary to explain that θ is the instantaneous deviation of the Z-axis from the z-axis, whereas the angle between the x-axis and the line of intersection of the moving XY plane and the stationary xy plane is ψ. Lastly, ϕ is the precession angle about the Z-axis in a counter-clockwise direction as visible in a body fixed frame. The Euler Lagrange's approach that yields Equation (2.9) is proposed in the derivation of equations of motion.

3.3.2 System constraints

Considering identical d.c. motors for the right and left rear wheels, the wheelchair's linear and angular speeds, V and $\dot{\phi}$, respectively, can be expressed in the body fixed coordinate frame, according to Equation (3.1) in terms of $\dot{\gamma}_{_R}$ and $\dot{\gamma}_{_L}$.

$$\begin{aligned} V &= {}^{r}/_{2}\,(\dot{\gamma}_{_R} + \dot{\gamma}_{_L}) \\ \dot{\phi} &= {}^{r}/_{2b}\,(\dot{\gamma}_{_R} - \dot{\gamma}_{_L}) \end{aligned} \tag{3.1}$$

In order to facilitate the computation of system constraints, the ideal non-slipping condition is initially considered. The body fixed linear velocity vector $[\dot{X}_g\ \dot{Y}_g\ \dot{Z}_g]$, of point C is expressed according to Equation (3.2), as a linear transformation of the inertial velocity vector. The rotational matrix, $\mathbf{R}$, of frame $\{X, Y, Z\}$ relative to $\{x, y, z\}$ is presented in Equation (3.3) in terms of Euler angles. In the rest of this

thesis, the elements of matrix $\mathbf{R}$ will be referred to as $\mathbf{R}_{XX}\,|_{X=1,2,3}$.

$$\left[\dot{X}_g\ \dot{Y}_g\ \dot{Z}_g\right]^T = [\mathbf{R}]\,[\dot{x}_g\ \dot{y}_g\ \dot{z}_g]^T \tag{3.2}$$

$$\mathbf{R} = \begin{bmatrix} \cos\phi\cos\psi - & \cos\phi\sin\psi + & \\ \sin\phi\sin\psi\cos\theta & \sin\phi\cos\psi\cos\theta & \sin\theta\sin\phi \\ -\sin\phi\cos\psi - & -\sin\phi\sin\psi + & \\ \cos\phi\sin\psi\cos\theta & \cos\phi\cos\psi\cos\theta & \sin\theta\cos\phi \\ \sin\theta\sin\psi & -\sin\theta\cos\psi & \cos\theta \end{bmatrix} \tag{3.3}$$

From Equation (3.1), it is easy to notice that $V = r\dot{\gamma}_R - b\dot{\phi} = r\dot{\gamma}_L + b\dot{\phi}$. Noting that V in Equation (3.1) $= \dot{X}_g$ in Equation (3.2), the pure rolling constraints of the right and left wheels that express how the longitudinal motion of the wheelchair's centre of mass is restricted by the longitudinal velocity of the wheels may be stated as follows:

$$\begin{aligned} \dot{X}_g &= r\dot{\gamma}_R - b\dot{\phi} \\ \dot{X}_g &= r\dot{\gamma}_L + b\dot{\phi} \end{aligned} \tag{3.4}$$

Moreover, the non-holonomic restrictions constraining the wheelchair's motion in the direction perpendicular to the driving axis of the wheels, and on the moving XY plane, (ground surface), could be presented as Equation (3.5):

$$\begin{aligned} \dot{x}_g\mathbf{R}_{21} + \dot{y}_g\mathbf{R}_{22} + \dot{z}_g\mathbf{R}_{23} - \dot{\phi}\bar{\bar{x}} &= 0 \\ \dot{x}_g\mathbf{R}_{31} + \dot{y}_g\mathbf{R}_{32} + \dot{z}_g\mathbf{R}_{33} &= 0 \end{aligned} \tag{3.5}$$

Being non-integrable and independent velocity constraints, the equations in (3.5) may be expressed in terms of Equation (3.6) with $\mathbf{A}(q_i)$ being a full rank matrix of size $m \times n$.

$$\mathbf{A}(q_i)\dot{\mathbf{q}} = 0 \tag{3.6}$$

The computation of the first order kinematic model in Equation (3.7) without slip, requires the full rank transformation matrix $\mathbf{S}(q_i) \in \mathcal{R}^{n\times(n-m)}$, which transforms the velocity vector $\boldsymbol{\nu} \in \mathcal{R}^{(n-m)\times 1}$, to the generalised velocity vector $\dot{\mathbf{q}}$. Both $\mathbf{S}(q_i)$ and $\boldsymbol{\nu}$ are presented in Equation (3.8). The matrix $\mathbf{S}(q_i)$ is formed by a set of smooth linearly independent vector fields that span the null space of $\mathbf{A}(q_i)$, such that the product $\mathbf{S}^T(q_i)\mathbf{A}^T(q_i) = 0$. It is evident from Equation (3.6), that $\dot{\mathbf{q}}$ is in the null space of $\mathbf{A}(q_i)$, and it accordingly follows that $\dot{\mathbf{q}} \in \text{span}\{\mathbf{S}(q_i)\}$. However, depending on the physical interpretation given to $\boldsymbol{\nu}$, different choices of $\mathbf{S}(q_i)$ may be possible.

$$\dot{\mathbf{q}} = \mathbf{S}(q_i)\boldsymbol{\nu}(t) \tag{3.7}$$

where

$$\mathbf{S}(q_i) = \begin{bmatrix} \mathbf{R}_{11} & \bar{\bar{x}}\mathbf{R}_{21} \\ \mathbf{R}_{12} & \bar{\bar{x}}\mathbf{R}_{22} \\ \mathbf{R}_{13} & \bar{\bar{x}}\mathbf{R}_{23} \\ 0 & 1 \end{bmatrix} \qquad \boldsymbol{\nu} = \begin{bmatrix} V \\ \dot{\phi} \end{bmatrix} \tag{3.8}$$

3.3.3 Kinetic and potential energy

Considering the wheelchair as a single non-elastic body, the kinetic energy T, of the wheelchair with reference to the centre of mass can be computed. Equation (3.9) observes the wheelchair symmetry, and therefore takes into account the assumption that the wheelchair's centre of mass is likely to lie along the longitudinal axis. This

implies that $\bar{y}$ could be considered equal to zero without loss of generality.

$$\begin{aligned} T &= \tfrac{1}{2}M\left(\dot{x}_g^2 + \dot{y}_g^2 + \dot{z}_g^2\right) + \\ &\quad \tfrac{1}{2}\left(I_{XX}\omega_X^2 + I_{YY}\omega_Y^2 + I_{ZZ}\omega_Z^2 - 2I_{XZ}\omega_X\omega_Z\right) + \\ &\quad M\left[\bar{\bar{x}}\left(\nu_{0Y}\omega_Z - \nu_{0Z}\omega_Y\right) + \bar{\bar{z}}\left(\nu_{0X}\omega_Y - \nu_{0Y}\omega_X\right)\right] \end{aligned} \tag{3.9}$$

where

- M is the total mass of the wheelchair including all its components.
- I_{XX}, I_{YY} and I_{ZZ} are the moment of inertia of the wheelchair about the X, Y and Z axis respectively through point O, while I_{XZ} is the product inertia about X and Z axis through the same point.
- ω_X, ω_Y and ω_Z are components of angular velocity ω of the wheelchair given by Equation (3.10) along the X, Y and Z axis respectively.

$$\begin{aligned} \omega_X &= \dot{\psi}\mathbf{R}_{13} + \dot{\theta}\cos\phi \\ \omega_Y &= \dot{\psi}\mathbf{R}_{23} - \dot{\theta}\sin\phi \\ \omega_Z &= \dot{\psi}\mathbf{R}_{33} + \dot{\phi} \end{aligned} \tag{3.10}$$

- ν_{0X}, ν_{0Y} and ν_{0Z} are components of inertial velocity of point C given by $[\dot{X}_g\ \dot{Y}_g\ \dot{Z}_g]^T$ along the instantaneous directions of X, Y and Z axis respectively.

Thus with potential energy $U = Mgz_g$, the Lagrange function $\mathcal{L}$ can be computed as Equation (3.11):

$$\begin{aligned} \mathcal{L} &= T - U \\ &= \tfrac{1}{2}M\left(\dot{x}_g^2 + \dot{y}_g^2 + \dot{z}_g^2\right) + \tfrac{1}{2}\left(I_{XX}\omega_X^2 + I_{YY}\omega_Y^2 + I_{ZZ}\omega_Z^2 - 2I_{XZ}\omega_X\omega_Z\right) + \\ &\quad M\left[\bar{\bar{x}}\left(\nu_{0Y}\omega_Z - \nu_{0Z}\omega_Y\right) + \bar{\bar{z}}\left(\nu_{0X}\omega_Y - \nu_{0Y}\omega_X\right)\right] - Mgz_g \end{aligned} \tag{3.11}$$

3.3.4 Dynamic model development

The inclusion of the potential energy of gravitational forces in the Lagrangian function has the logical effect that the resulting equations of motion naturally take into account the gravitational forces subjected to the wheelchair relative to its position in the configuration space. The dynamic equations of motion are computed in accordance with the Lagrangian formalism. This simplifies the modelling process of a rigid body's dynamics into a straightforward procedure that generates the matrices $\bar{\mathbf{M}}(q_i) \in \mathcal{R}^{n\times n}$, $\mathbf{G}(q_i) \in \mathcal{R}^{n\times 1}$ and $\bar{\mathbf{C}}(q_i, \dot{q}_i) \in \mathcal{R}^{n\times n}$ in Equations (3.12) and (3.13).

$$\bar{\mathbf{M}}(q_i) = \begin{bmatrix} M & 0 & 0 & -M\bar{\bar{x}}\mathbf{R}_{21} \\ 0 & M & 0 & -M\bar{\bar{x}}\mathbf{R}_{22} \\ 0 & 0 & M & -M\bar{\bar{x}}\mathbf{R}_{23} \\ -M\bar{\bar{x}}\mathbf{R}_{21} & -M\bar{\bar{x}}\mathbf{R}_{22} & -M\bar{\bar{x}}\mathbf{R}_{23} & I_{zz} \end{bmatrix}, \quad \mathbf{G}(q_i) = \begin{bmatrix} 0 \\ 0 \\ Mg \\ 0 \end{bmatrix} \tag{3.12}$$

$$\bar{\mathbf{C}}(q_i, \dot{q}_i) = \begin{bmatrix} 0 & 0 & 0 & M\bar{\bar{x}}(\dot{\phi}\mathbf{R}_{11} + 2\dot{\psi}\mathbf{R}_{22} - 2\dot{\theta}\sin\psi\sin\theta\cos\phi) \\ 0 & 0 & 0 & M\bar{\bar{x}}(\dot{\phi}\mathbf{R}_{12} - 2\dot{\psi}\mathbf{R}_{21} + 2\dot{\theta}\sin\theta\cos\phi\cos\psi) \\ 0 & 0 & 0 & M\bar{\bar{x}}(\dot{\phi}\mathbf{R}_{13} - 2\dot{\theta}\cos\phi\cos\theta) \\ 0 & 0 & 0 & 0 \end{bmatrix} \tag{3.13}$$

Because the kinetic energy equation, (3.9), is a quadratic function of the generalised velocity vector $\dot{\mathbf{q}}$, that is, $T = \frac{1}{2}\dot{\mathbf{q}}\bar{\mathbf{M}}(q_i)\dot{\mathbf{q}}$, the matrix, $\bar{\mathbf{M}}(q_i)$, could be referred to as the mass matrix, that relates T to $\dot{\mathbf{q}}$. The symmetric mass matrix $\bar{\mathbf{M}}(q_i)$ depends on the configuration of the dynamic system, and since T is always positive and bounded, matrix $\bar{\mathbf{M}}(q_i)$ is also positive definite and bounded. With these properties, $\bar{\mathbf{M}}(q_i)$ can be considered non-singular with positive eigenvalues. The product of $\dot{\mathbf{q}}$ and matrix $\bar{\mathbf{C}}(q_i, \dot{q}_i)$ in Equation (3.13) is the vector of centrifugal and Coriolis forces. It includes all the inertial forces resulting from centrifugal and Coriolis accelerations.

The matrices $\bar{\mathbf{M}}(q_i)$ and $\bar{\mathbf{C}}(q_i, \dot{q}_i)$ are related by the skew-symmetric matrix $\dot{\bar{\mathbf{M}}}(q_i) - 2\bar{\mathbf{C}}(q_i, \dot{q}_i)$. The $\mathbf{G}(q_i)$, also in Equation (3.13), is the vector of gravitational forces, and is often present in a dynamical system from the mechanical point of view. Since it is continuous and depends only on the generalised positions q_i, $\mathbf{G}(q_i)$ is bounded for each bounded q_i. Further details regarding these matrices may be found in the literature (Spong et al., 2006; Taghirad, 2013; Kelly et al., 2006). The ideal dynamic model that does not take the slipping effects into consideration, can therefore be computed as expressed in Equation (3.14).

$$\bar{\mathbf{M}}(q_i)\ddot{\mathbf{q}} + \bar{\mathbf{C}}\left(q_i, \dot{q}_i\right)\dot{\mathbf{q}} + \mathbf{G}(q_i) = \mathbf{E}(q_i)\boldsymbol{\tau} - \mathbf{F}(\dot{q}_i) + \mathbf{A}^T(q_i)\boldsymbol{\lambda} \tag{3.14}$$

The matrix $\mathbf{E}(q_i)$ presented in Equation (3.15) is also a transformation matrix, that transforms the inputs, motor torques $\boldsymbol{\tau}$, also in Equation (3.15), into the applied force components in the generalised coordinates, while, $\mathbf{F}(\dot{q}_i)$ is the vector of frictional forces described in section 3.4.3.

$$\mathbf{E}(q_i) = \frac{1}{r}\begin{bmatrix} \mathbf{R}_{11} & \mathbf{R}_{11} \\ \mathbf{R}_{12} & \mathbf{R}_{12} \\ \mathbf{R}_{13} & \mathbf{R}_{13} \\ b & -b \end{bmatrix} \qquad \boldsymbol{\tau} = \begin{bmatrix} \tau_{_R} \\ \tau_{_L} \end{bmatrix} \tag{3.15}$$

3.4 Slipping parameters and frictional force

3.4.1 Slipping parameters

In this study, a wheelchair is considered slipping if there exists a difference between the computed or theoretical wheel circumferential velocity $r\dot{\gamma}$, and the absolute or actual velocity V, at any given time instant. The slip ratio s_r is generally computed

by Equation (3.16), where r is the radius, and $\dot{\gamma}$ is the average rotational velocity of the driving wheel.

$$s_r = \begin{cases} \frac{r\dot{\gamma}-V}{r\dot{\gamma}} & \text{driving} : (r\dot{\gamma} > V) \\ \frac{r\dot{\gamma}-V}{V} & \text{braking} : (V > r\dot{\gamma}) \end{cases} \tag{3.16}$$

Apart from the road surface texture and mechanical load of the wheelchair, the frictional force between the tire and the road surface is also dependent upon the slip ratio s_r, because $\tau_{_R}$ and $\tau_{_L}$ are translated into wheelchair motion through the road-tire friction. If the slipping condition is allowed beyond a certain threshold, it lowers the traction force and significantly reduces the controllability. Regulation of wheel torques is therefore necessary to maintain traction within the acceptable limit. Slip detection could be a major challenge bearing in mind the slow steering speed of a wheelchair. However, considering that the front castor wheels are relatively far from the centre of mass compared to the hind wheels, it could be assumed as a result of force effect that the castor wheels experience no slip. The castor wheels are therefore considered to reflect the real or actual velocity of the wheelchair, while the motorised wheels reflect the theoretical velocity.

Chenier et al. (2011) originally proposed an open-loop observer method for estimating the orientational directions of each of the two castor wheels, based on the kinematics of the rear wheels, and without using encoders. However, this method is founded on the assumption that none of the wheels will slip. For this reason, a previously published method that requires no additional information regarding the environment or acceleration of the wheelchair is elaborated to take the effects of wheel rotations on linear velocity when driving on inclined paths into consideration (Emam et al., 2007). In this method, encoders are used in the determination of slipping velocity by measuring and comparing the actual and expected velocities of the wheelchair.

This procedure demands two encoders on each of the front wheels, one for wheelchair orientation measurement, and the other for measuring wheel rotational angle. Similarly, two odometers are required on the driving wheels for absolute velocity and orientation measurement.

3.4.2 Determination of real velocity

As indicated in the previous section, besides the wheelchair's geometry, the determination of the real centre of mass velocity is based on the utilisation of the orientational and rotational velocities of the castor wheels. Considering Figure 3.2, it is possible to derive Equations (3.17) - (3.19) that validate the possibility of representing the direction of the right castor wheel in terms of the left, thus reducing the number of front wheels encoders required for slip detection.

$$\dot{\phi}_f = \frac{\mathbf{v}_Y}{\bar{\bar{x}} + f} \tag{3.17}$$

$$\beta = \frac{\sin\alpha_L}{\cos\alpha_L + \frac{b}{\bar{\bar{x}}+f}\sin\alpha_L} \tag{3.18}$$

$$\alpha_R = \frac{\sin\alpha_L}{\cos\alpha_L + \frac{2b}{\bar{\bar{x}}+f}\sin\alpha_L} \tag{3.19}$$

(*derived in Appendix A*)

where $\dot{\phi}_f$ is the rotational velocity of the wheelchair on the XY plane due to $\mathbf{v}_Y$ and the radial distance $(f + \bar{\bar{x}})$ along the X-axis. The linear velocities $\mathbf{v}_R$ and $\mathbf{v}_L$, of the right and left castor wheels respectively, are considered to originate from the two components of rotational velocities in Equation (3.20), with each component being computed with respect to the point and axis of rotation. One component, $\mathbf{v}_{R_B}$ and $\mathbf{v}_{L_B}$, for the right and left castor wheels respectively, represents the effects of rotations about the centre of the wheels (point B in Figure 3.3). The other component, $\mathbf{v}_{R_A}$

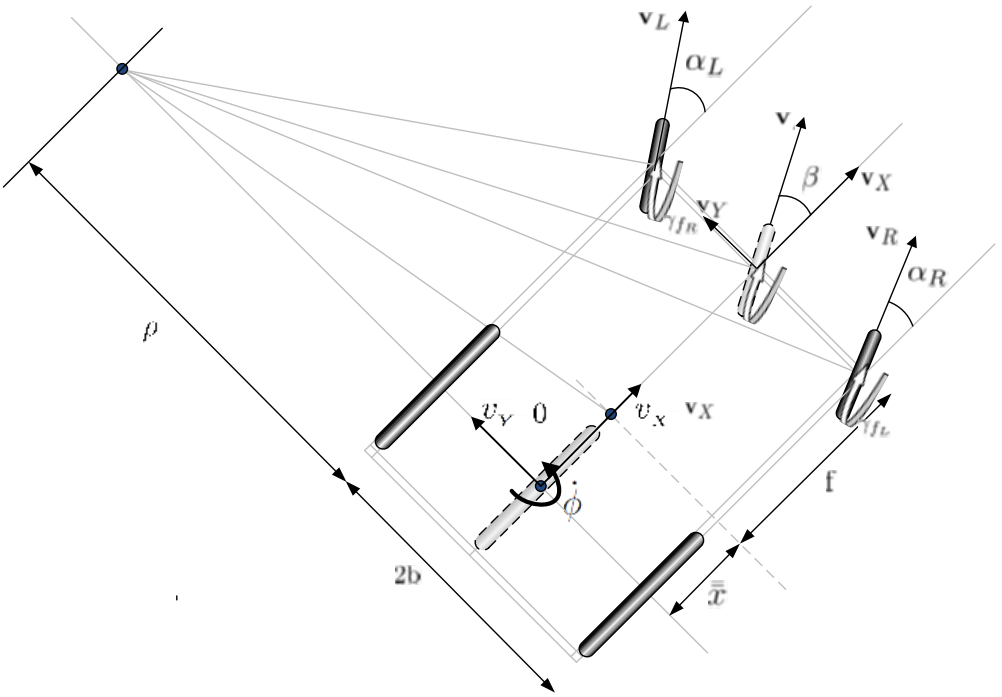

FIGURE 3.2: Geometrical representation of the wheelchair, with the parameters that have been utilised in deriving the velocity of the centre of mass from the castor wheels' velocities.

and $\mathbf{v}_{L_A}$, represents the effect of rotations about the point A in Figure 3.3, where the castor wheels are attached to the wheelchair. $\mathbf{v}_R$ and $\mathbf{v}_L$ can therefore be computed according to Equation (3.20).

$$\begin{aligned} \mathbf{v}_R &= \mathbf{v}_{R_B} + \mathbf{v}_{R_A} \\ \mathbf{v}_L &= \mathbf{v}_{L_B} + \mathbf{v}_{L_A} \end{aligned} \tag{3.20}$$

where

$$\mathbf{v}_{R_A} = \begin{bmatrix} \dot{\alpha}_R \mathrm{e}(\sin\alpha_R \cos\psi - \cos\alpha_R \sin\psi \cos\theta) \\ \dot{\alpha}_R \mathrm{e}(\sin\alpha_R \sin\psi - \cos\alpha_R \cos\psi \cos\theta) \\ \dot{\alpha}_R \mathrm{e}(\cos\alpha_R \sin\theta) \\ 0 \end{bmatrix} \tag{3.21}$$

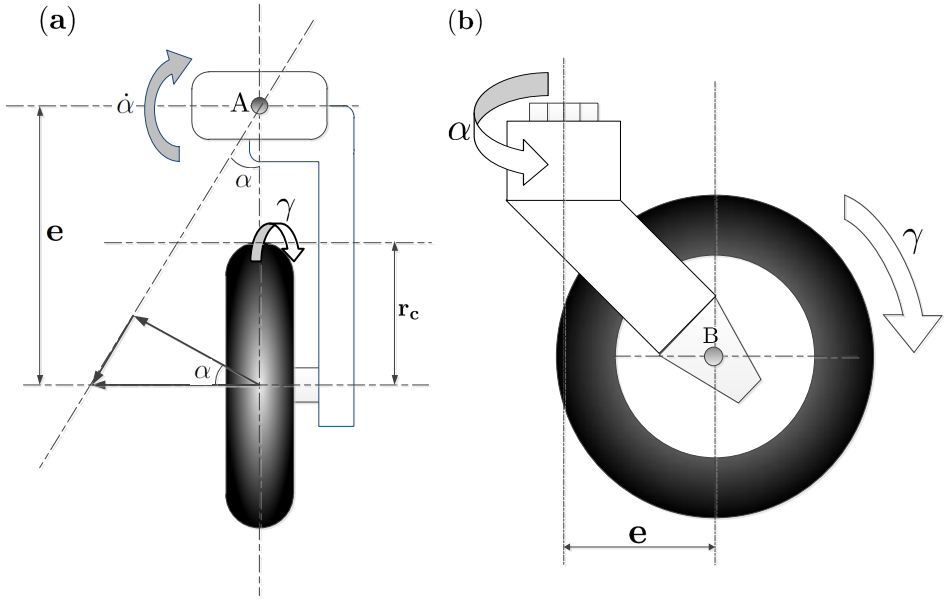

FIGURE 3.3: (a) Bird view and (b) side view schematic representation of a castor wheel.

$$\mathbf{v}_{R_B} = \begin{bmatrix} r_c\dot{\gamma}_{f_R}(\cos\alpha_R\cos\psi - \sin\alpha_R\sin\psi\cos\theta) \\ r_c\dot{\gamma}_{f_R}(\cos\alpha_R\sin\psi + \sin\alpha_R\cos\psi\cos\theta) \\ r_c\dot{\gamma}_{f_R}(\sin\alpha_R\sin\theta) \\ 0 \end{bmatrix} \tag{3.22}$$

$$\mathbf{v}_{L_A} = \begin{bmatrix} \dot{\alpha}_L e(\sin\alpha_L\cos\psi - \cos\alpha_L\sin\psi\cos\theta) \\ \dot{\alpha}_L e(\sin\alpha_L\sin\psi - \cos\alpha_L\cos\psi\cos\theta) \\ \dot{\alpha}_L e(\cos\alpha_L\sin\theta) \\ 0 \end{bmatrix} \tag{3.23}$$

$$\mathbf{v}_{L_B} = \begin{bmatrix} r_c\dot{\gamma}_{f_L}(\cos\alpha_L\cos\psi - \sin\alpha_L\sin\psi\cos\theta) \\ r_c\dot{\gamma}_{f_L}(\cos\alpha_L\sin\psi + \sin\alpha_L\cos\psi\cos\theta) \\ r_c\dot{\gamma}_{f_L}(\sin\alpha_L\sin\theta) \\ 0 \end{bmatrix} \tag{3.24}$$

$\mathbf{v}_{R_B}$, $\mathbf{v}_{R_A}$, $\mathbf{v}_{L_B}$ and $\mathbf{v}_{L_A}$ are given in Equations (3.21) to (3.24). The resultant velocity of the front wheels as conceived at the midpoint between the right and left castor wheels is then computed as Equation (3.25):

$$\mathbf{v} = \tfrac{\mathbf{v}_R+\mathbf{v}_L}{2} + \begin{bmatrix} 0 \\ 0 \\ 0 \\ \dot{\phi}_f \end{bmatrix} = \begin{bmatrix} \mathbf{v}_x \\ \mathbf{v}_y \\ \mathbf{v}_z \\ \dot{\phi}_f \end{bmatrix} \tag{3.25}$$

Translating $\mathbf{v}$ to point O (see Figure 3.1), the new velocity of point O denoted as $\mathbf{v}_O$ can be considered equal to V because of the non-holonomic constraint that restricts the lateral speed of the rear wheels, v_Y, to zero (see Figure 3.2). $\mathbf{v}_O$ can then be expressed in terms of $\mathbf{v}$ by relationship (3.26). The slipping parameters in Equation (3.27) may be computed from the actual and the relative centre of mass velocities.

$$\mathbf{v}_O = \mathbf{v} \odot [\mathbf{R}_{11}\ \mathbf{R}_{12}\ \mathbf{R}_{13}\ \ 1]^T \tag{3.26}$$

$$\epsilon = \begin{bmatrix} \dot{x}_{f_o} \\ \dot{y}_{f_o} \\ \dot{z}_{f_o} \\ \dot{\phi}_f \end{bmatrix} - \begin{bmatrix} \dot{x}_o \\ \dot{y}_o \\ \dot{z}_o \\ \dot{\phi} \end{bmatrix} \tag{3.27}$$

where $\dot{x}_{f_o}$, $\dot{y}_{f_o}$, $\dot{y}_{f_o}$ and $\dot{\phi}_f$ are the components of $\mathbf{v}_O$, while $[\dot{x}_o \quad \dot{y}_o \quad \dot{y}_o \quad \dot{\phi}]^T$ is

the velocity of wheelchair at point O translated from $[\dot{x}_g \quad \dot{y}_g \quad \dot{y}_g \quad \dot{\phi}]^T$ of point C. By super-positioning the slipping velocities, $\boldsymbol{\epsilon}$, and the generalised velocities without slip, $\mathbf{S}(q_i)\boldsymbol{\nu}$, presented in Equation (3.7), the kinematic model with slipping conditions taken into account may be expressed. Upon differentiation of the configuration velocity vector in Equation (3.28), the acceleration vector in Equation (3.29) may be expressed as follows:

$$\dot{\mathbf{q}}_\epsilon = \mathbf{S}(q_i)\boldsymbol{\nu}(t) + \epsilon \tag{3.28}$$

$$\ddot{\mathbf{q}}_\epsilon = \dot{\mathbf{S}}(q_i)\boldsymbol{\nu} + \mathbf{S}(q_i)\dot{\boldsymbol{\nu}} + \dot{\epsilon} \tag{3.29}$$

3.4.3 Frictional and resistive force modelling

Modelling the rolling friction involves determining the relationship between the driving velocity and the normal force at the area of contact between the wheels and the ground. Since the rolling friction is quite non-linear and depends on many parameters, a reduced formulation that only depends on the new generalised velocity vector, $\dot{\mathbf{q}}_\epsilon$, is considered. The reduced model in Equation (3.30) is a combination of viscous and Coulomb friction, with a dimensionless coefficient of rolling friction μ, that describes the ratio of the frictional force responsible for friction coupling between the wheels and the ground.

$$\mathbf{F}(\epsilon) = \mu_{\text{vis}}\ \dot{\mathbf{q}}_\epsilon + \mu_{\text{cmb}} N\ \text{sgn}(\dot{\mathbf{q}}_\epsilon) \tag{3.30}$$

where $\dot{\mathbf{q}}_\epsilon$ is the new vector of generalised velocities described in Equation (3.28) that includes the slipping parameters, N is the normal force at point O, while μ_{vis} and μ_{cmb} denote the coefficient of viscous friction and coefficient of Coulomb friction respectively. Nevertheless, considering the low driving speed involved in wheelchairs,

both μ_{vis} and $\dot{\mathbf{q}}_\epsilon$ may be considered very small, resulting in much greater Coulomb friction as compared to viscous friction. The viscous friction, $\mu_{\text{vis}}\ \dot{\mathbf{q}}_\epsilon$, may therefore be neglected to simplify the model without loss of generality. The frictional force expressed in Equation (3.30) is not smooth and therefore not differentiable at $\dot{\mathbf{q}}_\epsilon = 0$. Since a continuous and time differentiable friction model is required for simulation, an approximation in Equation (3.32) based on Equation (3.31) may be used, with k being a constant that determines the approximation accuracy.

$$\lim_{k\to\infty} \frac{2}{\pi} \arctan(k\dot{\mathbf{q}}_\epsilon) = \text{sgn}(\dot{\mathbf{q}}_\epsilon)|_{k>>1} \tag{3.31}$$

$$\text{sgn}(\dot{\mathbf{q}}_\epsilon) \approx \frac{2}{\pi} \arctan(k\dot{\mathbf{q}}_\epsilon) \tag{3.32}$$

The rolling friction model, $\mathbf{F}$, of the wheelchair is therefore expressed as follows:

$$\mathbf{F} = \frac{2}{\pi} N \mu_{\max} \begin{bmatrix} \arctan(k\dot{q}_{\epsilon x}) \\ \arctan(k\dot{q}_{\epsilon y}) \\ \arctan(k\dot{q}_{\epsilon z}) \\ \arctan(k\dot{q}_{\epsilon \phi}) \end{bmatrix} \tag{3.33}$$

The normal force N may be determined by solving the Lagrange multiplier related to the vertical velocity constraint at point O in the second component of Equation (3.5) according to Equation (3.34)

$$\begin{aligned} N &= \lambda(2) \\ &= -\left[\mathbf{A}\bar{\mathbf{M}}^{-1}\mathbf{A}^T\right]^{-1} \left[\dot{\mathbf{A}}\dot{\mathbf{q}}_\epsilon + \mathbf{A}\mathbf{M}^{-1}\left(\mathbf{E}\tau - \bar{\mathbf{C}} - \mathbf{G}\right)\right] \end{aligned} \tag{3.34}$$

where $\lambda(2)$ denotes the second element of the matrix. The general equations of motion (3.14) may then be transformed into a more appropriate form for control by including Equations (3.28) and (3.29). Since matrix $\mathbf{S}(q_i)$ spans the null space of $\mathbf{A}(q_i)$, multiplying the result by $\mathbf{S}^T(q_i)$ eliminates the constraint forces, and produces

a dynamic model in Equation (3.35) which takes the rolling friction and gravitational effects on the wheelchair into account.

$$\begin{aligned}\mathbf{S^T}\bar{\mathbf{M}}\mathbf{S}\dot{\boldsymbol{\nu}} + \mathbf{S^T}\bar{\mathbf{M}}\dot{\mathbf{S}}\boldsymbol{\nu} + \mathbf{S^T}\bar{\mathbf{C}}\mathbf{S}\boldsymbol{\nu} + \mathbf{S^T}\bar{\mathbf{M}}\dot{\epsilon} + \mathbf{S^T}\bar{\mathbf{C}}\epsilon \\ + \mathbf{S^T}G + \mathbf{S^T}\mathbf{F} = \mathbf{S^T}E\boldsymbol{\tau}\end{aligned} \tag{3.35}$$

The dynamic model may be simplified to Equation (3.36) with $\mathbf{G}_n$ being a full rank and non-singular matrix

$$\dot{\boldsymbol{\nu}} = [\mathbf{F}_n] + [\mathbf{G}_n]\,\tau \tag{3.36}$$

where

$$\begin{aligned}[\mathbf{F}_n] &= -\left(\mathbf{S}^T\bar{\mathbf{M}}\mathbf{S}\right)^{-1}\left(\mathbf{S}^T\bar{\mathbf{M}}\dot{\mathbf{S}}\boldsymbol{\nu} + \mathbf{S}^T\bar{\mathbf{C}}\mathbf{S}\boldsymbol{\nu} + \mathbf{S}^T\bar{\mathbf{M}}\dot{\epsilon}\right) \\ &\quad -\left(\mathbf{S}^T\bar{\mathbf{M}}\mathbf{S}\right)^{-1}\left(\mathbf{S}^T\bar{\mathbf{C}}\epsilon + \mathbf{S}^T\mathbf{G} + \mathbf{S}^T\mathbf{F}\right) \\ [\mathbf{G}_n] &= \left(\mathbf{S}^T\bar{\mathbf{M}}\mathbf{S}\right)^{-1}\left(\mathbf{S}^T\mathbf{E}\right)\end{aligned}$$

3.5 Simulation and results

The simulation results to validate the proposed open-loop dynamic model are elaborated in this section. The results comprise various centre of mass trajectories and velocities of the open-loop system based on the dynamic model parameters expressed in Table 3.1. A comparison of the dynamic model to other differential drive systems existing in the literature is also provided. The wheel torques τ_R and τ_L are considered in the open-loop model simulations as the system's inputs. Given that the two identical rear wheels are independently driven by identical *dc* motors, straight line trajectories are expected on flat non-slippery surfaces with equal values of $\tau_{_R}$ and $\tau_{_L}$, while circular trajectories are anticipated with non-equal torques. The simulation

TABLE 3.1: The dynamic model parameters used in simulation

Kinematics	$\bar{\bar{x}} = 0.2$	$\bar{\bar{y}} = 0$
	$b = 0.3$m	f $= 0.35$m
	$r_R = 0.15$m	$r_L = 0.15$m
Dynamics	$M = 120$Kg	$g = 9.81$m/s
	$k = 100$	$\mu_C = 0.0143$
Surface	$\mu_x = \mu_y = \mu_z = \mu_\phi = 0.3$	

results that follow demonstrate the 20 second behaviour of the open-loop model with various torque inputs.

3.5.1 A comparison: the model with and without rolling friction

Figure 3.4 presents the trajectories of point C, generated by $\tau_R = \tau_L$ on a flat surface. The simulation results of the model without rolling friction are shown in sub-plots A to C, while the equivalent with rolling friction are in sub-plots D to F. It is notable in sub-plots A and B, and correspondingly D and E, that longer distances are obtained with larger torque values, and in sub-plots C and F, that negative torques generate backward trajectories. This is consistent with the expectation. According to Hoffman et al. (2003) and Chua et al. (2010), the coefficients of rolling friction of a manual wheelchair vary significantly with the kind of floor/road surface. Typical values include $\mu_W = 0.0042$, $\mu_L = 0.0061$ and $\mu_C = 0.0143$, for wooden, linoleum and carpet floors respectively. However, higher coefficients would be expected from the heavier powered wheelchairs with smaller wheel diameters on non-normal outdoor surfaces. Considering a carpet floor with $\mu_C = 0.0143$ in sub-plots D to F, an error of 20.15% in terms of the distance covered is observable in sub-plot A without the rolling

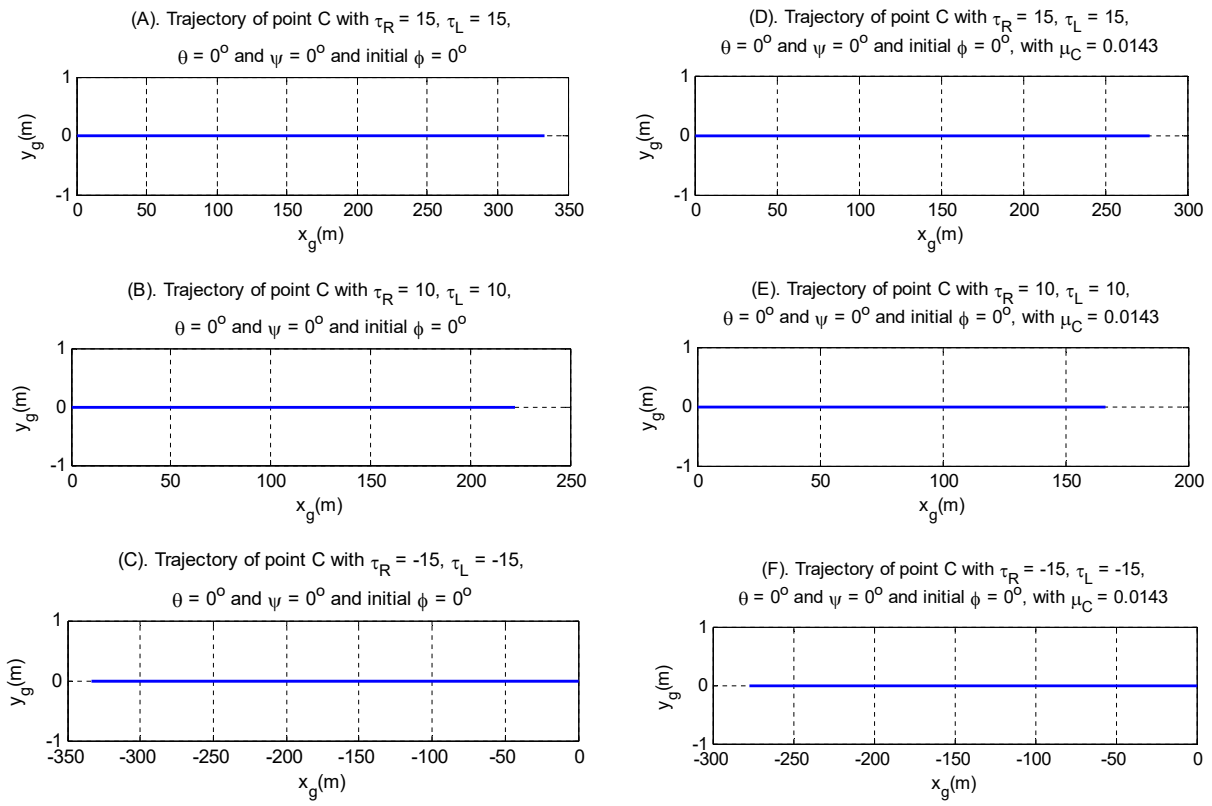

FIGURE 3.4: Straight line trajectories of wheelchair's centre of mass generated by torques $\tau_R = \tau_L$ on a flat surface from coordinate [0 0 0] in 20 seconds.

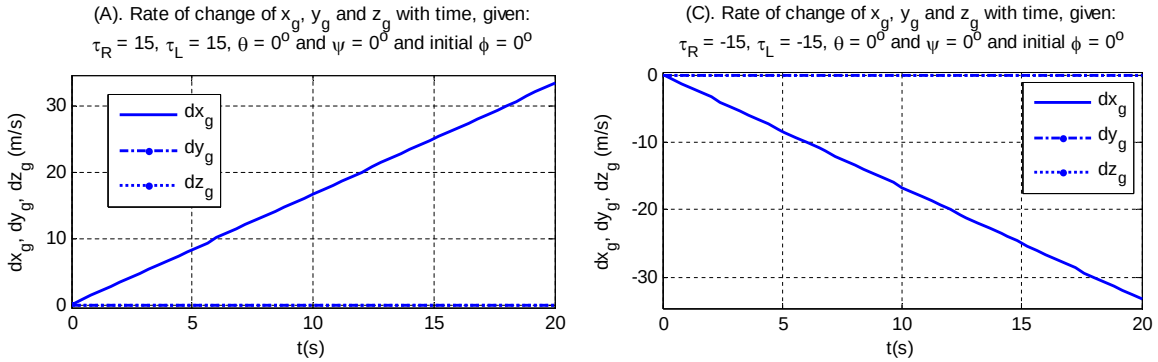

FIGURE 3.5: The velocity curves for trajectories (A) and (C) respectively in Figure 3.4.

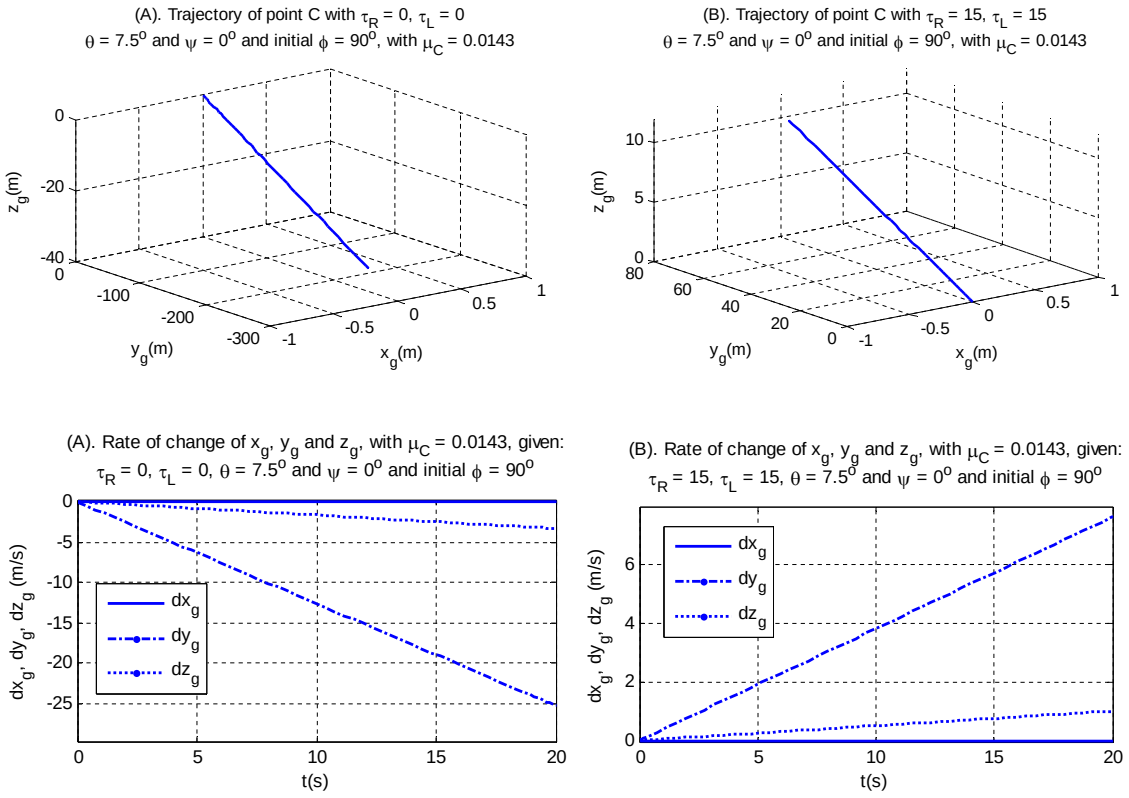

FIGURE 3.6: Straight line trajectories and rates of change of x_g, y_g and z_g generated from an inclined surface form an initial wheelchair position of [0 0].

friction as compared to sub-plot D with the rolling friction. Figure 3.5 presents the change rates of x_g, y_g and z_g for trajectories A and C for clearer perception of the model.

3.5.2 A comparison: the model with and without gravitation effects

The straight line trajectories and the corresponding change rates of x_g, y_g and z_g, generated from an inclined surface with $\theta = 7.5°$ and $\psi = 0°$ are shown in Figure 3.6. In both plots, the initial position is [0 0 0] with $\phi = 90°$. The wheelchair rolls backwards in sub-plot A when $\tau_R = \tau_L = 0$ due to gravitational potential, while in sub-plot B, the torques are high enough to enable frontwards motion. Comparing

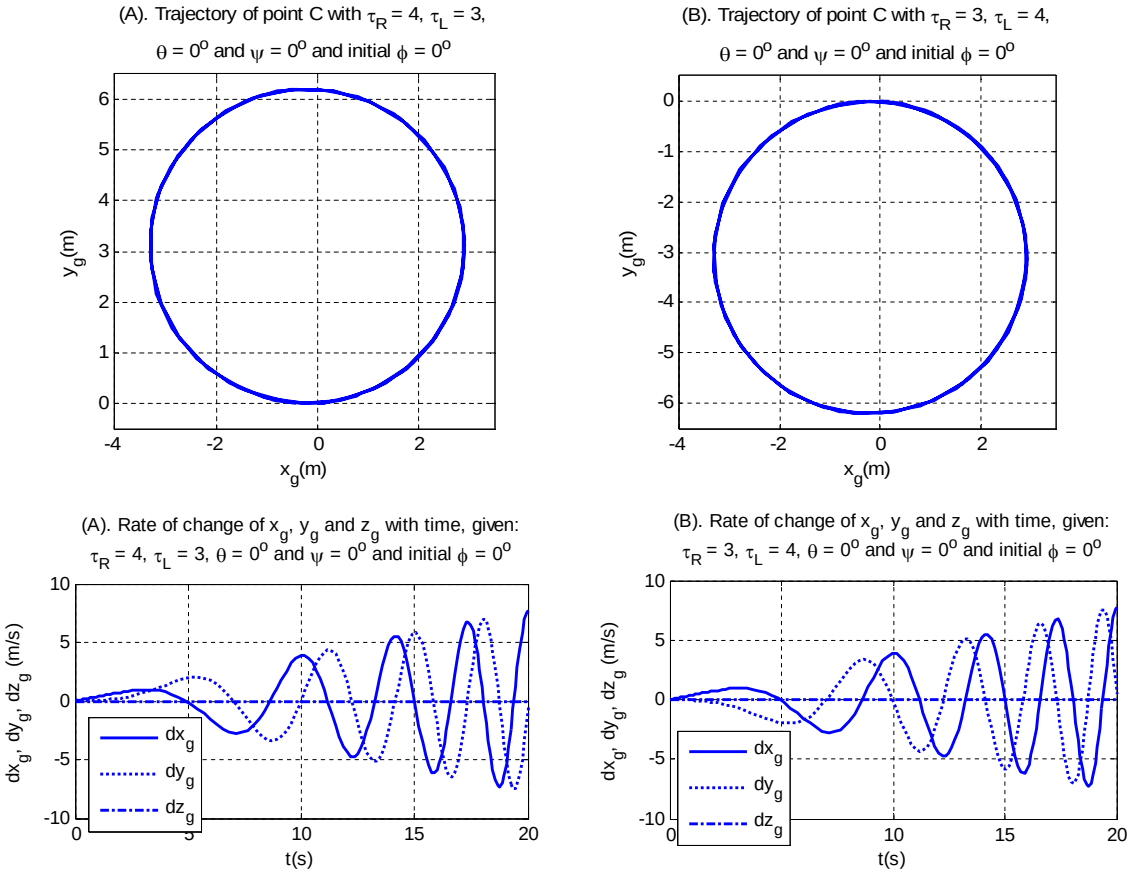

FIGURE 3.7: Circular wheelchair trajectories and rates of change of x_g, y_g and z_g generated on a flat surface from initial position [0 0] and initial direction $\phi = 0°$ with τ_R and τ_L equal to 4 and 3, and 3 and 4 in the first and the second sub-plot respectively.

sub-plots B in Figure 3.6 with D in Figure 3.4, in terms the distance covered given the same amount of torque and coefficient of rolling friction, one observes that the gravitational potential accounts for about 250% of the distance lost. A matching comparison between Chénier et al. (2015)'s recent model and the presented simulation model could not be possible in the absence of the user's propulsive-moment data. However, it may be observed that although the aforementioned model is based on experimental analysis, which makes its results more valid, its evaluation only regards manual propulsion, and does not consider the varying gravitational influence of inclined planes. Neglecting the contributions of both rolling friction and gravitation potential could therefore be inadequate in the dynamic model.

Two circular trajectories with their corresponding velocities are depicted in Figure 3.7. In the first case (case A) the wheelchair turns leftwards due to high τ_R as compared to τ_L while in the second case (case B) the opposite is true. Although not presented due to space limitation, simulation results show that the smaller the torque difference between the right and left wheels, the larger the radius of the circular trajectories and vice versa. Besides, circular trajectories of the same radius generated by equal but opposite τ_R and τ_L on flat surfaces have also been noticed, consistent with the expected behaviour.

The situations exemplified in Figure 3.8 arise on inclined surfaces, whenever the initial orientation is neither directly up nor directly down the slope. With $\tau_R = \tau_L = 3$ when the initial orientation is perpendicular to the direction of the slope, the S-shaped trajectory depicted in sub-plot A results. The left wheel, being raised compared to the right, has a higher potential energy which due to the force effect results in faster rotations. The wheelchair thus turns and a curved trajectory is observed. In the new direction, the right wheel is raised. Having a higher potential energy, it rotates faster than the left resulting in the second turning effect. This repetitive process generates the S-shaped trajectory. In sub-plot B, a larger torque is supplied to the right wheel to generate a counter-clockwise circular trajectory. The high torque overcomes the stronger gravitational effect on the raised wheel, the right wheel therefore rotates faster and a circular trajectory begins to form. However, when the right is raised compared to the left, its gravitational force together with its high torque creates a faster left turning effect and the wheelchair turns earlier. This generates the moving circular trajectory which seems to retard as the forces tends to equilibrium.

The explanation given for sub-plots A in the Figures 3.8 and 3.6 applies to first and second sub-plots in Figure 3.9 respectively. However it is important to notice the trajectory flip that resulted because of the initial $\psi = 90°$.

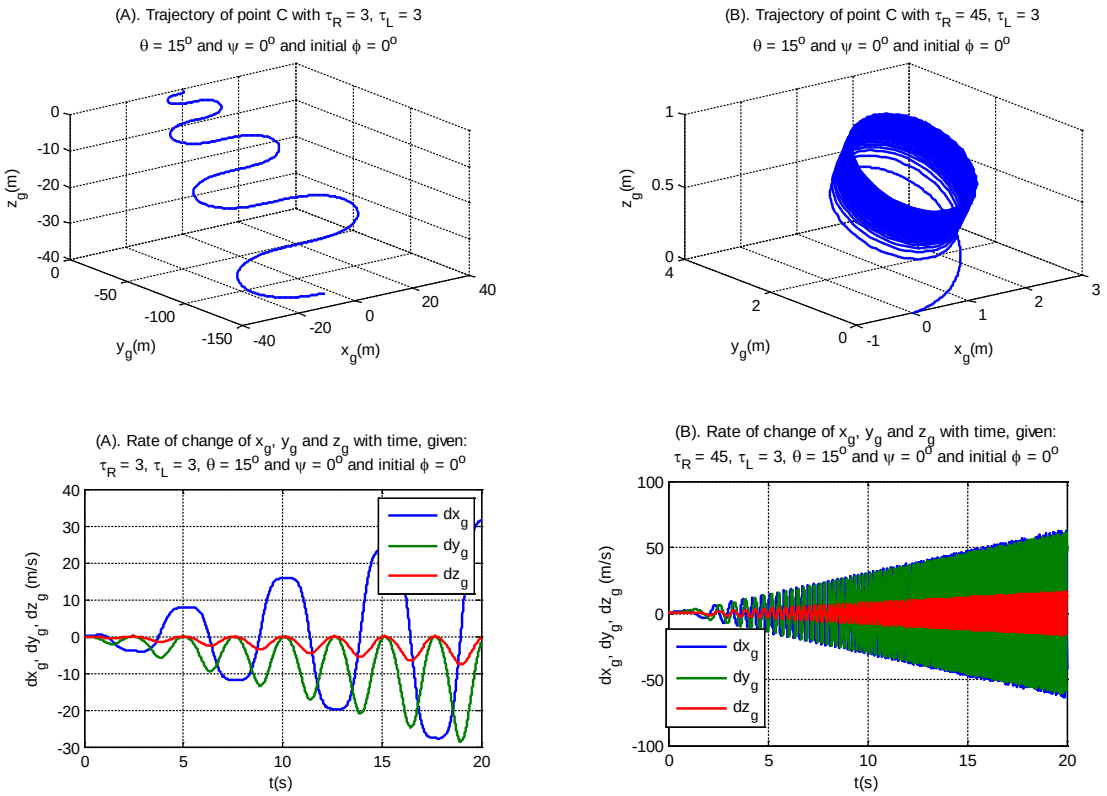

FIGURE 3.8: Trajectories and velocities generated when initial wheelchair orientation is neither directly up nor directly down the slope. The simulation have been conducted on a surface inclined by $\theta = 15°$ and $\psi = 0°$ from an initial [0 0] wheelchair position.

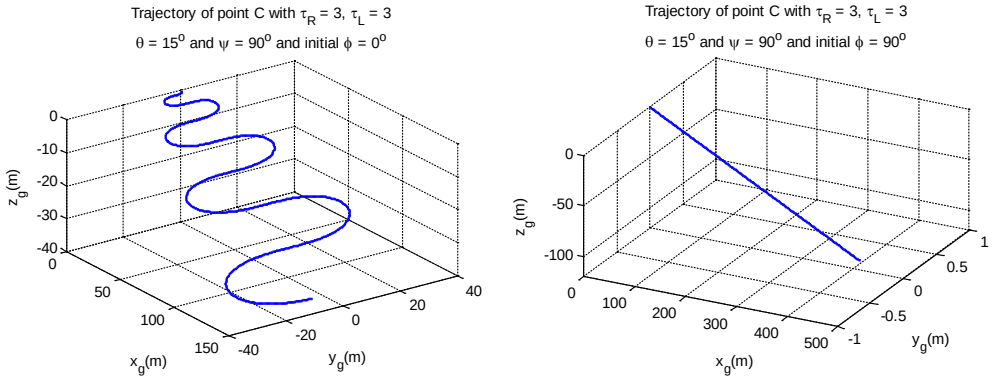

FIGURE 3.9: The trajectory observed due to ψ on a surface inclined by $\theta = 15°$ and $\psi = 90°$ from an initial [0 0] wheelchair position.

3.5.3 A comparison with other differential drive models

Table 3.2 compares the wheelchair model presented in this thesis with the previous models available in the literature, based on model's comprehensiveness and the employed modelling approach. The comparison is however limited to differential drive structures of wheeled-mobile systems with two front castor wheels.

TABLE 3.2: A comparison of the presented wheelchair model with other wheelchair models.

Study	Dynamic	Surface configuration		Frictional effects	Slip detection
		Non-inclined	Inclined		
Tashiro & Murakami (2008)	✓	✓			
Wang et al. (2009)	✓	✓	✓		
Onyango et al. (2009a)	✓	✓	✓		
Onyango et al. (2009b)	✓	✓	✓	✓	
Chénier et al. (2011)	✓	✓		✓	
Chénier et al. (2015)	✓	✓		✓	
Johnson & Aylor (1985)	✓	✓		✓	
Emam et al. (2007)	✓	✓			✓
The presented model	✓	✓	✓	✓	✓

3.5.4 Simulation with a slipping disturbance

By introducing a random slipping velocity, the deviations depicted in Figure 3.10 on a flat surface are observed. The simulation results depict the effect of slip in the open-loop model. A random slip introduces a disturbance that affects the model's ability to track the expected trajectory from the wheel torques. This therefore demonstrates the importance of a closed-loop model that takes into consideration/compensates the slipping disturbances. However, further experimental assessment using the encoders to estimate the slipping velocity according to the previous proposal may still be necessary for supplementary verification. Although the simulation results of the open-loop

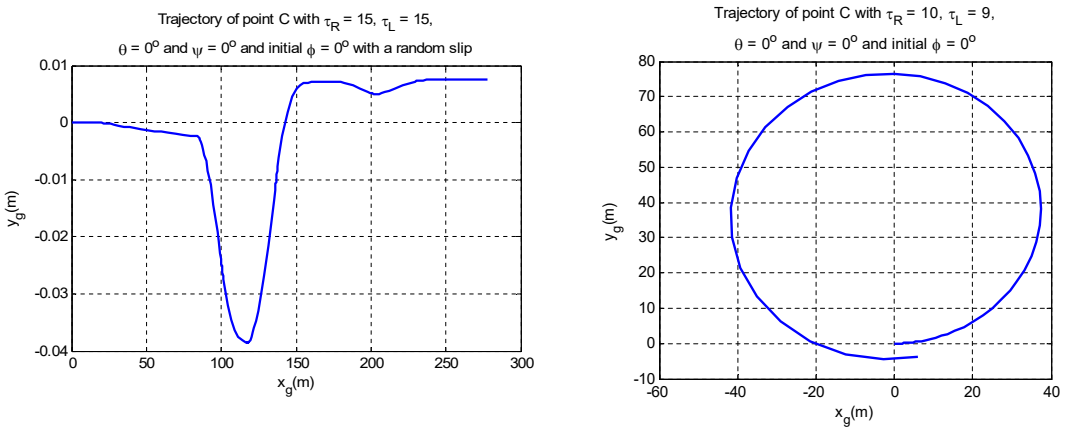

FIGURE 3.10: Resulting deviation from the intended trajectory on a flat surface with slight slip introduced into the model.

model are largely consistent with the expected behaviour, it is important to acknowledge the singularity effects of the time derivatives of Euler angles. The analysis and interpretation of simulation results involving such derivatives could sometimes be very complex. As a result, only trivial cases with $\dot{\psi} = 0$, $\psi = 90°$ or $\psi = 0°$ have been considered in the analysis.

3.6 Conclusions

This study intended to develop a comprehensive dynamic model that takes into consideration the effects of gravitational forces on inclined and non-inclined surfaces as well as the contributions of rolling friction. This also involved the estimation of slipping parameters and formulation of slipping velocities. A new dynamic model is therefore presented. With the simulation results that show consistency between the dynamic model's and the expected wheelchair behaviour, it is believed, that the new dynamic model gives a better representation of a real wheelchair. The introduced method of wheel-slip detection with a reduced number of slip detection encoders is

also considered a simple and cost effective solution. The dynamic model is therefore presumed to be comprehensive enough to enable accurate design, testing and validation of assistive controllers, to improve the wheelchair's safety and steering-ease.

Chapter 4

A DRIVING BEHAVIOUR MODEL OF ELECTRICAL WHEELCHAIR USERS

4.1 Introduction

According to Fehr et al. (2000), some powered wheelchair drivers still experience steering challenges and manoeuvring difficulties that limit their capacity to navigate effectively. Such drivers require steering support and assistive systems to supplement their steering capability. Besides, for a driver to appreciate fully the assistance of a steering support system, it may be necessary that the assistive control is adaptable to his/her steering behaviour. This chapter contributes to wheelchair steering improvement, by modelling the driving behaviour of a powered wheelchair user for wheelchair control. More precisely, the modelling is based on the improved directed potential field (DPF) method for trajectory planning. The proposed framework has facilitated the formulation of a simple driving behaviour model that is also linear in parameters. In the identification of the driving model's parameters, the steering data generated from the virtual worlds of an augmented wheelchair platform, is used. The estimation of parameters is facilitated by the least square method, with regression analysis results that accurately depict the observed driver-specific steering behaviours.

4.1.1 Background and Motivation

The manoeuvring difficulty experienced by wheelchair drivers with Parkinson's disease, multiple sclerosis and related handicaps is the main motivation in this chapter.

Such handicaps complicate the ability to effectively manipulate a conventional joystick, even within fairly simple environments (Eizmendi et al., 2007). According to Fehr et al. (2000), about 40% of the drivers struggle to steer standard powered wheelchairs with ordinary user interfaces. Fehr et al. (2000) further observe, that close to 50% of the affected user group can be assisted if better control methods, with supplemented user interfaces and/or support systems capable of accommodating their needs and preferences, were employed. Huge research on joysticks and related interfaces, including haptic systems, have emerged (Wei et al., 2011; Dicianno et al., 2010; Trujillo-León & Vidal-Verdú, 2014; Sorrento et al., 2011; Bauer et al., 2008), and new control models are continuing to develop (Ju et al., 2009; Vanacker et al., 2007). The available driving models, however, suffer lack of individuality, focusing mostly on common driver attributes, and assume that all drivers respond to particular navigational situations by similar general patterns (Diehm et al., 2013). Such driving models employ general parameters that barely correspond to measurements obtained from extreme drivers, and hardly take into consideration the contextual nature of human response to stimuli. Besides, the available control and assistive techniques rarely consider the fact that the steering capability of drivers with degenerative conditions (like ageing) deteriorate progressively over time. Adapting the wheelchair to the driver's best steering behaviour may simplify the general steering task and limit the steering troubles attributable to a worsening disability condition. This necessitates the modelling and identification of the driver's steering behaviour.

This chapter contributes to wheelchair driving by formulating a simple driving behaviour model that is also linear in parameters. The complexity of the steering model is considered instrumental in determining whether the model is usable on-line for real-time adaptation, or off-line for periodic or permanent adaptation. The driving model's derivation is based on deductive reasoning from known steering operations and systematic relationships between the driver's observable actions and wheelchair

reactions, taking into consideration the prevailing environmental situation. It, however, shuns the consideration of social events that occur within the driver's mind. To capture the driver's adaptable demands and preferences at the control and tactical levels, the driver-specific parameters are identified. The steering data generated from the augmented virtual-reality wheelchair platform, known as Virtual-Space 1 (VS-1), at FSATI[1] in TUT[2] (Steyn et al., 2013), is utilised. The identified parameters are then used to curve-fit and compare the model against other generated data. Due to its simplicity and linearity, the proposed model can be used as well in wheelchair self-tuning adaptive control, to observe the preceding behaviour and self-tune the control parameters to fit the observation.

The chapter is organised as follows: Section 4.1 has presented the background and motivation for modelling the driving behaviour of a wheelchair user. Section 4.2 presents a few approaches that have previously been used to represent the drivers' path planning behaviours, including the existing wheelchair driver behaviour models. Simulator evaluation is discussed in Section 4.3, while the driving behaviour model's formulation is presented in Section 4.4. In Section 4.5, the statistical analysis of the proposed driver behaviour model and its comparison to the generated data is discussed. Finally, the conclusion is presented in Section 4.6.

4.2 Path planning and driver adaptation models

The driving process often begins when the driver has conceived a desired path to the destination. This involves careful consideration of the entire workspace. Based on the associated constraints, the conception process may be accomplished either fully in advance before setting out the journey, or partly before, and continuously while

[1]FSATI is an acronym for French South-African Institute of Technology.
[2]TUT is an acronym for Tshwane University of Technology.

driving. Path planning for robotic automation has been achieved in the literature by deliberate and reactive planners (Zeng et al., 2015; Gamarra & Guerrero, 2015).

The deliberate path planning methods that consist of cell decomposition, road-maps and evolutionary algorithms ensure prior plan of the whole journey, but entail expensive computations that limit their practical implementation in higher dimensional configurations. As a result, they are commonly applied in confined environments. On the contrary, the reactive planners provide cheap trajectory planning algorithms based on the local (sensor captured) information. These planners ensure both faster and real-time information update, and reactive response to stimuli. In consequence, they are commonly used to represent the drivers' reactive behaviours towards the surrounding risks. Nonetheless, the paths obtained from these approaches may not be optimal, and the vehicle could be trapped into local minima. The use of reactive planners, in global or local path planning, is therefore considered inefficient without deliberate planners. As a result, hybrid path planning approaches that integrate the reactive and deliberate planners into unified structures have been proposed to overcome the drawback of the individual planners (Masehian & Sedighizadeh, 2007).

Although driving involves both global and local planning, the actual control or steering behaviour may be considered local, characterised by the drivers' reactive adaptations in response to perceived risks and undesired situations. For this reason, the reactive path planners have been used in the formulation of driver obstacle and collision avoidance behaviours. Furthermore, in wheelchair steering, the common limitations of reactive planners are naturally eliminated because the driver is personally available to solve the unknown trajectory as well as the global and non-optimality problems.

The reactive path planning approaches consist of nearness diagram, dynamic window, velocity obstacle and potential field. The strength of the nearness diagrams

approach is based on the situation analysis performed to select the new direction of motion that reduces the local minima. The dynamic window and velocity obstacle approaches operate in the vehicle's velocity space, by admitting all velocities that allow stopping without collision. However, they are more computationally intensive (Fraichard, 2007). The velocity obstacle approach also requires complete knowledge of other agents in the environment, including their future dynamics. Besides, the implementation of their analytical solutions is more difficult with environmental uncertainties and noisy data (Kruse et al., 2013). On the contrary, the potential field method is known to be 'elegant' and compatible to most real-time problem solving tools with minimal computational demands.

4.2.1 The potential field method

The artificial potential field (APF) method is therefore considered. The APF method allocates a potential function, expressed according to Equation (4.1), in the configuration space by representing the goal as an attractor and obstacles as repellers. The APF function denoted as U_{art}, is defined as a sum of the attractive potential U_{att} and repulsive potential U_{rep}, and the resulting force function is obtained by computing the negative integral of the APF function (Khatib, 1985; Ge & Cui, 2002)

$$U_{\text{art}} = U_{\text{att}} + U_{\text{rep}} \tag{4.1}$$

The attractive force, commonly represented to attain its minimum at the intended goal, is often considered to have a direct or quadratic relationship with the goal distance X_{goal}, while the repulsive potential is assigned an inverse relationship with the square of the obstacles distance X^2_{obst}. In the literature, the following representations are commonly used to express the repulsive potential:

Minimum distance representation: where the repulsive force is computed out of the minimum distance between the obstacle and the vehicle at each time instant k according to Equation (4.2). The positive constant, k_{o}, scales the repulsive potential, while $\mathrm{X}_{\mathrm{obst}}(\mathbf{r}, \mathbf{r}_{\mathrm{obst}})$ represents the distance between the vehicle at position $\mathbf{r}$, and the obstacle at position $\mathbf{r}_{\mathrm{obst}}$.

$$\mathbf{F}_{\mathrm{rep}_k} = k_{\mathrm{o}} \frac{1}{\min\left(\mathrm{X}^2_{\mathrm{obst}_k}\right)} \tag{4.2}$$

Multiple distance representation: where several i equidistant points on the obstacle are selected, and a repulsive force directed towards the vehicle is computed at each time instant k, according to Equation (4.3).

$$\mathbf{F}_{\mathrm{rep}_k} = \sum_{i=1}^{N} k_{\mathrm{o}} \frac{1}{\mathrm{X}^2_{\mathrm{obst}_{i_k}}} \tag{4.3}$$

Representation with restricted radius of influence: Both minimum and multiple distance representations may introduce unnecessary obstacle effects on the vehicle when the distance, $\mathrm{X}_{\mathrm{obst}_i}$, is large enough to allow safe passage. Latombe (1991), therefore, proposed an adjustment to the conventional repulsive potential by limiting the radius of influence $\mathrm{X}_{0_{\mathrm{obst}}}$ of the obstacle to eliminates the unnecessary influence.

$$U_{\mathrm{rep}} = \begin{cases} \frac{1}{2} k_{\mathrm{o}} \left(\frac{1}{\mathrm{X}_{\mathrm{obst}}} - \frac{1}{\mathrm{X}_{0_{\mathrm{obst}}}} \right) & \mathrm{X}_{\mathrm{obst}} \leq \mathrm{X}_{0_{\mathrm{obst}}} \\ 0 & \mathrm{X}_{\mathrm{obst}} > \mathrm{X}_{0_{\mathrm{obst}}} \end{cases} \tag{4.4}$$

DPF: This approach proposed by Taychouri et al. (2007) is of special interest. Although it uses the distance representation methods and takes the obstacle's position and direction of motion into account, it also allocates maximal repulsive potential whenever the vehicle is moving directly towards the obstacle, and

negligible potential whenever the obstacle is at right angle to the direction of motion. Due to its strength and ingenious simplicity, the DPF formulation in Equation (4.5) is considered to represent the subjective risk function of the driver's steering behaviour, where m is the gain constant and ϕ_i is the angle between point i of the obstacle and the direction of motion of the vehicle.

$$\mathbf{F}_{\mathrm{rep}_k} = \sum_{i}^{N} k_{\mathrm{o}} \frac{(\cos \phi_i)^m}{\mathrm{X}^2_{\mathrm{obst}_{i_k}}} \tag{4.5}$$

4.2.2 DPF and other modified APF methods: A comparison

The non-globality (i.e. local minima and trap situations), non-optimality, and goals non-reachable with obstacles nearby (GNRON) (Raja et al., 2015; Montiel et al., 2014; Ahmed & Deb, 2013) are the primary causes of discontent that have seen several modifications in the APF approach. One of the recent APF modifications is the evolutionary artificial potential field (EAPF) method, which integrates APF with genetic algorithms to derive an optimal potential field function, that ensures global planning without local minima (Vadakkepat et al., 2000). The model uses multi-objective evolutionary algorithm (MOEA) to identify the most optimal potential field function, and escape force algorithm to avoid local minima. The other modification is the concept of parallel evolutionary artificial potential field (PEAPF) introduced by Montiel et al. (2014), as a new path planning method in mobile robot navigation. PEAPF improves the earlier EAPF method by making the controllability of the vehicle in real-world scenarios with dynamic obstacles possible. The recent bacterial evolutionary algorithm (BEA), also compares closely with PEAPF, introducing an enhanced flexible planner to improve the EAPF method (Montiel et al., 2015). While these algorithms always provide solutions for the APF drawbacks, the logical consideration of these modifications with regard to real-time applications turns

out, in most cases, to be unrealistic because the resulting models involve expensive computational steps (Barraquand et al., 1992).

Because the driver is always available in the wheelchair to solve the APF limitations, the important considerations in the approach of choice for the driving model include features that enhance the model's adaptational behaviour in the local environment. Global planning at the expense of computational simplicity may therefore constitute a worthless trade-off. The features of consideration regarded in this study include computational complexity, path smoothness, context scalability, directionality and handling capability in complex environments.

Computational complexity: The implementation of a control model in a real-time application is strongly influenced by the amount time it take to compute the control signal that generates both feasible path and desired speed. According to Barraquand et al. (1992), it is more suitable to have a very fast path planner for real-time applications, than to perceive a vehicle that only learns its workspace to memorise a variety of standard paths. Thus, a finite horizon that only encompasses the perceivable workspace may be considered to increase planner's computational speed.

Path smoothness: This regards the planner's capability to interpret the dynamic and static behaviours of other agents within the workspace in order to execute the adaptive control progressively without jerks. The planner's response speed and the computed magnitude of the steering signal are very crucial in determining the quality of the resulting path. A driver model with smooth planning capability could be instrumental in the assistance of wheelchair drivers with disabilities like hand tremors and cognitive disorders.

TABLE 4.1: Comparison of the potential field modifications based on their applicability in the formulation steering behaviour of wheelchair users.

	APF	EAPF	PEAPF	BPF	DPF
Smooth planning	✓	✓	✓	✓	✓
Local planning	✓	✓	✓	✓	✓
Global planning		✓	✓	✓	
Complex environments			✓	✓	✓
Highly scalable			✓	✓	✓
Directionality					✓
Min. computational time					✓

Context scalability: It is important that only behaviours of the agents that influence the driver's subjective risk are taken into consideration. For instance, scaling down the entire workspace to an area enclosed by a look-ahead radius, and further into a smaller area encompassing only the driver's field-of-view may reduce the complexity of analysis and enhance the quality of control.

Directivity: This concerns the amount of influence imposed on the driver by virtue of the agents' position relative to the vehicle's direction of motion. Directed models enhance smoother time variations in the sensor signals to improve the quality of the resulting path.

Handling capability in complex environments: This regards the planner's computational speed, and its ability take into consideration the dynamic behaviour of other agents in the configuration space.

Table 4.1 compares the features of the recent modified potential field methods with the proposed DPF, based on their computational complexity, path smoothness, context scalability, directionality and handling capability in complex environments.

4.3 Simulator evaluation and steering data

4.3.1 Evaluation of the VS-1 simulator

The steering data required to identify the driving behaviour is generated in a simulated environment, on the VS-1 simulator depicted in Figure 4.1. The platform's basic components include the visual interface, the motion platform, and the controller (Steyn, 2014). The visual interface presents a synchronised virtual world to the user through a stereoscopic head mounted display (HMD) or a four-connected screens display. The motion platform consists of a user ramp, a roller system for the right and left driving wheels, and a stage that hosts either a powered or a manual wheelchair. Lastly, the controller interlinks the motion platform and the display unit. The roller system depicted in Figure 4.2 enables rotational motion of the wheels on the platform, and facilitates the mapping of wheel motion into the virtual world. This is aided by the rollers' force effect that results from the wheelchair's and the user's weights. Each roller system consists of a pulse generating rotary encoder, mounted to enable the determination of the wheelchair's position, velocity and acceleration in the virtual space, and to facilitate the measurement of the wheelchair's differential drive motion.

In similar simulators, the slip dynamics at the point of contact between the driving wheel and the roller constitutes a possible source of error that could lead to inaccurate representation of the wheelchair's behaviour in the virtual world. Since the absolute translational velocity of the wheelchair on the motion platform is zero, the theoretical difference between the rotational velocity of the driving wheel and the rollers is used to account for possible wheel-slip errors in the simulator. A comparison between the driving motors' current and the wheels' velocity with respect to the driving wheels' torques is also made to determine the possible instability of the wheelchair. In the

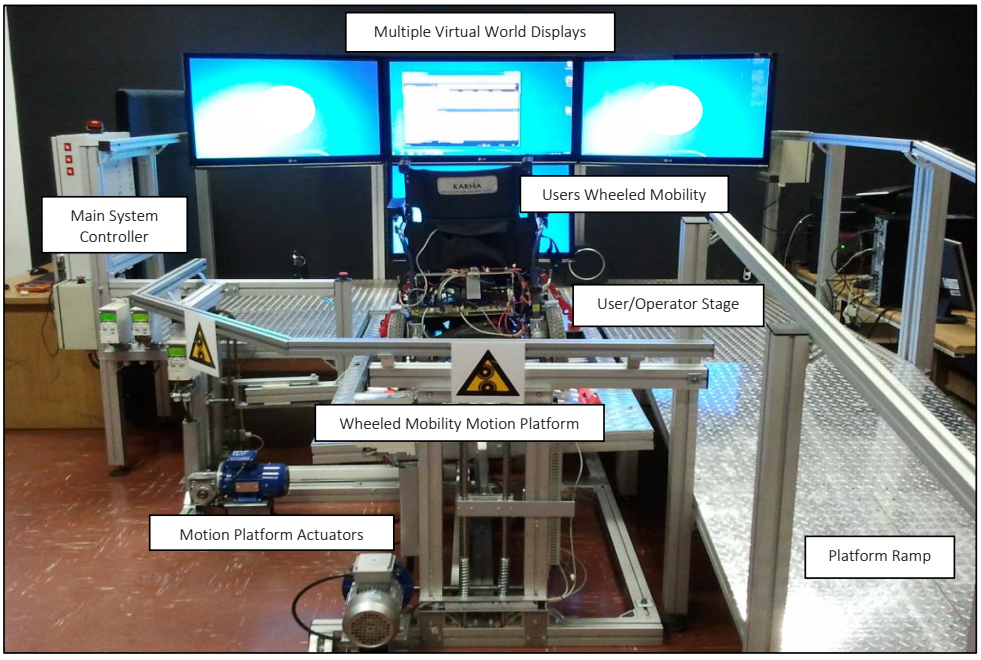

FIGURE 4.1: Virtual-reality System 1 (VS-1): The augmented virtual and motion simulator at FSATI for wheelchair simulations.

case of instability, a method for auto-mobile traction control proposed by Hori et al. (1998) is used in the stabilisation (Steyn, 2014).

The simulator possesses an important advantage of allowing full access and control of the steering variables. Besides, the following desirable characteristics of the VS-1 platform regarding this study are noted: 1) It eliminates the need for sensor installation. 2) It introduces a synchronised feeling of the pitch and roll rotational motions on flat and inclined surfaces, reducing the possibility of simulator sickness. 3) It allows the use of manual or powered wheelchair in the evaluation of steering behaviour. Moreover, the powered wheelchair can be steered using the standard wheelchair embedded joystick or any other compatible user interface. 4) Lastly, the virtual worlds can be modified to provide a close representation of a desired real environment.

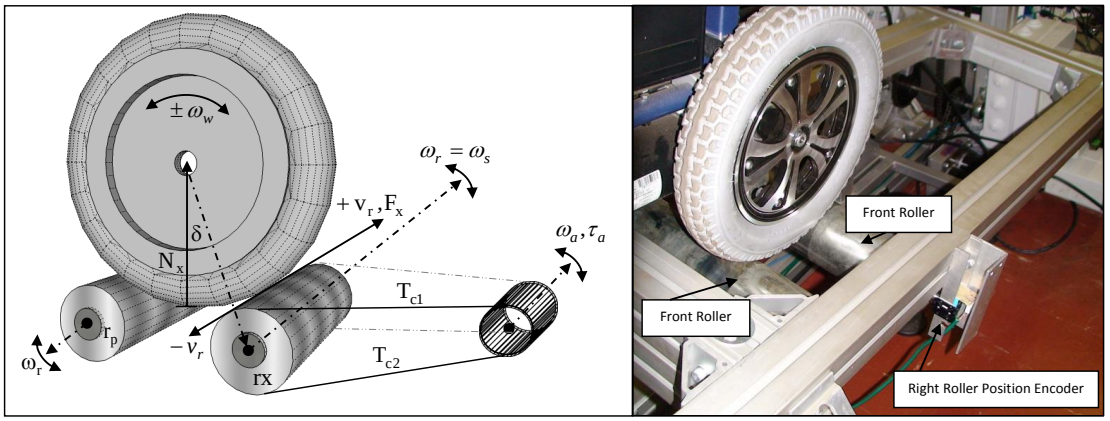

FIGURE 4.2: The roller system on the motion platform that enables both rotational motion of the wheels, and the mapping of the wheel's motion into the virtual world.

Notwithstanding the above advantages, the potential usefulness of the motion platform in the evaluation of driver behaviour, can only be acceptable if the virtual world and the impression of motion in the simulated environment conform to the real world to a certain extent. A study evaluating the participants' perception of degree of presence and comparing the usability of the simulated and reality world is conducted by Steyn (2014). The degree of presence in the simulator, compared to the real world, is evaluated in terms of spacial presence, involvement, realism and system value. A portion of evaluation outcome is presented in Figure 4.4.

Spacial presence indicates the extent to which the user acknowledges his/her existence in the environment in the actual sense, while involvement concerns the response of the simulator towards the driver inputs and the resulting motion feedback. Realism is expressed by the use of a real wheelchair and the rotational motion of VS-1 platform, while system value represents the degree to which users recognise the motion platform in general as an evaluation aid.

According to the study (Steyn, 2014), the participants experienced 75% disorientation with regard to the steering tasks and platform usage at the beginning of evaluation in

FIGURE 4.3: A user steering the wheelchair in a living room set-up in both virtual and reality environments.

both reality and simulated world. However, adaptation was much faster in both cases, with 81% adaptation rate in the reality world, and 69% in the virtual world. Based on the presented tasks, the participants observed 73% and 75% challenges/uncertainties in the reality and simulated worlds respectively. The study, thus, demonstrates a fair similarity between the steering experience observed within the virtual and reality worlds. Figure 4.3 for instance, shows a user steering the wheelchair within a living-room environment in both virtual and reality worlds during the evaluation.

Like in most simulators, the existence of cue conflicts that result from the absence of translational motion between the motion platform and the virtual world, and the sensory simulation artefacts like reduced field of view in the virtual world, must be acknowledged. Moreover, a simulation task, however important it is, will always be perceived as a simulation exercise, with few risks for careless actions and few rewards for desired behaviours. Nevertheless, studies have demonstrated the feasibility of simulation techniques, and have shown that simulation results approximate those obtained by other methods (Beare & Dorris, 1983). The relative validity of the VS-1 platform is therefore trusted as sufficient for driver behaviour assessment.

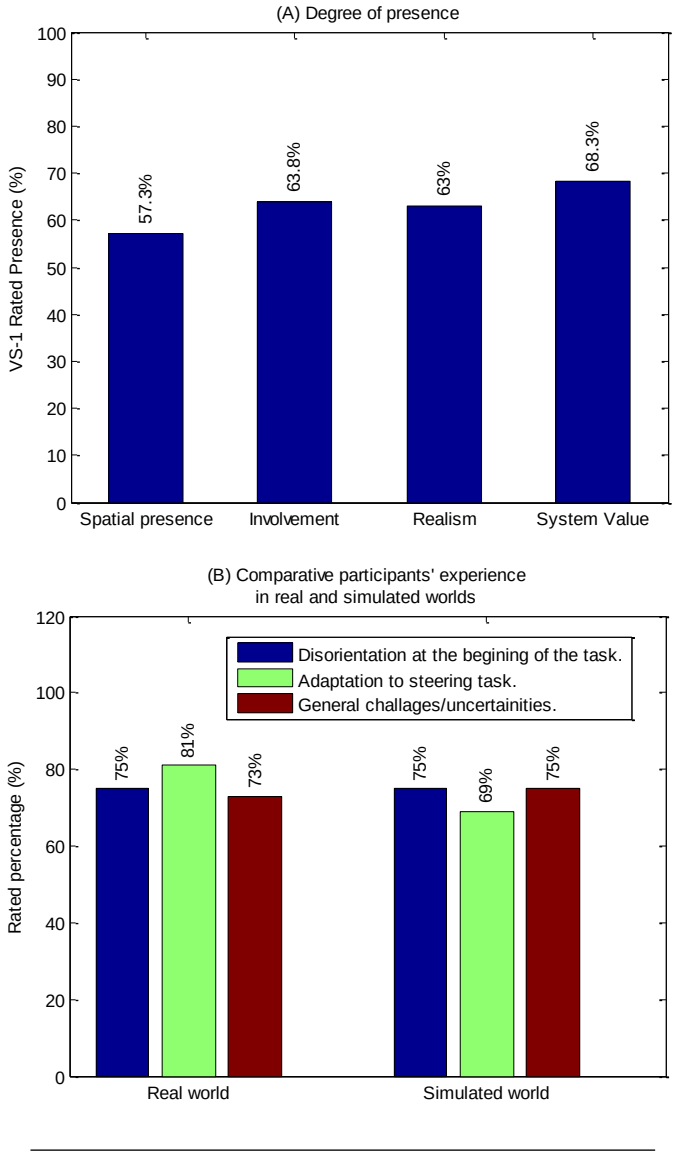

FIGURE 4.4: Virtual-reality System 1 (VS-1): The augmented virtual and motion platform at FSATI for wheelchair simulations.

4.3.2 Steering data and implied behaviour

A powered wheelchair employing the standard embedded joystick was used in the generation of steering data. In order to effectively evaluate the steering behaviours in relation to the general and familiar environments, the virtual worlds attempted as much as possible to represent the actual areas. Accordingly, seven data sets comprising the following information, were generated in similar virtual environments

on the augmented platform to represent seven different cases of steering behaviours.

1. Distance between the wheelchair and other agents (X_{obst})
2. Wheelchair velocity relative to other agents (ν_{obst})
3. Orientation of the agents relative to the wheelchair's direction of motion (ϕ_{obst})
4. Absolute velocity of the wheelchair (ν_k)
5. Yaw angle (ϕ_k), yaw rate, pitch angle and roll angle

The steering behaviour observed in the following virtual environments is described using a portion of the steering data.

4.3.2.1 A risk free environment

The word risk is used to represent objects or agents that the driver would not wish to steer over, closer to or collide into. In this environment, goal positions G_1 to G_5 are set 4m away from the starting position S, at angles 90°, 60°, 30°, 0°and -30°respectively. The wheelchair is then driven from the starting point to each goal. Initially in each trip, the wheelchair is positioned at S, oriented towards G_1. One set of the trajectories and speeds observed in this environment is shown in Figure 4.5. It may be noticed, that driving towards G_1 compared to other goals involved an initial steeper rise in the steering speed. The more skewed the goal directions relative to the initial orientation at position S, the slower initial accelerations. The explanation regarding this behaviour is considered common knowledge: that drivers constantly perceive an instantaneous look-ahead goal whose position from the vehicle is a function of the available driving space and path curvature. According to Figure 4.5, the skewed global goals involve highly curved paths at the beginning, implying that drivers prefer

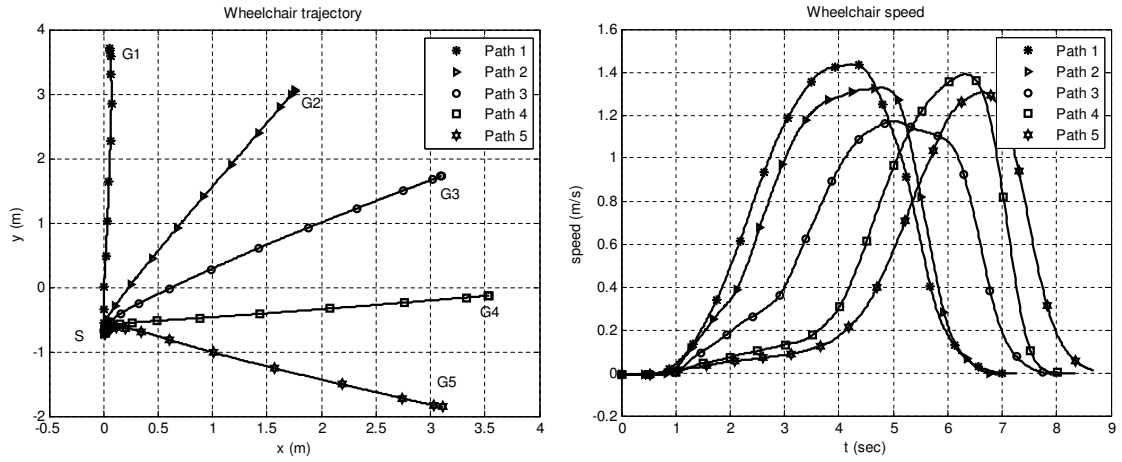

FIGURE 4.5: Wheelchair trajectories and speeds observed in a risk free environment.

to align the wheelchair to the global goal at the beginning of the journey. Once aligned, a steeper rise in the driving speed is observed. It is presumed that closer instantaneous goals with slower accelerations were considered in the curved paths, to facilitate the process of aligning the wheelchair towards the skewed global goals. The position of the instantaneous goals then shifted at accelerated rates towards the global goals as the path curvature reduced. In consequence, the local driving speed in a risk free environment is considered a function of the instantaneous goal position and path curvature. Although this pattern is observed, the rate at which the path curvature and the instantaneous goal position influences the desired speed is considered subjective.

4.3.2.2 A minimal risk environment

The second environment presumed a configuration with an object placed 4m, 8m and 12m away from the starting point in the first, second and third trip respectively. In each trip, the wheelchair is driven from the starting point, near position (0,0), in Figure 4.6, to the goal approximately 15m away. Figure 4.6 depicts the trajectories and

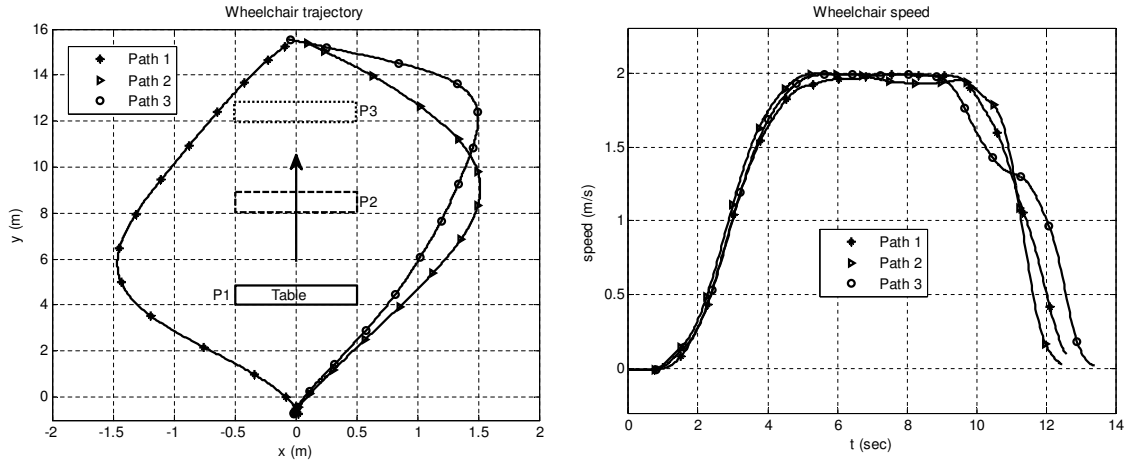

FIGURE 4.6: Trajectories and speeds of wheelchair observed in a minimal risk environment.

speeds generated in one case. It is observable that although the chosen trajectories deviated away from the observed risk, the sufficient space within the configuration enabled the consideration of paths with little effect on the desired steering speed.

4.3.2.3 A living-room environment

In this case, an example of the living-room environment depicted in Figure 4.3 and Figure 4.7 is considered. The wheelchair is steered to the goals G_1, G_2 and G_3 from the starting point S, without speed or path restrictions. Interestingly, the paths and speeds depicted in Figure 4.8 were mostly considered, with additional steering priority allocated to avoid the local risks. Also, it may be important to note that longer safer paths as opposed to shorter riskier paths were preferred; the risk magnitude in this case concerns the amount steering accuracy required to avoid collision. Additionally, in Figure 4.8 at positions A, B, C and D, the reduction in the immediate forward space along the perceived curved path and the apparent possibility of collision with furniture, compelled the consideration of closer instantaneous goals. This accordingly,

FIGURE 4.7: The considered virtual living room environment (perimeter wall not shown for clarity reason).

resulted in the steering speed reduction at the respective points as depicted in Fig 4.9.

4.4 Modelling the driving behaviour

According to the 'intentional stance' strategy, Dennett (1989) treats an entity as a rational agent having the ability to regulate its choice of action by its desires and beliefs. Dennett (1989) then defines a 'behaviour' as a goal oriented activity of an agent that can only be understood by assigning intentions or goals to the agent. The modelling of driver behaviour, therefore involves defining one of the numerous goals that the driver may want to reach, and determining the activities that the driver performs to arrive at the goal. Generally, different drivers demonstrate different driving actions and reactions within the same environment to achieve the same objective. These subjective behaviours are commonly related to the driver's

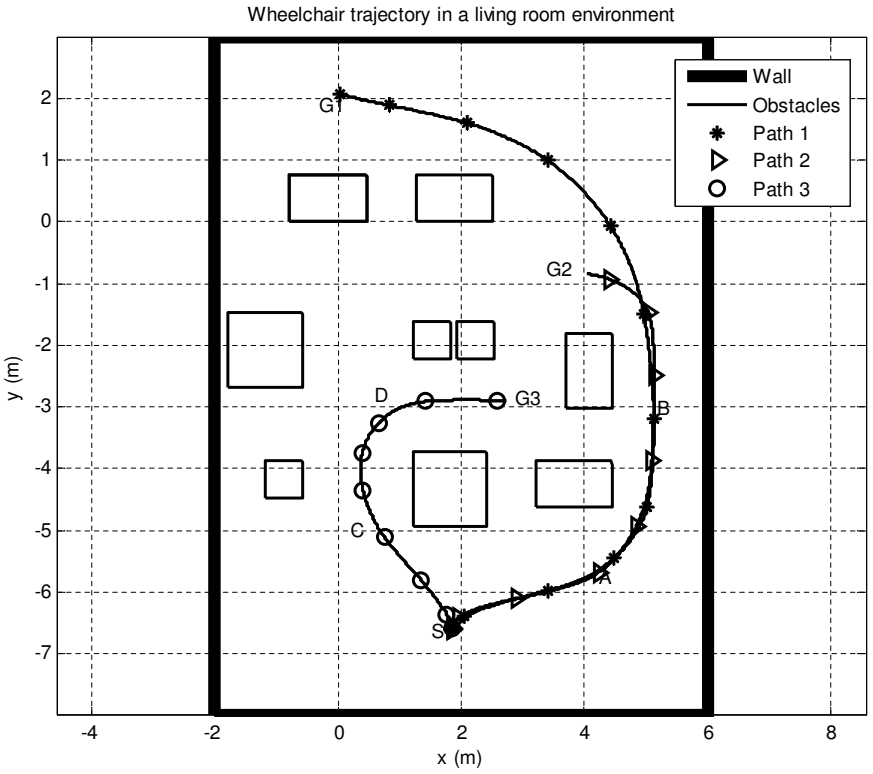

FIGURE 4.8: Wheelchair trajectories observed in a living-room environment. The rectangular shapes in the configuration space represent the living room furniture.

capability in terms of decision making (choice) and risk taking (desires), and are affected by personality, experience, state of driver, task demand and environment.

Adapting the wheelchair to exhibit the desired characteristics of the driver, taking into account the evolving and dynamic behaviour of the driver and other agents is a complex task that may be approached in the following two ways:

System training: In this case, the model learns by observing over time the way drivers execute the driving tasks. Once a task is perfectly learned, the model can proceed to learning other tasks. This approach is applicable to motor-vehicle driving, because the required tasks are well-defined, performed in regular configurations, and can be represented by heuristics. However, in the wheelchair

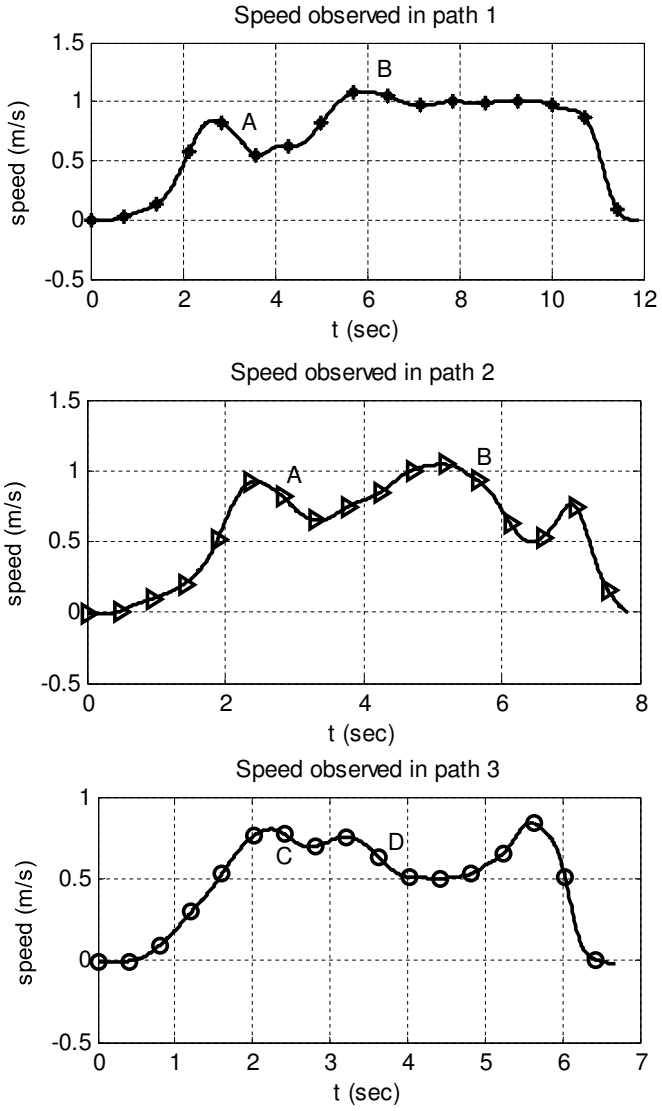

FIGURE 4.9: Wheelchair speeds observed in the living room environment.

case, the workspace is highly complex, undefined and involves tasks that lack chronological rules of execution, making system training difficult to consider.

Representing the entire driving behaviour theoretically: This is the approach considered in this study. All local tasks performed by the driver are considered together to realise the driving behaviour. The theoretical driver behaviour models of this nature are initially limited in scope, and may not perfectly represent certain specific driving tasks. However, they can be advanced over time

to closely predict the actual driving behaviour. The theoretical driver model of this nature can be validated by comparing the model's outputs against real driving data.

4.4.1 Dynamic representation of driving behaviour

Four major factors are considered to influence wheelchair driving: The first that prompts the user to exert some force, to begin or continue in motion, pertains to the difference between the actual wheelchair position and the target position (in this case the instantaneous goal). This is the primary motivating factor that instigates the driver to steer. As long as it exists, the driver is presumed to apply the driving force. The second factor influences the amount of force exerted to minimise the positional difference. This factor, the desired velocity, is related to the urgency or average time required by the driver to accomplish the driving task. The desired velocity may be considered as a function of disposition and the prevailing personal desire and priorities of the driver. The third factor concerns risk assessment and involves the driving capability and the driver's opinion of safety about the driving environment. These factors contribute concurrently to the varying driving velocity of the wheelchair towards the global goal during motion. In fact, there exist an interrelationship between the three factors: the driver establishes a subjective constant risk level, when this is exceeded, a compensation mechanism is activated. The compensatory mechanism may involve altering the position of the instantaneous goal, which then alters the direction and speed of travel. Finally, it is important to observe that the amount of force exerted is constrained by physical limits of the wheelchair. The local driving velocity, ν, is therefore limited by the maximum velocity, $\nu_{\max}$ of the wheelchair. In this study, ν is considered a function of the instantaneous goal,

$\nu_{\text{des}}(g_i)$, and environmental situation, $\nu_{\text{env}}(env)$, according to Equation (4.6).

$$\nu = |\nu_{\text{des}}(g_i) + \nu_{\text{env}}(env)| \leq \nu_{\max} \tag{4.6}$$

4.4.2 Desired steering velocity

In normal situations, drivers are believed to prefer some constant driving speeds in environments with minimal risk factors. The desired speed is a personality factor that varies from one individual to another. It is affected not only by the composition of the workspace, but also by the implied steering complexity and driver experience. The composition of the workspace introduces an aspect of risk and safety, that compels a driver to presume an adaptation mechanism that limits the perceived risk to an acceptable subjective threshold. Such adaptive mechanisms generally confine the local driving speed to a safe minimum. A discussion in this regard is presented in Section 4.4.3. On the other hand, the steering complexity pertains to influence of complex orientational manoeuvres involved in the steering task, including the effects path curvature.

Disassociating the influence of environmental risks from the desired speed, and considering the speed as a function of the steering complexity alone, results in Equation (4.7), that expresses the desired velocity as a function of path curvature in the direction of the instantaneous goal. As presented, the desired velocity in a risk free environment only takes into consideration the observable variables (i.e. path curvature and the instantaneous goal direction) that have systematic relationships with the driver's steering behaviour. The formulation avoids the effects of non-quantifiable subjective factors including the driver's experience and task urgencies that are also

know to influence the driving behaviour.

$$\nu_{\text{des}} = V_{\text{des}} \cos^{p}(\phi_{k} - \phi_{k-1})\bar{\mathbf{e}} \tag{4.7}$$

In Equation (4.7), p is a constant, V_{des} is the desired driving speed, ϕ_{k} is the orientation of the wheelchair at the time instant k. The function, $\cos^{p}(\phi_{k} - \phi_{k-1})$, represents the influence of path curvature on the desired speed, and $\bar{\mathbf{e}}$, expressed in Equation (4.8), is the direction of desired velocity.

$$\bar{\mathbf{e}} = \frac{\mathbf{r}_{L_k} - \mathbf{r}_k}{|\mathbf{r}_{L_k} - \mathbf{r}_k|} \tag{4.8}$$

In Equation (4.8), $\mathbf{r}_{L_k}$ is the position of the instantaneous/look-ahead goal, while $\mathbf{r}_k$ is the instantaneous position of the wheelchair.

4.4.3 Influence of risk and driver adaptation mechanisms

Collision or threat avoidance and goal-seeking reactions constitute the driver's fundamental behaviours. Indeed, the capability of wheelchair drivers is commonly evaluated based on their dexterous ability to avoid threats and collisions when driving. Besides, common wheelchair accidents that have resulted in severe damages and injuries to the driver, can be related to collision. Collision avoidance is, therefore, elemental to the driver's and wheelchair's safety. Drivers often presume some constant risk thresholds and safety margins to observe in the vicinity of danger during steering. When such thresholds are exceeded, certain risk-compensating mechanisms are initiated to minimise the risk level. In the Taylor's risk-speed compensation model (Taylor, 1964), it is observed that drivers regulate their driving speeds in accordance with the magnitude of the perceived risk in such a way that larger magnitudes result in slower speeds. To adapt the wheelchair to such behaviours and eliminate the

common variations in the drivers' level of attention, proper risk detection systems need to be instituted on the wheelchair. The following two hypothesis are considered in this thesis as the main adaptation references that drivers commonly presume to confine wheelchair within the limits of safety.

1. Time-to-risk (TTR)

2. Distance-to-risk (DTR)

The time-to-contact with a risk, is influenced by the distance and speed of travel of the wheelchair towards the risk. The consideration of TTR naturally implies that the wheelchair can basically reach or get very close to an objects at very low velocities. On the other hand, with DTR, the driver maintains a comfortable distance from the risk. The expression in Equation (4.9) is considered to represent the drivers' risk avoidance behaviour in the configuration space.

$$\nu_{\text{env}_k} = -k_{\text{env}} \sum_{i=1}^{N} \frac{\cos^m \left(\phi_{\text{obst}_i} - \phi_k \right)}{\mathcal{A}_i^n} \tag{4.9}$$

In Equation (4.9), k_{env}, m, n and N are constants, ϕ_{obst_i} is the instantaneous direction of point i on the risk from the position of wheelchair, ϕ_k is wheelchair direction at the time instant k, while $\mathcal{A}$ is the adaptation mechanism presumed by the user. Figure 4.10 depicts the variation of Equation (4.9) with respect to the different positions and directions of the risks in the workspace, with DTR presumed as the main adaptation reference. The strength of Equation (4.9) is based on the idea that the driver's steering behaviour is affected, mostly, by the risks within the field of view. The risks considered closer and directed to the driver have greater influence compared to those viewed as skewed and further away. It, therefore, scales down the workspace to a smaller workable field of consideration. Taking both Equations (4.7) and (4.9) into

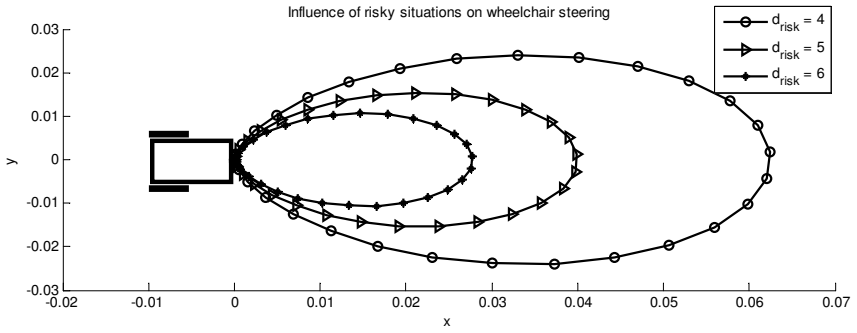

FIGURE 4.10: Influence of risky situations on wheelchair steering with m and $n = 2$, and with distance-to-risk d_{risk} considered as the main adaptation reference.

account, the model considered to represent the local driving behaviour of a wheelchair user may be expressed by Equation (4.10).

$$\nu_{k+1} = \nu_k + k_\nu \left(\nu_{\text{des}} - \nu_k\right) - k_{\text{env}} \sum_{i=1}^{N} \frac{\cos^m \left(\phi_{\text{obst}_i} - \phi_k\right)}{\mathcal{A}_i^n} \tag{4.10}$$

4.5 Simulation, results and discussion

4.5.1 Parameter identification and adaptation mechanism

The linearity of Equation (4.10) in the parameters has facilitated the use of ordinary least squares method in the identification of parameters. The moving average filter with a span of 20 was also considered in the smoothing of generated data. The result of the model's regression analysis is presented in Table 4.2, where the DTR criteria presented in Equation (4.11) is considered as the primary adaptation mechanism presumed to avoid collision risks, and also in Table 4.3, where TTR in Equation

(4.12) is the primary adaptation mechanism:

$$DTR_k = \mathrm{X}_{\mathrm{obst}_{k_i}} \bar{x} + \mathrm{X}_{\mathrm{obst}_{k_j}} \bar{y} \tag{4.11}$$

$$TTR_k = \frac{\mathrm{X}_{\mathrm{obst}_{k_i}}}{\nu_{k_i}} \bar{x} + \frac{\mathrm{X}_{\mathrm{obst}_{k_j}}}{\nu_{k_j}} \bar{y} \tag{4.12}$$

Regarding Equations (4.11) and (4.12), $\mathrm{X}_{\mathrm{obst}_k} = \mathbf{r}_{\mathrm{obst}} - \mathbf{r}_k$ is the instantaneous distance between the risk at position $\mathbf{r}_{\mathrm{obst}}$ and the wheelchair at position $\mathbf{r}_k$, while ν_k is the instantaneous velocity of the wheelchair.

Table 4.2 contains the identified parameter values, constant p, standard error (in value and percentage), t-statistics, maximum deviation between the fitted and the generated data, and coefficients of determination of the analysis for each of the seven data sets. The optimised values of constants m and n used in the identification process are 4 and 2 respectively. These values represent a pair that resulted in the highest coefficient of determination with regards to majority of the presented cases. The value of constant m, according to Figure 4.10, defines the shape of the contours along which risks possess the same magnitude of influence on the driver. A higher value represents a driver who is less bothered about the skewed risks and more concerned about the risks perceived along the direction of wheelchair orientation. Referring to Equation (4.9), $m = 1$ produces a circular contour, while higher values ($m > 1$) results in oval contour shapes. The high value of constant m considered in the identification process thus represents a reduced influence of side risks on the driver's steering behaviour. Constant n, on the other hand, determines the magnitude of influence of the risks based on the presumed adaptation mechanism. Higher values imply that the magnitude of influence is considerably high within the close neighbourhood of the observed risk, but negligible outside.

In parameter identification, the navigation data generated in Section 4.3, have been

utilised. Of the data, 85% are used in the identification of the driver-specific model parameters to ensure that the observed values represent well the natural driving behaviour, while only 15% is used in the curve fitting validation. The observed values of coefficient of determination R^2, in Table 4.2 demonstrate how well the model replicates the generated data. Besides, the resulting large values of t-statistics establish the significance of the identified coefficients of the driver behaviour model. It is noticeable that higher values of t-statistics corresponding to k_ν as compared to k_{env} are obtained, indicating the general stronger impact of the driver's desired velocity compared to risks avoidance. This is presumed to have resulted from the drivers' subjective goal reaching urgencies during steering. The variability of ν_{des} with respect to each of the presented seven cases demonstrates the importance of identifying the individual's driving behaviour, denoting the different preferred driving speeds.

Table 4.3 adopts the TTR criteria, and considers the constants presented in the previous table to compare and determine the relevance of the two hypothesised risk adaptation mechanisms. The observed results are found to be very close to those in Table 4.2. Nonetheless, the slightly lower values of coefficient of determination and t-statistics obtained with TTR may be realised. Besides, the model parameters in Case 6 and 7 may not represent the actual driving behaviour because ν_{des} and k_ν are negative, and the identified desired velocity in Case 7 is unreasonable. These may have resulted from the driver's preferences and their choice of the adaptation criteria. For instance, because of the slow wheelchair speed, drivers with confidence in the braking system may only observe the distance-to-risk criteria by applying sudden brakes at sufficient distances to avoid collision. It is considered that TTR is not observed if there is no progressive reduction in the travel speed as the driver approaches the threats. Presuming TTR in such cases, may produce the observed invalid results. It may therefore be concluded, that the consideration of DTR as

the principal adaptation criteria that wheelchair drivers adopt in the vicinity of risks corresponds well with most wheelchair drivers.

p	Parameters		Std Error		$\frac{1}{t_{stat}}$	Max. Dev	R^2
Case 1							
2	k_ν	0.0023296	0.0000493	2.12%	0.021145	0.0066778	0.9998727
	k_{env}	0.0000607	0.0000042	6.92%	0.069456		
	ν_{des}	2.1620485	0.0000664	0.003%	0.000031		
Case 2							
1	k_ν	0.0013058	0.0000457	3.50%	0.034998	0.0044821	0.9998751
	k_{env}	0.0000168	0.0000050	29.8%	0.297619		
	ν_{des}	3.1936471	0.0000572	0.002%	1.791e-5		
Case 3							
2	k_ν	0.0016111	0.0000638	3.96%	0.039600	0.0282700	0.9998215
	k_{env}	0.0001812	0.0000042	2.32%	0.023179		
	ν_{des}	2.9748170	0.0000809	0.003%	2.720e-5		
Case 4							
1	k_ν	0.0022988	0.0000481	2.10%	0.020924	0.0096421	0.9998336
	k_{env}	0.0001566	0.0000041	2.62%	0.026181		
	ν_{des}	1.5590495	0.0000483	0.003%	3.098e-5		
Case 5							
1	k_ν	0.0011705	0.0000330	2.82%	0.028193	0.0048858	0.9999171
	k_{env}	0.0000525	0.0000024	4.57%	0.045714		
	ν_{des}	2.3263703	0.0000322	0.001%	1.384e-5		
Case 6							
2	k_ν	0.0033319	0.0003469	10.4%	0.104115	0.0288915	0.9992932
	k_{env}	0.0002114	0.0000097	4.59%	0.045885		
	ν_{des}	2.0650043	0.0003439	0.017%	1.665e-4		
Case 7							
2	k_ν	0.0007837	0.0000496	6.33%	0.063290	0.0108345	0.9998355
	k_{env}	0.0001583	0.0000048	3.03%	0.030322		
	ν_{des}	5.5191529	0.0000688	0.001%	1.247e-5		

TABLE 4.2: Statistical analysis of the model employing DTR as the adaptation mechanism. The indicated values of constant p represent those that resulted in the highest coefficient of determination.

p	Parameters		Std Error		$\frac{1}{t_{stat}}$	Max. Dev	R^2
Case 1							
2	k_ν	0.0022305	0.0000508	2.28%	0.022775	0.0051076	0.9998726
	k_{env}	0.0000116	0.0000024	20.7%	0.206897		
	ν_{des}	2.1419324	0.0000642	0.003%	2.997e-5		
Case 2							
1	k_ν	0.0012839	0.0000472	3.68%	0.036763	0.0042400	0.9998751
	k_{env}	0.0000059	0.0000018	30.51%	0.305085		
	ν_{des}	3.2207044	0.0000570	0.002%	1.770e-5		
Case 3							
2	k_ν	0.0011325	0.0000646	5.70%	0.057042	0.0077142	0.9998197
	k_{env}	0.0000370	0.0000027	7.30%	0.072973		
	ν_{des}	3.3136044	0.0000776	0.002%	2.342e-5		
Case 4							
1	k_ν	0.0017910	0.0000473	2.64%	0.026410	0.0053594	0.9998327
	k_{env}	0.0000718	0.0000043	5.99%	0.059889		
	ν_{des}	1.5635212	0.0000435	0.003%	2.782e-5		
Case 5							
1	k_ν	0.0010542	0.0000339	3.22%	0.032157	0.0042527	0.9999171
	k_{env}	0.0000403	0.0000018	4.47%	0.044665		
	ν_{des}	2.4670341	0.0000319	0.001%	1.29e-05		
Case 6							
2	k_ν	-0.001482	0.0004203	-28.4%	-0.28360	0.0274354	0.9992838
	k_{env}	0.0002261	0.0000146	6.46%	0.064573		
	ν_{des}	-1.513273	0.0002957	-0.02%	-1.95e-4		
Case 7							
2	k_ν	-0.000199	0.0000442	-22.2%	-0.22211	0.0059510	0.9998381
	k_{env}	0.0000659	0.0000031	4.70%	0.047041		
	ν_{des}	-13.54669	0.0000522	-0.00%	-3.85e-6		

TABLE 4.3: Statistical analysis of the model employing TTR as the main adaptation mechanism, with the same constants as Table 4.2.

4.5.2 Trajectory fitting

Because of space limitations, curve fitting results of only two of the seven cases are presented to validate the driving behaviour model. The presented curves include a comparison between the model and generated data, the observed instantaneous errors

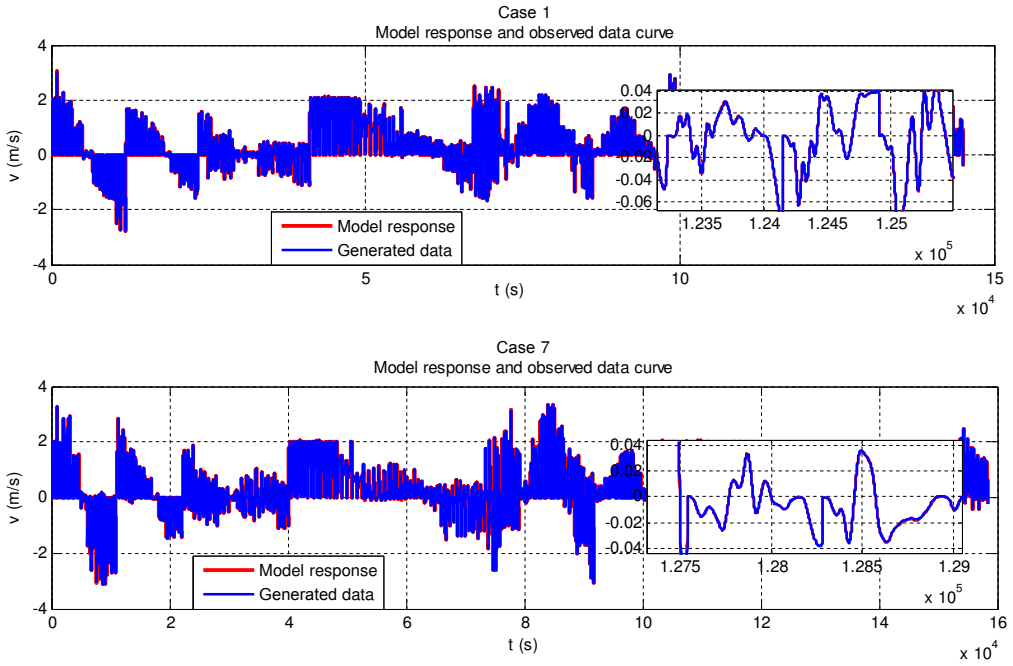

FIGURE 4.11: The generated linear velocity and model response in Case 1 and Case 7.

between the model and generated data, as well as the trajectory and steering velocity of the wheelchair in the two cases. Figure 4.11 depicts the relationship between the generated data and the driving model's response, and shows the amount of data used in the least squares estimation of the model's parameters. It is interesting to observe, with these constants and parameters, how close the driving model represents generated data. The observed difference between the model's output and the generated data as presented in Figure 4.12 basically represents a white noise. The generated and modelled trajectories and linear velocities in Case 1 and Case 7 are also depicted in Figure 4.13 and Figure 4.14 respectively. A visual comparison between the two trajectories and linear velocities presented in the two figures, demonstrate an accurate correspondence between the model's behaviour and the actual driver's behaviour.

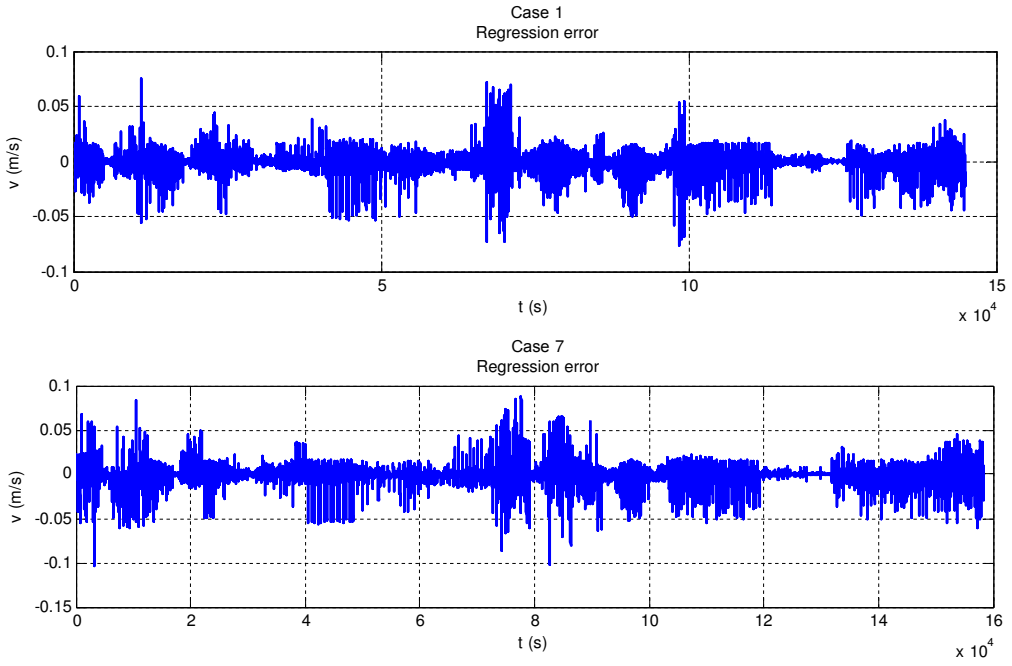

FIGURE 4.12: Regression errors in Case 1 and Case 7.

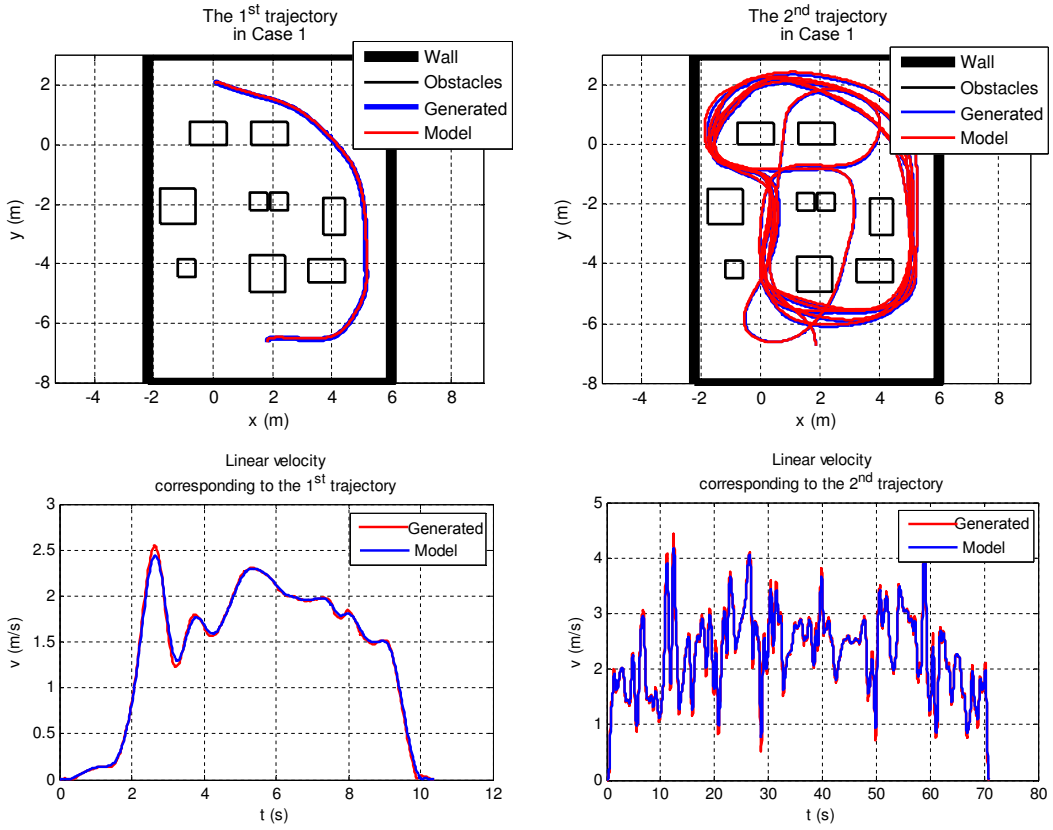

FIGURE 4.13: Generated trajectories and linear velocities in Case 1.

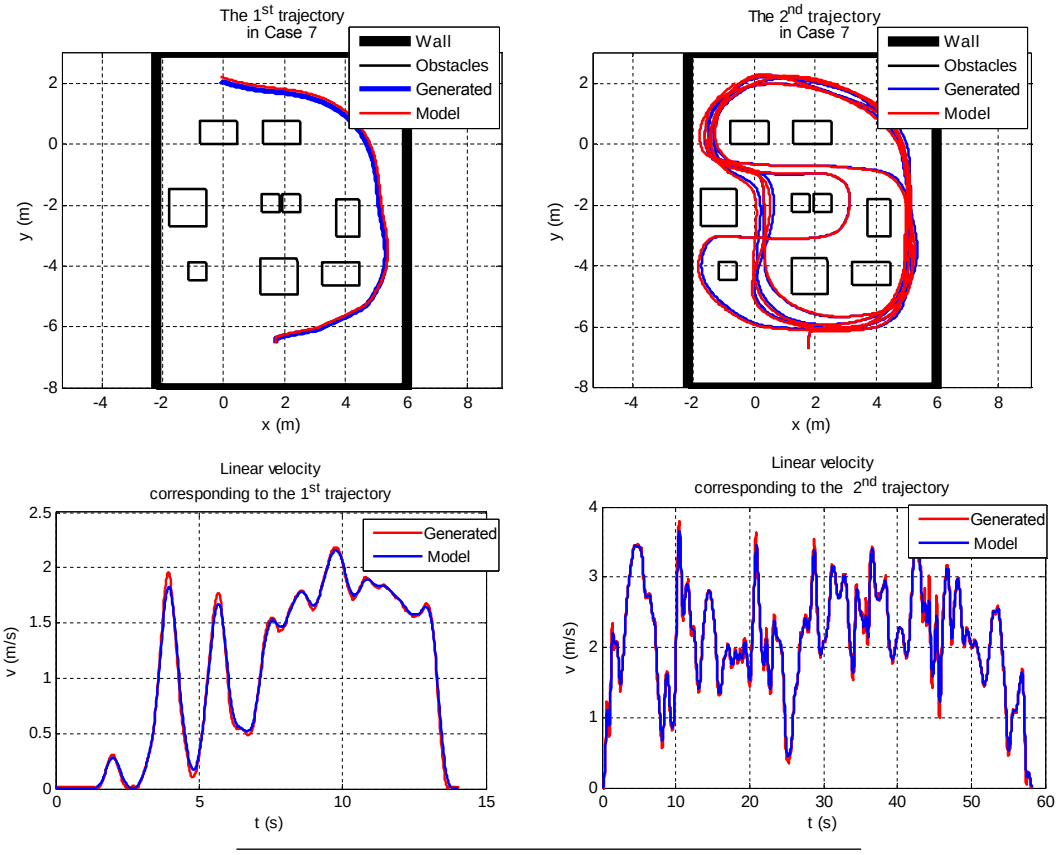

FIGURE 4.14: Generated trajectories and linear velocities in Case 7.

4.5.3 A comparison with Emam et al (2010)'s driver behaviour model

A curve fitting comparison between the presented model and Emam et al. (2010)'s model is also provided in Figure 4.15. The second trajectory in Figure 4.13 depicting Case 1's behaviour is used in the comparison, with DTR as the adaptation criteria. It can be seen that the presented model performs better, with a closer fitting compared to Emam et al. (2010)'s model. In addition, Table 4.4 presents the estimated parameter values, standard error, t-statistics, maximum deviation and coefficient of determination of Emam et al. (2010)'s model for the seven cases. Comparing the regression analyses in Table 4.2 and Table 4.4, it is apparent that the presented linear model performs better, noting the higher values of standard errors and maximum

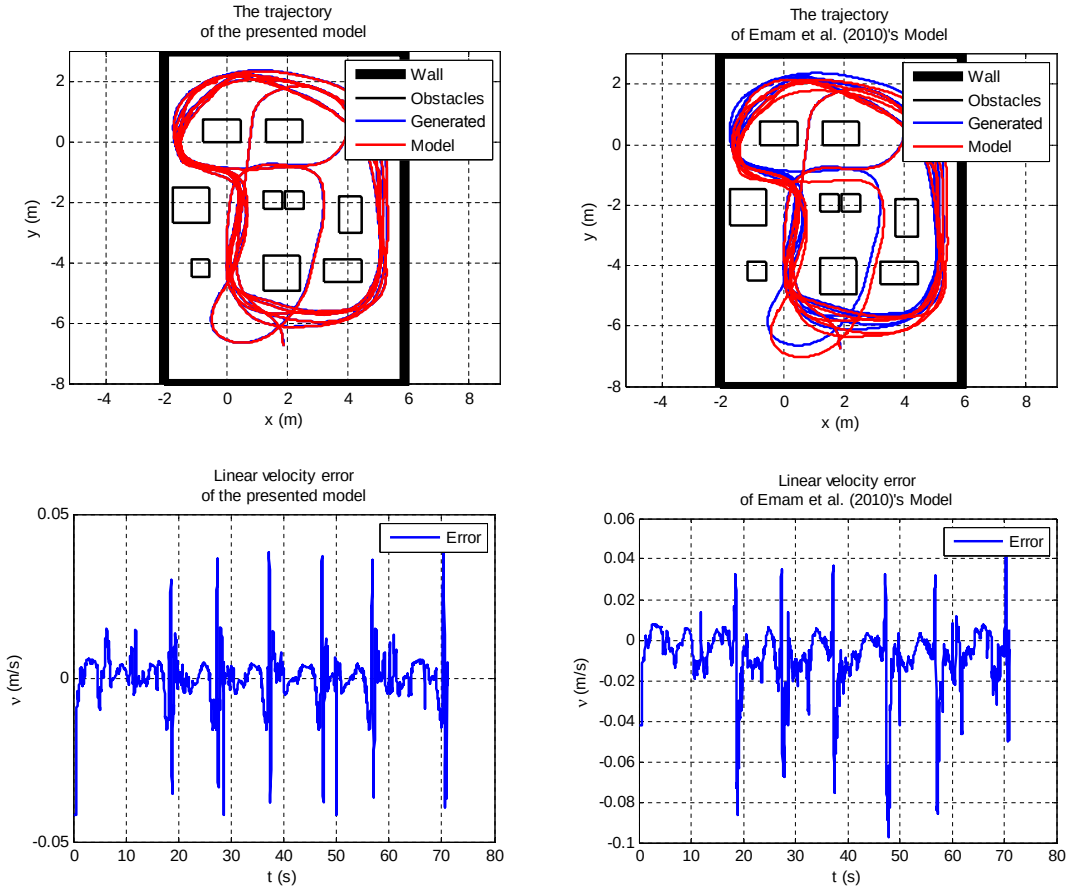

FIGURE 4.15: The curve-fitting comparison between the presented model and Emam et al. (2010)'s Model

deviation in Table 4.4 compared to Table 4.2. Besides, some negative parameters value were obtained in the identification.

4.6 Conclusion

This chapter intended to formulate a driver model that represents the driving behaviour of a wheelchair user in a local environment. A simple driving behaviour model that is linear in parameters is therefore presented. The model assumes explicit knowledge of the driver's subsequent intentions in order to generate the necessary adaptation signals required to adapt the wheelchair to the driver's driving

	Param. value	**Std Error**		$\frac{\mathbf{1}}{\mathbf{t_{stat}}}$	**Max. Dev**	$\mathbf{R^2}$
Case 1						
$K(1)$	-0.00097	0.00033	-34.184%	-0.3418	0.39777	0.99258
$K(2)$	-0.99680	0.00074	-0.0744%	-7.44e-4		
$K(3)$	0.002372	0.00132	55.4434%	0.55443		
$K(4)$	2.666837	0.47865	17.9482%	0.17948		
Case 2						
$K(1)$	0.000822	0.00169	2.062e2%	2.06227	0.55602	0.99266
$K(2)$	-0.99650	0.00075	-0.0756%	-7.56e-4		
$K(3)$	0.002030	0.00117	57.8637%	0.57864		
$K(4)$	2.914947	0.51880	17.7981%	0.17798		
Case 3						
$K(1)$	0.007529	0.00099	13.1842%	0.13184	0.36037	0.99245
$K(2)$	-0.99562	0.00063	-0.0629%	-6.29e-4		
$K(3)$	0.001935	0.00106	54.7612%	0.54761		
$K(4)$	2.720196	0.51956	19.1000%	0.19100		
Case 4						
$K(1)$	5.4794e-5	2.577e-5	47.0383%	0.47038	0.58585	0.99193
$K(2)$	-0.99611	0.00053	-0.0528%	-5.28e-4		
$K(3)$	0.000754	0.00028	37.4431%	0.37443		
$K(4)$	3.414773	0.31000	9.07842%	0.09078		
Case 5						
$K(1)$	0.001279	0.00086	67.1672%	0.67167	0.29464	0.99237
$K(2)$	-0.99631	0.00069	-0.0693%	-6.93e-4		
$K(3)$	0.001302	0.00093	71.2194%	0.71219		
$K(4)$	2.802759	0.61846	22.0662%	0.22066		
Case 6						
$K(1)$	0.003097	0.00096	30.9182%	0.30918	0.01506	0.99205
$K(2)$	-0.99582	0.00063	-0.0633%	-6.33e-4		
$K(3)$	-0.00016	0.00123	-7.82e2%	-7.8198		
$K(4)$	0.645253	11.9476	1.851e3%	18.5161		
Case 7						
$K(1)$	0.002894	0.00192	66.2751%	0.66275	0.66898	0.99254
$K(2)$	-0.99636	0.00071	-0.0708%	-7.08e-4		
$K(3)$	0.001286	0.00064	49.5301%	2.01897		
$K(4)$	3.589096	0.46016	12.8211%	0.12821		

TABLE 4.4: The regression parameters obtained with Emam et al. (2010)'s model

behaviour. It is observed from the identified parameters that although similar driving behaviours are exhibited, an implied uniqueness with respect to each case can still be observed. This validates the need for modelling and identification of the driver's steering behaviour. Because of the model's simplicity and linearity in parameters, the ordinary least square method has been used in parameter identification. The curve-fitting and regression analysis of the model with the identified parameter values produced results that accurately depict the generated driver-specific steering behaviours. Although the driving behaviour took into consideration the DPF algorithm, the model is uniquely formulated to account for user disposition like desired velocity. Besides, to the best our knowledge, a wheelchair driving model with similar simplicity and the accuracy with which its trajectory tracks/fits the actual may not available.

Chapter 5

A CLOSED-LOOP CONTROL WITH HUMAN-IN-THE-LOOP

5.1 Introduction

Human-in-the-loop control represents a framework for modelling systems that involve human interactions. Contrary to conventional control systems where a human model is included as an external input into the closed-loop system, the contemporary technological developments regard a human model as an active participant, capable of both judgement and decision making. In this way, human-in-the-loop technologies enable thorough analysis and understanding of the existing complex interaction between humans and machines under operational conditions, from a holistic perspective. The possibility of realising control systems with human-in-the-loop has become more and more practical with the rapid development of fast electronic systems and sensor technologies. A few implementations have been realised in automotive environments, to reduce car accidents and improve traffic safety. This chapter presents a closed-loop control system for a differential drive wheelchair, that also includes a driving behaviour model. Instead of a fully autonomous system, the architecture emphasises driver assistance, by adapting the wheelchair to the driving behaviours and preferences of the driver. The presented closed-loop model utilises the input-output feedback controller to track the driver inputs through torque compensation, and ensures the optimality of the resulting minimum-phase system through the performance index of the non-linear continuous-time GPC.

5.2 The control tool

Generally a classical controller is preferred where a model exists. Several classical control techniques applicable to nonlinear systems including numerical evaluation, Lyapunov theory and feedback linearisation exist. Although numerical techniques are widely applied to evaluate the performance of nonlinear systems, these techniques commonly suffer time and global stability issues. This is because a numerical simulation only depicts the response corresponding to one input sequence and a set of operation conditions at a time. It is therefore difficult to completely prove stability of a system with numerical simulations only. Lyapunov theory on the other hand plays a central role in the study of the controllability and stabilisability of control systems. However, except for passive systems, Lyapunov theory lacks a systematic procedure for constructing a positive definite control function that contains the system variables. This restricts the applicability of methods like sliding mode control which also necessitates a positive-definite energy function with negative derivative. On the other hand, feedback linearisation techniques may be applied in the control of nonlinear systems through state transformations and feedback, to algebraically linearise the system, leaving the equations of the nonlinear system intact. Linearisation techniques have been used successfully in high performance systems like robots and aircraft. It may, however, be impossible to algebraically linearise some nonlinear systems. In such cases, feedback linearisation technique only provides a partial linearisation with no guarantee of global stability. Nonetheless, the attractive characteristic of feedback linearisation is that, it has a systematic linearisation procedure. Besides, once a system is linearised, linear techniques may be used in a simple way to control the system. These motivate our feedback linearisation choice.

5.3 Feedback linearisation background

The differential drive structure of the wheelchair with two passive front castor wheels have restricted mobility and reduced number of actuators, and are therefore both non-holonomic and non-linear. This reduces the feasibility of computing their optimal controllers (Bloch & McClamroch, 1989; Campion et al., 1991). The classical controller synthesis methods that have previously been employed for non-holonomic and non-linear systems include feedback linearisation and Lyapunov theory (Isidori, 1999). The latter has previously been considered in the control of simple non-holonomic models, that did not take into account the effects of rolling friction as well as the varying gravitational potential of inclined grounds (Fierro & Lewis, 1997; Yang & Wang, 2011). This is because it lacks a systematic procedure for constructing the control function, except for passive systems (Spong & Vidyasagar, 2008). The former method, employed in this study, is commonly preferred for non-linear minimum and non-minimum-phase systems because of its systemstic linearisation procedure. Although Bloch & McClamroch (1989) and Campion et al. (1991) demonstrated that it was not possible to stabilise non-holonomic systems to a single equilibrium by smooth feedback, Sarkar & Kumar (1994) showed that the input-output feedback method could still be used to control such systems. Feedback control theories have been used widely in the execution trajectory tracking, path following and point stabilisation controls in both linear and non-linear systems (Khosla & Kanade, 1988; De Luca, 2000; Laumond, 1998). Recently, a global path-following feedback controller for a mobile robot is presented by Do (2015) at a dynamic level, based on level curve approach, under slow and constant time-varying disturbances with negligible derivatives. The design considered the Lyapunov's backstepping and direct methods to track a desired linear velocity in the path following problem with an observer that estimates the subjected disturbances and robot's velocity. The use of input-output

feedback linearisation techniques is also considered by Bidram et al. (2014) to design a controller for multi-agent systems with diverse non-identical and non-linear dynamics. The authors used the procedure to transform the non-identical and non-linear dynamics into identical linear dynamics, and designed a fully distributed controller, that ensures that the only information required for the control is the state of the agent and its neighbours. In a similar case, Rahimi et al. (2014) used the technique in the time varying formation control of collaborative multi-agent systems. Li & Yang (2012) carried out a non-linear controller design for a model-based inverted pendulum vehicle, whose accurate dynamic model could not be guaranteed because of the presence of uncertain vehicle and operator behaviours. They based the design on the input-output feedback linearisation control coupled with adaptive neural network (NN) and a linear dynamic compensator, to accomplish the tracking of desired trajectories and ensure a stable dynamic balance. In (Palli et al., 2008), a full-state feedback linearisation via static feedback is employed to linearise and control the position and stiffness of manipulator joints with multiple degrees of freedom and variable joints stiffness. The authors showed that it is possible, by static-state feedback, to impose a desired behaviour on the robot's motion in a decoupled way. In other applications, Eghtesad & Necsulescu (2004) performed an experimental study of feedback linearisation of a dynamic autonomous ground vehicle to ascertain asymptotic point stabilisation in curvilinear coordinates, while Bortoff (1997) presented an algorithm to construct a state-feedback linearising controller in such a way that certain part of the state coordinate transformation can be used as an output function.

5.4 Configuration of the control system

The proposed structure of the closed-loop model comprises the driver, the driving behaviour model, the wheelchair model, the driving environment and the controller, according to Figure 5.1. The controller design is based primarily on the presence of accurate models of the wheelchair and the driver's steering behaviour. In Chapter 3, a dynamic model of a differential-drive wheelchair is derived, using the Euler Lagrange procedure, to facilitate the design of assistive control systems in the presence of gravitational, frictional and slipping forces that act on the wheelchair during motion. The modelling considered the effects of wheel-slip, gravitational potential and rolling friction on the road-load force, on both inclined and non-inclined surfaces, and determined the slipping parameters by an approach that reduces the conventional number of slip-detection encoders. Derivation of the driving behaviour model and identification of driver-specific steering behaviours is carried out in Chapter 4. The driving model utilises the driver-specific parameters, the real-time steering signals, the state of the wheelchair and the sensor captured environmental information to compute, at each time instant, a reactive signal that drives the wheelchair to an instantaneous look-ahead goal, while at the same time circumventing collision incidents. The behaviour model thus executes the adaptive action on the joystick signals by applying the identified driver-specific parameters, to guarantee that the succeeding wheelchair states will track the steering behaviour of the driver, and avoid collision situations without the driver's conscious effort. The formulation of the driving model is based on deductive reasoning from the known steering operations and systematic relationships between the drivers' observable behaviours and wheelchair responses. The model however does not take into account the non-perceivable and interpersonal events that occur within the driver's mind. Although this study presumes a driver

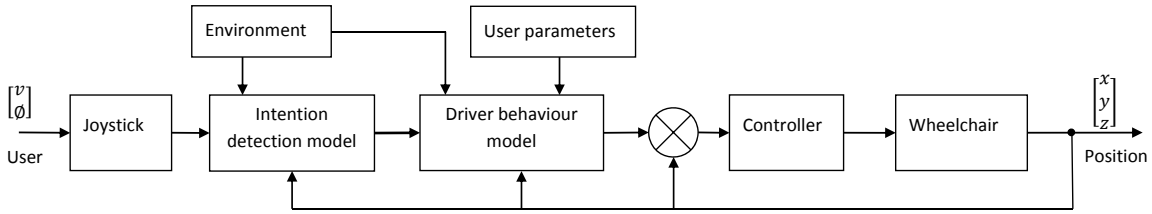

FIGURE 5.1: The control diagram of a wheelchair with integrated driver behaviour model and intention detection model.

capable of relatively reliable directional signals, in the case of extreme steering disability, an intention detection model may be instituted between the driver and the driving behaviour model according to Figure 5.1 to assist the driver.

5.5 System description

In this and the following sections, the wheelchair dynamic model and the driving behaviour model presented in Equations (3.36) and (4.10) respectively, will be considered to ensure tracking and stabilisation of the driver's commands. Equation (5.1) expresses the non-linear dynamic model of the wheelchair in a state space form:

$$\begin{aligned} \dot{\boldsymbol{\chi}}(t) &= \mathbf{f}_1\left(\boldsymbol{\chi}(t)\right) + \mathbf{g}_1\left(\boldsymbol{\chi}(t)\right)\mathbf{u}(t) \\ \boldsymbol{\mathcal{Y}}(t) &= \mathbf{h}\left(\boldsymbol{\chi}(t)\right) \end{aligned} \tag{5.1}$$

where $\boldsymbol{\chi}(t) \in \mathcal{R}^n = \begin{bmatrix} v & \dot{\phi} \end{bmatrix}^T$ is the state vector, $\mathbf{u}(t) \in \mathcal{R}^n = [\tau_R \;\; \tau_L]^T$ is the input vector and $\mathbf{h}\left(\boldsymbol{\chi}(t)\right) \in \mathcal{R}^n = [v \;\; \phi]^n$ is the output vector of the system. In addition, the non-linear functions $\mathbf{f}_1 : \mathcal{R}^n \rightarrow \mathcal{R}^n$ and $\mathbf{g}_1 : \mathcal{R}^{n\times n} \rightarrow \mathcal{R}^n$ describe the dynamics of the system, while $\mathbf{h} : \mathcal{R}^n \rightarrow \mathcal{R}^n$ gives the output expression $\boldsymbol{\mathcal{Y}}(t)$. Finally, $\dot{\boldsymbol{\chi}}(t)$ represents the derivative of the state vector $\boldsymbol{\chi}(t)$ with respect to time t. For clarity reasons, the time index will not be indicated in this and the following sections, unless

its indication is necessary to clear a possible confusion. Because the functions $\mathbf{f}_1$, $\mathbf{g}_1$ and $\mathbf{h}$ are smooth, it logically follows that the mappings $\mathbf{f}_1 : \mathcal{R}^n \rightarrow \mathcal{R}^n$ and $\mathbf{g}_1 : \mathcal{R}^{n\times n} \rightarrow \mathcal{R}^n$, expressed in Equations (5.2) and (5.3) respectively, are vector fields on $\mathcal{R}^n$.

$$\mathbf{f}_1(x) = \begin{bmatrix} -\bar{\bar{x}}\cos\theta\dot{\psi}\dot{\phi} - g\sin\phi\sin\theta \\ -\frac{Mg\bar{\bar{x}}\sin\theta\cos\phi}{\left(I_{ZZ}-M\bar{\bar{x}}^2\right)} \end{bmatrix} \tag{5.2}$$

$$\mathbf{g}_1(x) = \begin{bmatrix} \frac{1}{Mr} & \frac{1}{Mr} \\ \frac{b}{r\left(I_{ZZ}-M\bar{\bar{x}}^2\right)} & \frac{-b}{r\left(I_{ZZ}-M\bar{\bar{x}}^2\right)} \end{bmatrix} \tag{5.3}$$

The proposed input-output feedback linearisation entails inverting the non-linear system dynamics through a change of coordinates to globally linearise the model. A feedback control law can then be implemented on the linearised system to ensure that it tracks the reference inputs. This involves the consideration of both lie derivatives and relative degree of the non-linear system according to the following definitions:

Lie derivatives: Given system (5.1), computing the derivative of the output $\boldsymbol{\mathcal{Y}}$ with respect to time result in the following Equation (5.4):

$$\begin{aligned} \dot{\boldsymbol{\mathcal{Y}}} &= \frac{\partial \mathbf{h}}{\partial x}\dot{\boldsymbol{\chi}} \\ &= \frac{\partial \mathbf{h}}{\partial x}\left[\mathbf{f}_1(x) + \mathbf{g}_1(x)\,\mathbf{u}\right] \\ &= L_f h(x) + L_g h(x)\mathbf{u} \end{aligned} \tag{5.4}$$

where

$$L_f h(x) = \frac{\partial \mathbf{h}}{\partial x}\mathbf{f}_1(x) \qquad \text{and} \qquad L_g h(x) = \frac{\partial \mathbf{h}}{\partial x}\mathbf{g}_1(x)$$

The function $L_f h(x)$ denotes the Lie derivative of $h(x)$ along $\mathbf{f}_1(x)$, while $L_g h(x)$ is the Lie derivative of $h(x)$ along $\mathbf{g}_1(x)$.

Relative Degree: The relative degree, ρ, of a non-linear system refers to the number of times the output $\boldsymbol{\mathcal{Y}} = \mathbf{h}(x)$ of the system is differentiated with respect to time for the input $\mathbf{u}$ to appears explicitly in the resulting equations. A system is therefore said to have a relative degree of ρ such that $1 \leq \rho \leq n \in \mathcal{R}^n$ if $\forall x \in \mathcal{R}^n$:

$$L_g L_f^{i-1} h(x) = 0 \qquad i = 1,\ 2,\ \cdots,\ \rho - 1$$
$$L_g L_f^{\rho-1} h(x) \neq 0$$

where $L_g L_f^{i-1} h(x) = L_g \left[L_f^i h(x) \right]$, $L_f^i h(x) = L_f \left[L_f^{i-1} h(x) \right]$ and $L_f^0 h(x) \triangleq h(x)$

5.6 Feedback linearisation and controller design

The appropriate controller design approach is generally determined by the complexity of the dynamic system as well as the control task that the system has to accomplish. Normally, in order to obtain a locally linearised approximation, the non-linear state-space system expressed in Equation (5.1) could be controlled in a classical way by estimating its first-order dynamics around the origin, $\boldsymbol{\chi} = 0$, using a linear controller. However, the lie derivatives of the smooth non-linear wheelchair model derived in Chapter 3 does not satisfy the involutivity condition (Isidori, 1999; Yun et al., 1992; Sarkar & Kumar, 1994). As a result, the proposed dynamic model is not full-state feedback linearisable. However, the non-approximating input-output feedback technique can be used to achieve the linearisation with a proper choice of the output variables. As previously stated in this thesis, a typical problem of wheelchair velocity control is considered. The problem is translated into torque regulation task, that necessitates the coupling and linearisation of the system's dynamic properties between the input and the output. This solves the velocity control problem by

computing the wheel torques that guarantee tracking of the steering commands from driving behaviour model on flat, inclined and slippery surfaces; and by optimising the closed-loop gains through the performance index of the non-linear continuous-time GPC.

5.6.1 Navigation task

In practice, in order to direct the wheelchair according to path geometry to a desired destination, the steering task is executed by continuous specification the of steering signals through the available interface by the driver. The proposed closed-loop control model is not intended to withdraw this driver's responsibility, but to simplify the driver's steering task. A linearised system is necessary in this respect, because it aids the driver to make a proportional judgement of the inputs quantities required to produce a desired output. The non-linear wheelchair system in Equation (5.1) is therefore linearised with respect to the output variables of a conventional wheelchair joystick to ensure practicality of the steering task. Since the proposed wheelchair dynamic model in Equation (3.36) has two inputs, it is possible to choose any two output variables to achieve the input-output feedback linearisation. The problem of linear speed and angular position control of a conventional wheelchair is therefore considered with an intention of tracking the specified input signals. This is accomplished by ensuring that the linear speed and angular position errors, $\mathbf{e} = [\ e_1^1 \quad e_1^2\ ]^T$, specified in Equation (5.5) results in $\lim_{t\to\infty}[\mathbf{e}] = 0$.

$$\begin{aligned} e_1^1 &= V - V_r \\ e_1^2 &= \phi - \phi_r \end{aligned} \tag{5.5}$$

5.6.2 Relative degree of the system (ρ)

It is observable in Equation (5.6), that the first derivative of the output variable vector **e**, lacks the control signal **u**, in the second element. This explains why Equation (5.1) could not be linearised by exact feedback linearisation. The control signal **u**, however, appears by delaying the first element of the first derivative $\dot{\mathbf{e}}$, while performing the second differentiation on the second output element:

$$\begin{aligned} \dot{e}_1^1 &= -\bar{\bar{x}}\cos\theta\dot{\psi}\dot{\phi} - g\sin\phi\sin\theta - \dot{v}_r + \tfrac{1}{Mr}(\tau_R + \tau_L) \\ \dot{e}_1^2 &= e_2^2 \\ \dot{e}_2^2 &= -\tfrac{Mg\bar{\bar{x}}\sin\theta\cos\phi}{\left(I_{ZZ} - M\bar{\bar{x}}^2\right)} - \ddot{\phi}_r + \tfrac{b(\tau_R - \tau_L)}{r\left(I_{ZZ} - M\bar{\bar{x}}^2\right)} \end{aligned} \tag{5.6}$$

As a result, the relative degree of the first output element e^1, is one, while the second element e^2, has a relative degree of two. Since the sum of the components of vector relative degree is greater than the state dimension of the system, the state extension is performed to enable computation of the outcome for every state. A linearised Equation (5.7) of the system is therefore presented as follows:

$$\begin{bmatrix} \dot{e}_1^1 \\ \dot{e}_2^2 \end{bmatrix} = \begin{bmatrix} -\bar{\bar{x}}\cos\theta\dot{\psi}\dot{\phi} \\ -g\sin\phi\sin\theta - \dot{v}_r \\ -\tfrac{Mg\bar{\bar{x}}\sin\theta\cos\phi}{\left(I_{ZZ} - M\bar{\bar{x}}^2\right)} - \ddot{\phi}_r \end{bmatrix} + \begin{bmatrix} \frac{1}{Mr} & \frac{1}{Mr} \\ \frac{b}{r\left(I_{ZZ} - M\bar{\bar{x}}^2\right)} & \frac{-b}{r\left(I_{ZZ} - M\bar{\bar{x}}^2\right)} \end{bmatrix} \mathbf{u} \tag{5.7}$$

5.6.3 The control law

Considering that the synthetic control inputs need to equalise the rate of change of errors $\dot{\mathbf{e}} = [\dot{e}_1^1 \quad \dot{e}_2^2]^T$, and that, the two-rank decoupling matrix is invertible and non-singular unless $r = 0$ or $I_{ZZ} - M\bar{\bar{x}}^2 = 0$, the state feedback law required to provide a compensation for the input-output non-linearities can be computed. Since r cannot be equal to zero it is possible to ensure, through proper wheelchair design,

that $I_{zz} - M\bar{\bar{x}}^2 \neq 0$ throughout. I_{zz}, M and $\bar{\bar{x}}$ are therefore carefully chosen in this thesis to realise a decoupling matrix that is always invertible. The input, $\mathbf{u}$ that drives Equation (5.1) to a desired response is then be computed as follows:

$$\mathbf{u} = \begin{bmatrix} \frac{1}{Mr} & \frac{1}{Mr} \\ \frac{b}{\left(I_{ZZ} - M\bar{\bar{x}}^2\right)r} & \frac{-b}{\left(I_{ZZ} - M\bar{\bar{x}}^2\right)r} \end{bmatrix}^{-1} \times \left[\begin{pmatrix} \dot{e}_1^1 \\ \dot{e}_2^2 \end{pmatrix} - \begin{pmatrix} -\ddot{\bar{x}}\cos\theta\dot{\psi}\dot{\phi} \\ -g\sin\phi\sin\theta - \dot{v}_r \\ -\frac{Mg\bar{\bar{x}}\sin\theta\cos\phi}{\left(I_{ZZ} - M\bar{\bar{x}}^2\right)} - \ddot{\phi}_r \end{pmatrix} \right] \tag{5.8}$$

where $\dot{e}_i = -\sum_{j=0}^{\rho_i - 1} K_{ij} L_f^j \left(h_i\right)|_{i=1,2.}$ with ρ_i being the relative degree of the i^{th} output element. To guarantee stability of the closed-loop system, positive values of the tracking coefficients K_{11}, K_{21} and K_{22} are considered in the control law in Equation (5.9):

$$\boldsymbol{\mathcal{U}} = \begin{pmatrix} \dot{e}_1^1 \\ \dot{e}_2^2 \end{pmatrix} = \begin{bmatrix} -K_{11}e_1^1 \\ -K_{21}e_1^2 - K_{22}e_2^2 \end{bmatrix} \tag{5.9}$$

Redefining the $\mathbf{h}(\boldsymbol{\chi})$ in Equation (5.1) as $[e_1^1 \;\; e_2^2]^T$ the internal dynamics of the system may be analysed as follows: The error $e_1^1 = 0$ implies that $\dot{e}_1^1 = 0$. However, $e_2^2 = 0$ means that $\dot{e}_2^2 = -K_{21}e_1^2$. This means that the error e_2^2 is governed by $\dot{e}_2^2 = -K_{21}e_1^2$. But since K_{21} is positive, the internal dynamics are stable and the system is well-behaved.

5.7 Non-linear continuous-time GPC

In this section, the non-linear continuous-time generalised predictive control is utilised to validate and provide an optimal design of the input-output controller gains through its performance index. The output, $\boldsymbol{\mathcal{Y}} = \mathbf{h}(\boldsymbol{\chi})$, of the wheelchair system in Equation

(5.1) with $\boldsymbol{\chi} \in \mathbf{X} \subset \mathcal{R}^n, \boldsymbol{\mathcal{Y}} \in \mathbf{Y} \subset \mathcal{R}^m \,|m = n$ is considered in the receding horizon performance index in Equation (5.10), where T_1 and T_2 are the minimum and maximum prediction time respectively, defined such that $T_1 \leq \bar{\tau} \leq T_2$:

$$J = \frac{1}{2}\int_{T_1}^{T_2} \left[\boldsymbol{\mathcal{Y}}\left(t+\bar{\tau}\right) - \boldsymbol{\mathcal{Y}}_r\left(t+\bar{\tau}\right)\right]^T \left[\boldsymbol{\mathcal{Y}}\left(t+\bar{\tau}\right) - \boldsymbol{\mathcal{Y}}_r\left(t+\bar{\tau}\right)\right] d\bar{\tau} \tag{5.10}$$

The predicted output, $\boldsymbol{\mathcal{Y}}(t+\bar{\tau})$, is computed by Taylor series expansion to the order of the corresponding relative degree of its elements as given by Equation (5.11) below:

$$\boldsymbol{\mathcal{Y}}_i\left(t+\bar{\tau}\right) = \sum_{k=0}^{\rho_i} \frac{\bar{\tau}^k}{k!}\boldsymbol{\mathcal{Y}}_i^{(k)}(t) + \left.H(\bar{\tau})\right|_{k>\rho_i} \tag{5.11}$$

In the Equations (5.10) and (5.11), t is the current time, $t+\bar{\tau}$ is the duration of prediction and $\left.H(\bar{\tau})\right|_{k>\rho_i}$ are the higher order terms of the expansion. Defining the error within the prediction duration as $\mathbf{e}(t+\bar{\tau}) = \boldsymbol{\mathcal{Y}}(t+\bar{\tau}) - \boldsymbol{\mathcal{Y}}_r(t+\bar{\tau})$, and neglecting the higher order terms of Equation (5.11), the Taylor expansion yields:

$$\mathbf{e}(t+\bar{\tau}) = \boldsymbol{\Gamma}(\bar{\tau})\tilde{\mathbf{E}}(t) \tag{5.12}$$

where $\boldsymbol{\Gamma}(\bar{\tau})$ is an $(n \times \sum_i (r_i+1))$ matrix whose elements are $(n \times n)$ diagonal matrices, and $\tilde{\mathbf{E}}(t)$ is a vector of errors expressed in Equation (5.13).

$$\boldsymbol{\Gamma}(\bar{\tau}) = \begin{bmatrix} \mathbf{I} & \bar{\tau} & \bar{\tau}^2/2! & \dots & \bar{\tau}^p/p! \end{bmatrix}$$

$$\tilde{\mathbf{E}}(t) = \begin{bmatrix} \phi(t) - \phi_r(t) \\ v(t) - v_r(t) \\ \dot{\phi}(t) - \dot{\phi}_r(t) \\ \dot{v}(t) - \dot{v}_r(t) \\ \ddot{\phi}(t) - \ddot{\phi}_r(t) \end{bmatrix} = \begin{bmatrix} e_1^2 \\ e_1^1 \\ e_2^2 \\ f_{11} - \dot{v}_r(t) + \frac{\tau_L}{Mr} + \frac{\tau_R}{Mr} \\ f_{12} - \ddot{\phi}_r(t) - \frac{b\tau_L}{r\left(I_{ZZ} - M\bar{x}^2\right)} + \frac{b\tau_R}{r\left(I_{ZZ} - M\bar{x}^2\right)} \end{bmatrix} \tag{5.13}$$

Equation (5.10) is then simplified to:

$$J = \frac{1}{2}\tilde{\mathbf{E}}^T(t)\mathbf{\Lambda}\left(T_1, T_2\right)\tilde{\mathbf{E}}(t) \tag{5.14}$$

where the 'prediction matrix', $\mathbf{\Lambda}$, is defined as:

$$\mathbf{\Lambda}\left(T_1, T_2\right) = \int_{T_1}^{T_2} \mathbf{\Gamma}^T(\bar{\tau})\mathbf{\Gamma}(\bar{\tau})d\bar{\tau}$$

Minimising the cost expressed in Equation (5.14) with respect to the control parameter $\mathbf{u}$ results in the following control law:

$$\mathbf{u} = \boldsymbol{\mathcal{D}}^{-1}{\mathbf{\Lambda}_{ss}}^{-1}\mathbf{\Lambda}_s \begin{bmatrix} -e_1^2 & -e_1^1 & -e_2^2 & -f_{11} + \dot{v}_r & -f_{12} + \ddot{\phi}_r \end{bmatrix}^T \tag{5.15}$$

where $\boldsymbol{\mathcal{D}}$ is the decoupling matrix in Equation (5.7), while ${\mathbf{\Lambda}_{ss}}^{-1}\mathbf{\Lambda}_s\left(T_1, T_2, \rho\right) = \mathbf{K}$ with

$$\mathbf{\Lambda}_{ss} = \begin{bmatrix} \frac{\left({T_2}^3 - {T_1}^3\right)}{3} & 0 \\ 0 & \frac{\left({T_2}^5 - {T_1}^5\right)}{20} \end{bmatrix} \tag{5.16}$$

$$\mathbf{\Lambda}_s = \begin{bmatrix} 0 & \frac{\left({T_2}^2 - {T_1}^2\right)}{2} & 0 & \frac{\left({T_2}^3 - {T_1}^3\right)}{3} & 0 \\ \frac{\left({T_2}^3 - {T_1}^3\right)}{6} & 0 & \frac{\left({T_2}^4 - {T_1}^4\right)}{8} & 0 & \frac{\left({T_2}^5 - {T_1}^5\right)}{20} \end{bmatrix} \tag{5.17}$$

$T_1 = 0$ and $T_2 = T$ is opted for in this simulation, for simplicity reasons. However, the control law applies as well to problems with $T_1 \neq 0$. The optimised gain matrix $\mathbf{K}\left(T,\ \rho\right)$ in Equation (5.18) can thus be expressed to obtain the alternative control law in Equation (5.19):

$$\mathbf{K}\left(T, \rho\right) = \mathbf{\Lambda}_{ss}\mathbf{\Lambda}_s\left(T, \rho\right) = \begin{pmatrix} 0 & \frac{3}{2T} & 0 & 1 & 0 \\ \frac{10}{3T^2} & 0 & \frac{5}{2T} & 0 & 1 \end{pmatrix} \tag{5.18}$$

$$\mathbf{u} = \begin{bmatrix} \frac{1}{Mr} & \frac{1}{Mr} \\ \frac{b}{r\left(I_{ZZ} - M\bar{\bar{x}}^2\right)} & \frac{-b}{r\left(I_{ZZ} - M\bar{\bar{x}}^2\right)} \end{bmatrix}^{-1} \times \begin{bmatrix} -f_{11} - \frac{3e_1^1}{2T} + \dot{v}_r \\ -f_{12} - \frac{10e_1^2}{3T^2} - \frac{5e_2^2}{2T} + \ddot{\phi}_r \end{bmatrix} \tag{5.19}$$

When Equation (5.9) is substituted into Equation (5.8), the generalised predictive control law in Equation (5.19) resembles the input-output control law in Equation (5.8) except for the difference in the gain matrices $\mathbf{K}(T, \rho)$ that produces the most accurate prediction over the chosen time horizon. This characterises the closed-loop tracking stability of the wheelchair.

5.7.1 Closed-loop stability of the wheelchair system

Although closed-loop stability is one of the non-linear continuous-time GPC's constraints, the corrected control law procedure that guarantees the stability of a closed-loop system could be applied (Dabo et al., 2009). However, since $\rho_i \ngeq 4| \ \forall i$, the corrected control law procedure does not apply, but the following demonstrates that the asymptotic stability of the closed-loop system in Equation (5.19) is guaranteed. Representing the coefficients of e_1^1, e_1^2 and e_2^2 as K_{11}, K_{21} and K_{22} respectively, and with the invertability of the decoupling matrix in the control law in Equation (5.19), Equation (5.1) can be expressed as follows:

$$\begin{bmatrix} -K_{11}e_1^1 + \dot{v}_r - \dot{v} \\ -K_{21}e_1^2 - K_{22}e_2^2 + \ddot{\phi}_r - \ddot{\phi} \end{bmatrix} = 0$$

or simply as

$$\begin{bmatrix} -K_{11}e_1^1 - \dot{e}_1^1 \\ -K_{21}e_1^2 - K_{22}\dot{e}_1^2 - \ddot{e}_1^2 \end{bmatrix} = \begin{bmatrix} 3e_1^1/2T + \dot{e}_1^1 \\ 10e_1^2/3T^2 + 5\dot{e}_1^2/2T + \ddot{e}_1^2 \end{bmatrix} = 0 \tag{5.20}$$

The closed-loop stability of the system can be established by letting the reference signals, v_r and ϕ_r equal to zero because they do not affect the stability of the linear system in Equation (5.20). The poles of Equation (5.20) then becomes $-1.5/T$ and

$-1.25 \pm 1.3307j/T$ respectively, ensuring that $\lim_{t\to\infty}\{e_1^1, e_1^2\} = 0$, a sufficient condition for the closed-loop system to be asymptotically stable. The wheelchair system in Equation (5.1) is therefore asymptotically stable given the control law in Equation (5.19). The poles of the closed-loop system depend linearly on the prediction time T, thus given a small prediction time, the controlled output will rapidly track the reference signal at the expense of large control torques. Control torques can therefore be regulated by appropriate selection of the prediction time T.

5.8 Simulation results of the closed-loop model

This section presents some simulation results to support the proposed closed-loop control model of the wheelchair with human-in-the-loop. The presented validations include plots of various centre of mass trajectories and velocities of the system, with and without the driving behaviour model. The dynamic model parameters and the default controller gains used in the simulation are shown in Table 5.1. Unlike the open-loop model simulations in Section 3.5, that considers the wheel torques as the system inputs, the reference linear speed V_r and angular position ϕ_r are considered in the closed-loop model simulations.

5.8.1 Simulation without the driving behaviour model

In the absence of the driving behaviour model, the proposed controller independently regulates the wheel torques to track the reference signals, based on the prevailing steering situation. Two simulation results are presented to this effect, and a consideration is made in each case to a slippery surface condition. In Figure 5.2 for instance, a reference angular orientation in the form of a unit slope ramp, with a

TABLE 5.1: Dynamic model and controller parameters used in simulation

Kinematics	$\bar{\bar{x}} = 0.2$	$\bar{\bar{y}} = 0$
	$b = 0.3$m	f $= 0.35$m
	$r_R = 0.15$m	$r_L = 0.15$m
Dynamics	$M = 120$Kg	$g = 9.81$m/s
	$k = 100$	$\mu_C = 0.0143$
Default	$K_{11} = 3$	$K_{22} = 13.33$
	$K_{21} = 5$	
Surface	$\mu_x = \mu_y = \mu_z = \mu_\phi = 0.3$	
Prediction horizon	$T = 0.5s$	

reference speed of $V_r = 1.5$, an initial surface inclination angle of $\theta = 15°$ and an initial ψ of 90°, generated the circular trajectory shown in the first sub-plot. During the simulation, a random slip was introduced at time $t = 20s$ for the rest of the simulation time. As depicted in the wheel-torques time-series curve, the controller automatically adjusted the torques to track the specified user inputs. The linear velocity time-series curve and angular orientation error illustrate how accurate the controller tracked the desired inputs in spite of the effects of gravitational potential and the slipping situation. Similar results are plotted in Figure 5.3, where the controller tracked a unit amplitude sinusoidal input, to produce the desired sine wave trajectory. Although a tracking error is evident in the orientation, the error is steady state with much smaller magnitude compared to the desired output. Thus, the simulated behaviour of the closed-loop model is considered largely consistent with the expected response of a wheelchair system in a practical situation.

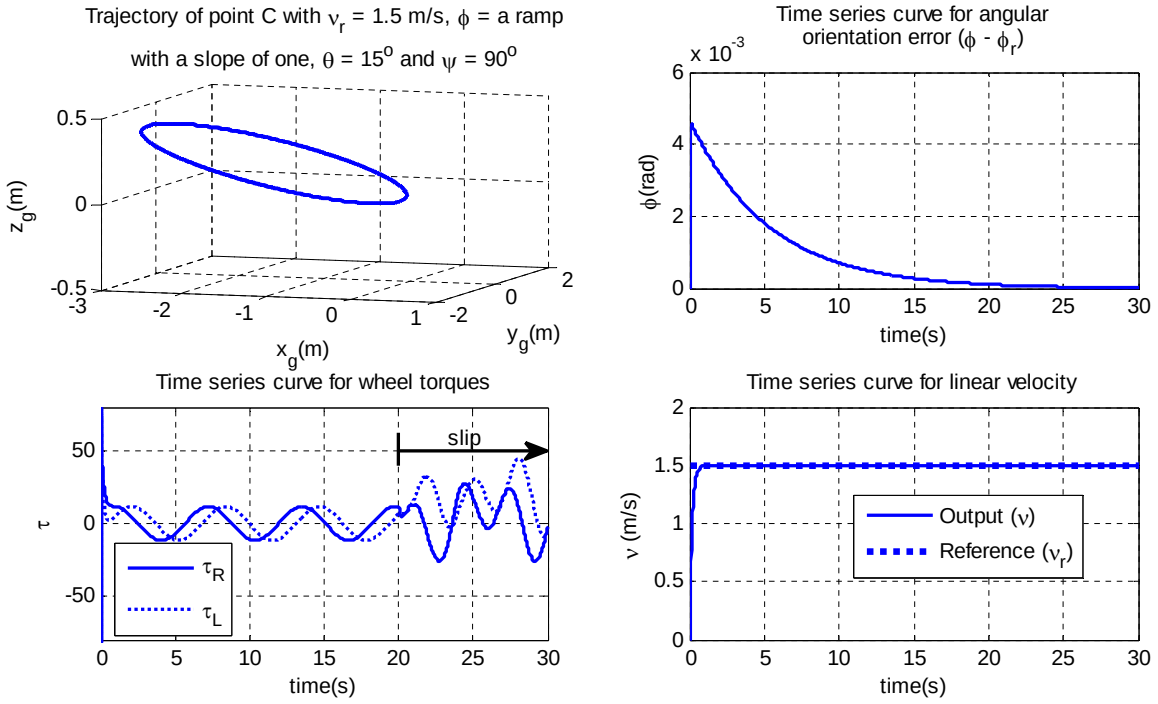

FIGURE 5.2: Circular wheelchair trajectory generated by considering a ramp input for reference angular orientation and $V_r = 1.5$ at $\theta = 0°$ and $\psi = 90°$. As depicted in time series curve for wheel torques, random slip introduced at time $t = 20s$ for the rest of simulation time does not affect the ability of controller to automatically adjust the torques in order to track the specified user inputs.

5.8.2 Simulation with the driving behaviour model

Figure 5.4 and 5.5 depicts simulation results of the closed-loop wheelchair with a driving behaviour model in the loop. The results intended to show the ability of the closed-loop controller to track the driver's commands and reproduce the wheelchair's trajectory. In Figure 5.4, both the original trajectory of the driver's steering speed and directional commands, and the controller's new trajectory in Case 1 and Case 7 are shown in sub-plots A and B respectively. Similarly, Figure 5.5 presents the original and controller computed linear speeds and their corresponding linear speed-errors in Case 1 and Case 7 in the first and second columns respectively. As depicted, the controller accurately tracks the reference speeds and trajectories of the drivers.

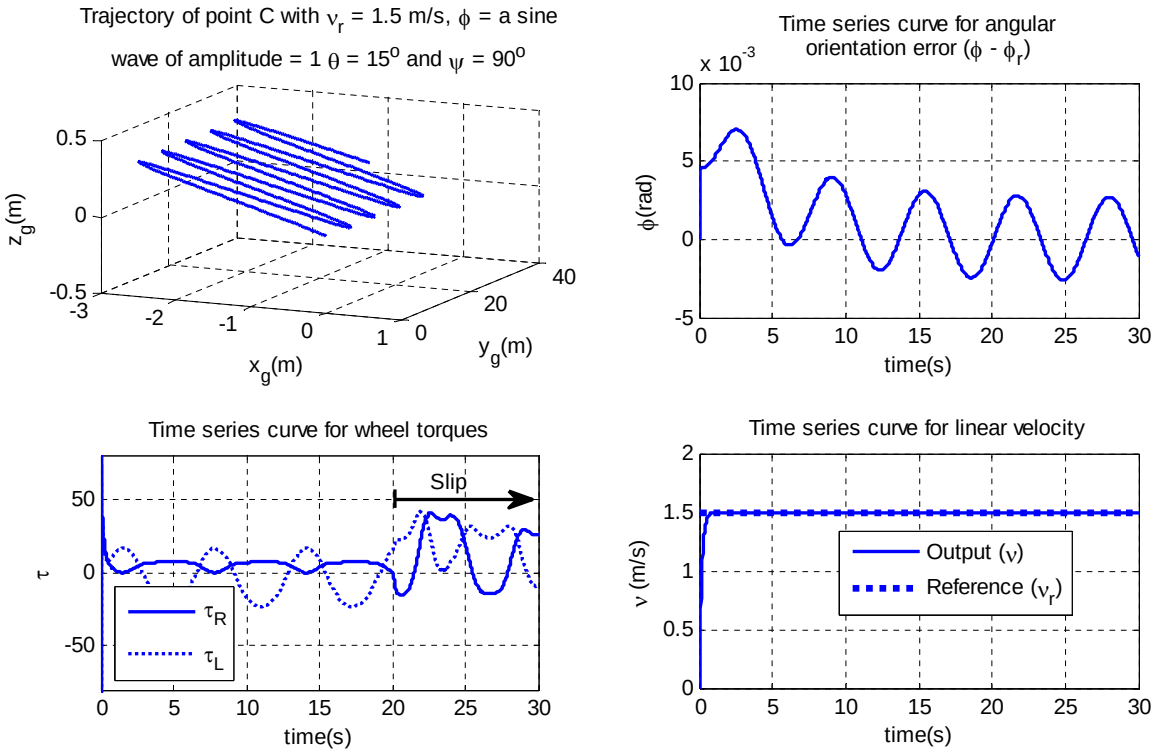

FIGURE 5.3: Sinusoidal wheelchair trajectory generated by considering a sine wave input for reference angular orientation and $V_r = 1.5$ at $\theta = 0°$ and $\psi = 90°$. Similarly, the random slip introduced at time $t = 20s$ does not affect the ability of controller to regulate wheel torques.

However, because none of the cases represented a steering disability condition, it was not possible to present the assistive contribution of the driving behaviour model on drivers with steering disability. A typical steering handicap signal is therefore modelled and added to the generated signals to help depict the significance of including the driving behaviour model in the control loop.

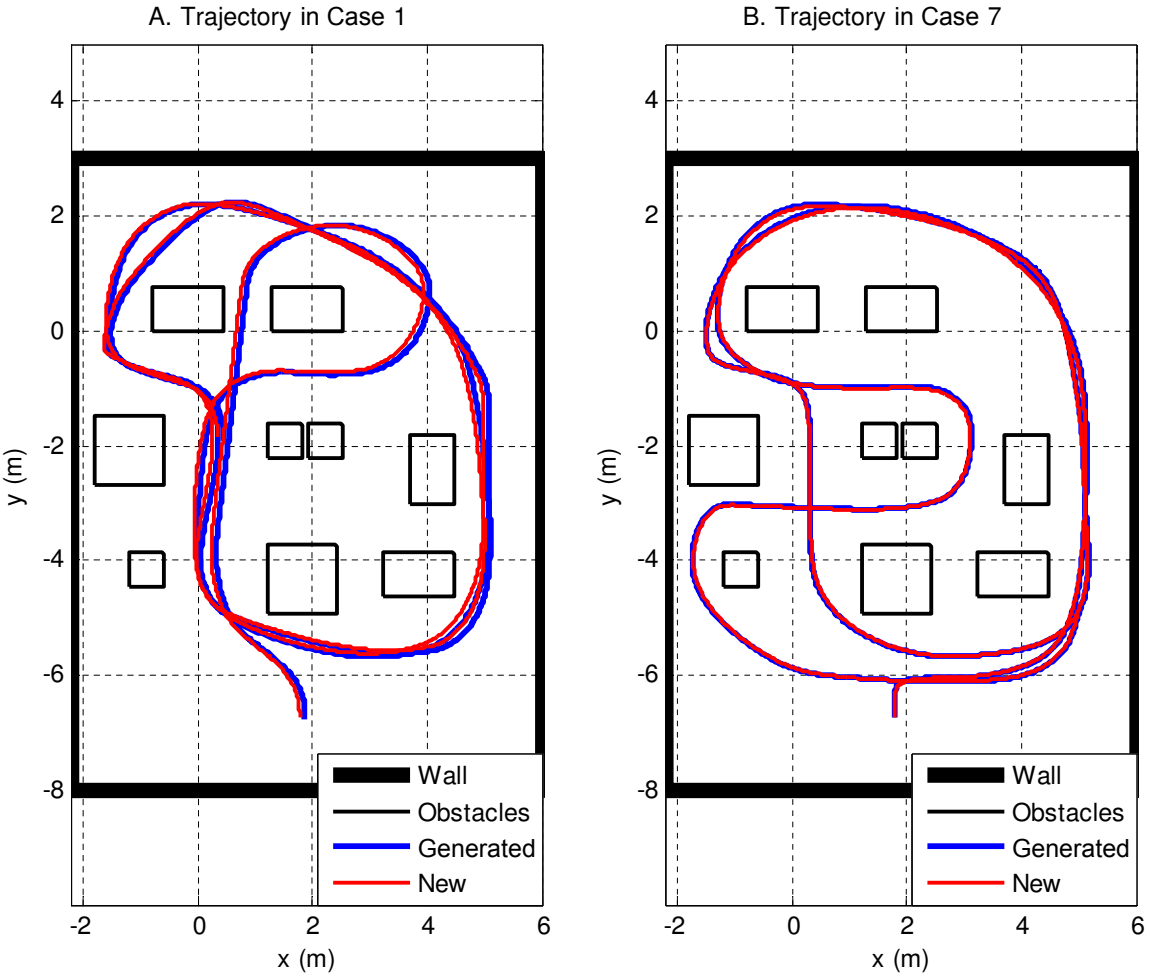

FIGURE 5.4: The original trajectory generated from the speed and directional commands of the driver and the new controller computed trajectory in Case 1 and Case 7.

5.8.3 Simulation with induced disability

In order to simulate signals with steering disability, a steering handicap is modelled and superimposed on the normal drivers' signals. The steering handicap model formulated the signal of a wheelchair driver with wrist extension problems. In particular, a driver with limited capability of pointing the joystick towards the right-side direction (negative directional changes) and making small variations in the translational speed is considered. The positive directional variations as well as considerably bigger

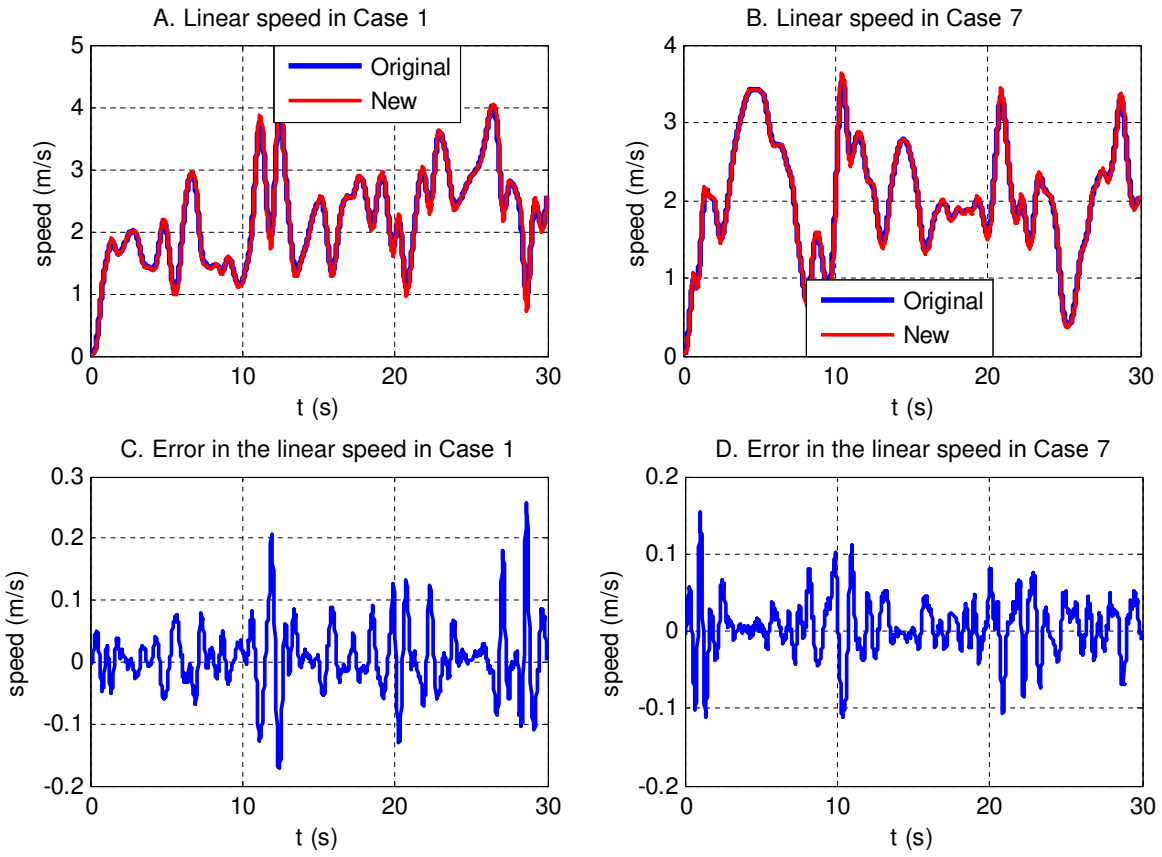

FIGURE 5.5: The original and controller computed linear speeds and their corresponding errors in Case 1 and Case 7.

changes in the linear speed are left unaffected. The disability model is presented in Equation (5.21), where a_k and ω_k denote linear acceleration and angular velocity respectively, s_h and s_w denote hand and wrist stiffness constants respectively, k represents the time instant while k_1 and k_2 are other constants.

$$\begin{aligned} \omega_k &= \begin{cases} \omega_k - s_h \cdot \sin(\omega_k) & \omega_k < 0 \\ \omega_k & \text{otherwise} \end{cases} \\ a_k &= a_k + s_w \cdot \arctan(k_1 \cdot a_k) \cdot \mathbf{e}^{-\,|k_2 \cdot a_k|} \end{aligned} \tag{5.21}$$

The effect of superimposing the disability model on a normal driving signals is depicted in Figure 5.6, showing the angular velocity and linear acceleration signals in sub-plots A and B respectively, and the corresponding angular position and linear

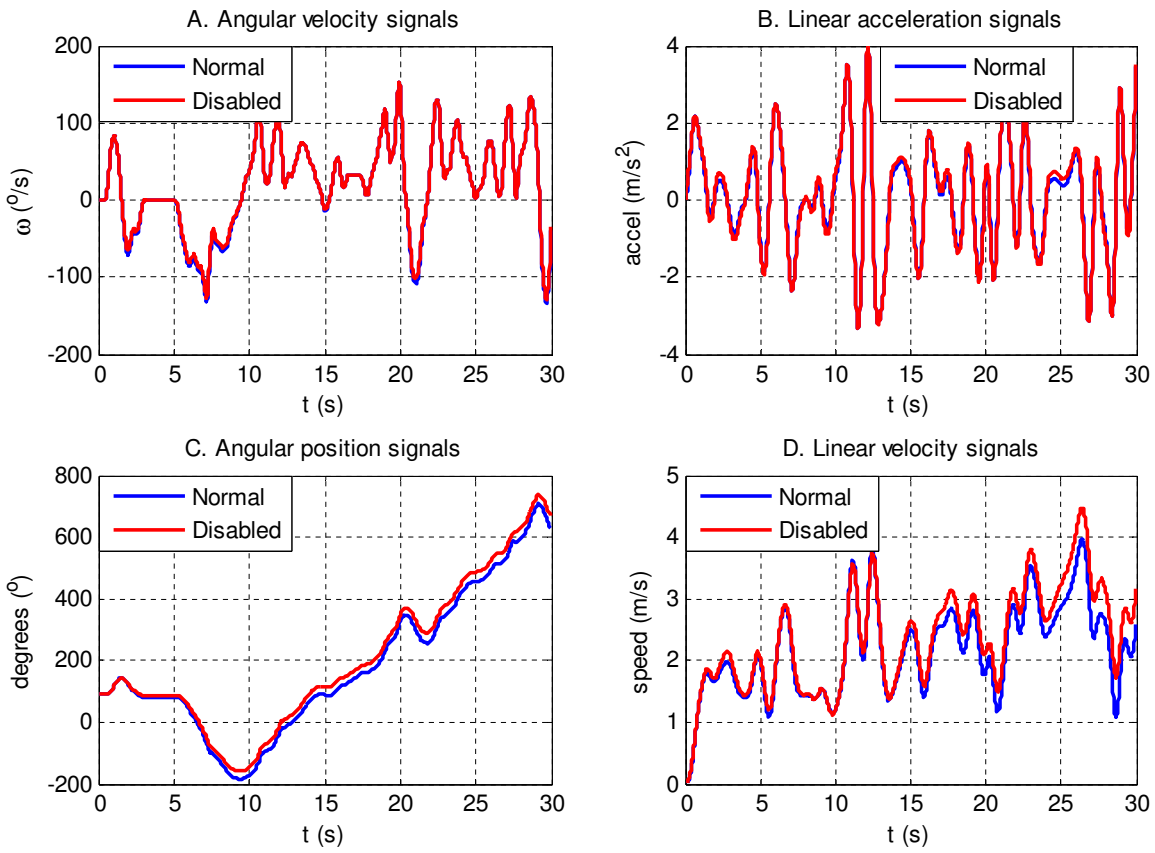

FIGURE 5.6: The resulting effect of the disability model on the angular velocity and linear acceleration signals and its corresponding contribution on the angular position and linear velocity.

velocity signals in sub-plots C and D respectively.

The simulation results of the two cases with superimposed steering disability are shown in Figure 5.7 and Figure 5.8. Each figure depicts a normal driver's trajectory, a trajectory with superimposed steering disability and the resulting controller generated trajectory in Case 1 and Case 7 in the first and second columns respectively, for comparison. It may be observed in Figure 5.7 that the trajectory with superimposed steering disability is quite poor, extending very close to the furniture with collision and near collision instances. In both cases, the controller computed signals produced better and more centralised trajectories. Although at some instances the controller

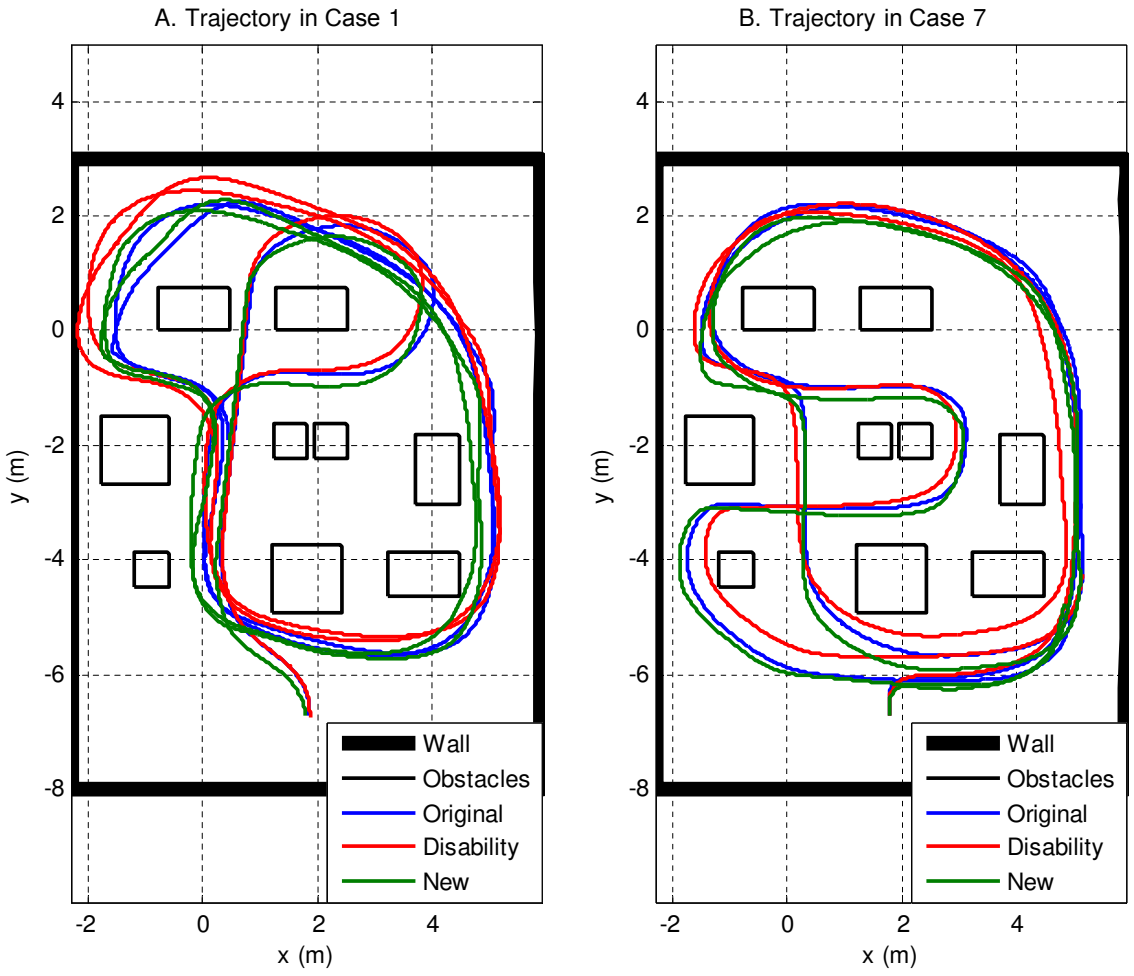

FIGURE 5.7: The wheelchair trajectory of a normal driver, the trajectory with superimposed steering disability and the resulting controller generated wheelchair trajectory, in Case 1 and Case 7.

signals deviate from the original able driver's signal, the presented results of the human-in-the-loop controller depict a forward progress towards the intended driver assistance and steering ease enhancement. Besides, the speed-errors in sub-plots C and D of Figure 5.8, produced by the controller with human-in-the-loop, are normally distributed with a smaller magnitude compared to the speed-errors of the disabled signal. Accordingly, the resulting speeds and trajectories of the human-in-the-loop controller relative to the speeds and trajectories with actual steering disabilities could be much better.

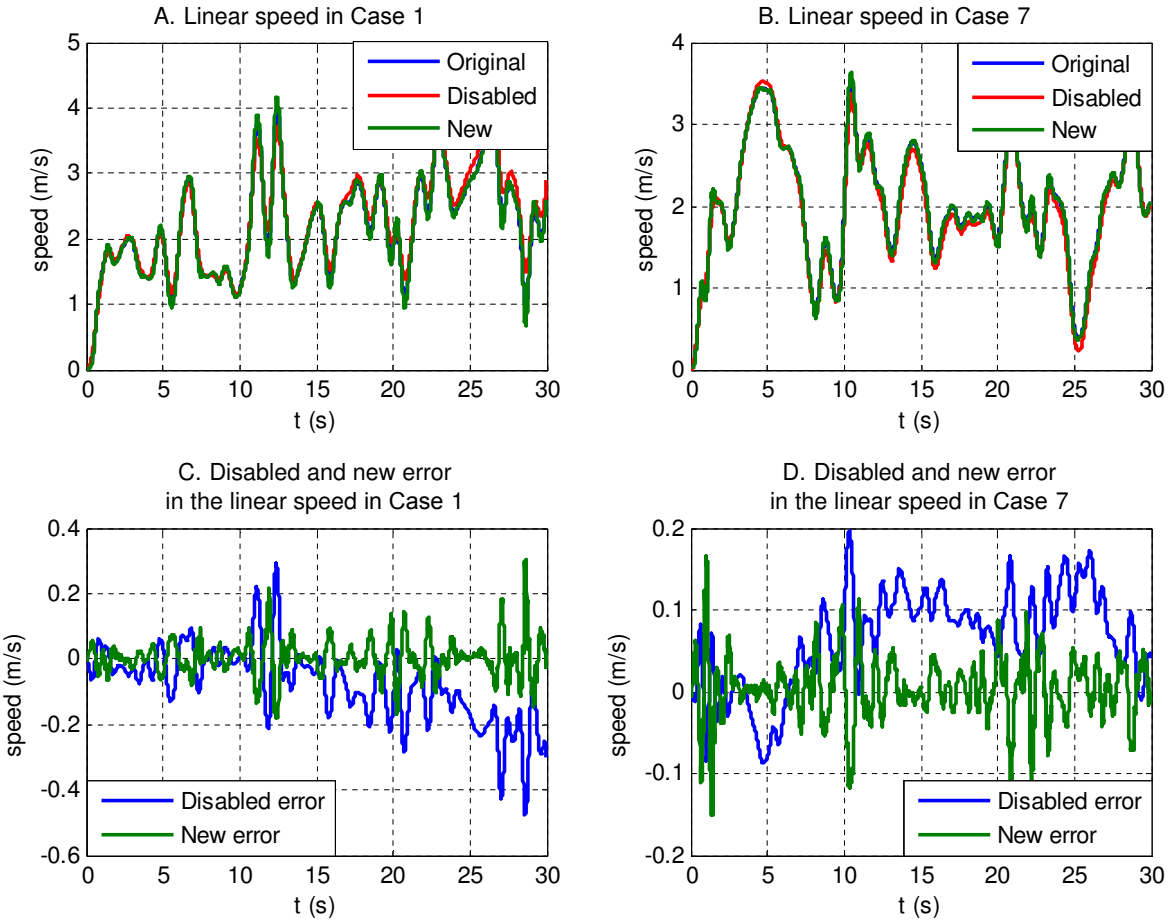

FIGURE 5.8: Sub-plots A and B depict linear wheelchair speeds produced by a normal user produced, a disabled user and the human-in-the-loop controller, while sub-plots C and D shows the resulting velocity errors in the disabled and controller computed signals relative to the normal user's, in Case 1 and Case 7.

Although the controller produces a reactive response to avert the possible dangerous situations, human drivers are also known, in practice, to observe and use the feedback result to improve their subsequent undertakings. The lack of practical implementation due to time constraints made it difficult to study the actual effects of the human-in-the-loop controller in the presence of human feedback. However, it is presumed that in a practical implementation with a driver's utilisation of the steering feedback, higher quality trajectories could be produced.

5.9 Conclusions

This chapter proposed a closed-loop controller with human-in-the-loop to adapt the steering of the wheelchair to the driver's behaviour. The linearisation of the closed-loop model is accomplished using the classical input-output feedback technique through torque compensation, and the linearised system is controlled using a simple proportional controller. To ensure an optimal tracking performance of the closed-loop control model, the performance index of the non-linear continuous-time generalised predictive control is used. Moreover, the presented simulation results have shown that it is possible to assist a wheelchair driver in the steering task, and that the control model may be used by both normal and non-normal drivers with steering problems to reduce the extra steering attention observed in typical environments. Furthermore, the results have shown the accurate tracking performance of the controller with regards to the steering signals of normal drivers, and considerable improvements in the resulting trajectory and driving speed of drivers with steering handicaps. It may however be noted that linearisation control techniques can sometimes be a real problem because the dynamics (operator included) must compensated first by the engines before the trajectory tracking, all in spite of the available power of the engine. A validation in this regard could not be accomplished due to time constraint and will therefore be necessary in future.

Chapter 6

CONCLUSION AND FUTURE WORK

6.1 Conclusion

The extensive literature survey carried out in this thesis has shown the important need for user adapted assistive systems, especially in applications like wheelchair, where the service machine forms an integral component of the user's life. It is observed that human operators exhibit diverse handling behaviours, and appreciate assistance not only because the assistive system performs the intended task to a desired conclusion, but also based on how the process executes the assistance. This makes it necessary to synthesise the behaviour of the operator into the control system. In this thesis, the control of wheelchair has been considered with a special focus on the steering support. It is observed that the contemporary wheelchair functionalities are directed towards user-suited interfaces with numerous autonomous control and hands-free navigation proposals. However, these functionalities often fail to empower the infirm users with the full control independence and self-esteem that the stronger drivers experience, and commonly disregard user disposition. Rather than the autonomous controllers, it is preferred in this thesis that the higher-level decision making tasks and control processes are granted to the driver, while the controller executes the necessary steering support in the background.

The primary objective of this study, was to advance the contemporary wheelchair steering task, by synthesising the user's driving behaviour into the control system, to implement a driver-specific background steering support. The proposed assistance was required to apply to all users in spite of their handicap conditions, and to reduce

the workload in fine control without limiting the driver's responsibility in the steering decisions. The implementation entailed integrating a driving behaviour model and a wheelchair model in the control system, to adapt the control of wheelchair to the driver's steering behaviour. This objective is accomplished by formulating the wheelchair dynamic model, by formulation and identification of the driving behaviour model and by proper implementation of the presented closed-loop control architecture.

In order to validate the proposed assistive system, it was important that the actual wheelchair dynamics and the driving behaviour of the user, are represented as much as possible in the close-loop control system. In consequence, a dynamic model of a differential drive wheelchair structure with two front castor wheels has been derived based on the Euler Lagrange formalism. Unlike the dynamic models in the literature that restrict the wheelchair motion to flat surfaces, the presented model also takes into consideration the effects of gravitational forces on the wheelchair on non-horizontal surfaces. The Lagrangian function was based on both kinetic and gravitational potentials to account for the dynamic properties of the wheelchair on both inclined and non-inclined configurations. Besides, the slipping parameters of the wheelchair are derived and integrated to represent the wheelchair slipping situations.

The formulation of the driving behaviour model was based on the reactive potential field approach on account of two fundamental sources of information: the empirical wheelchair steering knowledge, and the microscopic steering data generated by the wheelchair in different virtual environments. The DPF method has particularly been considered in the formulation of the user's risk detection and avoidance behaviours since it accounts for both distance and velocity representation, considers risks dissemination and allocates variable repulsive potential on the relative direction of a

potential risk. To present the specific behaviour of the driver, the best-fitting parameters, identified using the ordinary least square procedure from the driver's steering data, were incorporated in the driving behaviour model.

In the closed-loop system implementation, the proposed wheelchair dynamic model did not satisfy the full-state feedback linearisation conditions. The use of partial-state feedback linearisation technique, was therefore considered to track the user inputs by torque compensation. Interestingly, a minimum-phase closed-loop system resulted with stable internal dynamics. The performance index of the non-linear continuous-time GPC was also used to ensure the optimality of the resulting closed-loop system.

The primary contribution of the study lies in the use of the proposed reactive driving behaviour model, with driver-specific parameters, to represent the acceptable subjective risks and steering preferences of the driver. The simulation results have demonstrated that it is possible to improve wheelchair control and implement fine steering manoeuvres, as well as risk and collision avoidance behaviours through background steering support, by adapting the steering velocity of the wheelchair to the identified driver-specific parameters. The proposed driving model is simple and linear in the parameters, and therefore very convenient for on-line application as a real-time co-driver to predict and implement local corrective solutions to possible steering errors and emergency collision situation. The study has also contributed to the development of wheelchair dynamic model and derivation of slipping parameters. The dynamic model takes into account the effects of rolling friction, slipping parameter and gravitational potential of the wheelchair, on both inclined and non-inclined surfaces.

It was concluded from the comprehensiveness and simulation results of the wheelchair dynamic model, that it gives a better representation of the dynamic behaviour of a reality wheelchair in normal and non-normal indoor and outdoor driving conditions,

and that the reduction in the number of slip detection encoders makes it a cost effective model alternative. From the regression analysis and curve-fitting results of the driving model, it was concluded that it is possible to represent the local behaviour of a wheelchair driver using a simple reactive model that is linear in parameters. The presented driving behaviour model that modifies the driver's signals based on the contextual situation, to adapt the wheelchair to the driver's behaviour is assumed to have explicit knowledge of the driver's subsequent intentions. It was concluded from the identification parameters that although the drivers exhibit similar driving behaviours, there is always an implied uniqueness with each driver making it necessary to model and identify the driver's behaviour. It is presumed from these conclusions, that the wheelchair dynamic model and the driving behaviour model can be used in the implementation of the proposed wheelchair control with human-in-the-loop. The accurate tracking results of the closed-loop control system validates this presumption.

6.2 Recommendations for future works

The study concentrated on the utilisation of user-specific steering behaviours to adapt the control of wheelchair to the driver's driving preferences. However due to time constraints, the presented model is only validated by simulation. Furthermore, besides the superimposed modelled disability, the steering data used in the validation did not include the actual disability signal. A practical implementation of the human-in-the-loop control is necessary with real disability signals, in an actual steering situation under clinical supervision, to ensure a conclusive validation of the support system. It may be necessary that this also takes into consideration the reaction delay of the driver. Besides, the study presumed a driver with relatively predictable steering signals, but it may be necessary in the case of serious steering disability to establish the

driver's explicit intention. This justifies the important need to integrate an intention detection system in closed-loop model. The usability of the intention detection models should therefore be considered in future. This entails further study and research on novel input techniques like eye-tracking, and use of BCI and brain-actuated systems to acquire the necessary information for wheelchair control. It may also be noticed, that the presented driving behaviour model only took into consideration the observable driver actions and wheelchair reactions. However, numerous cognitive processes are also known to affect the driving behaviour, further study is necessary in this respect.

Adapting the wheelchair to common user environments may as well be very important to ensure inclusivity of the user community. Certainly, this includes obstacle and collision avoidance tasks that have received significant attention in the wheelchair literature. These tasks require the accurate sensors that often come with prohibitive costs. Sensor related studies are therefore still necessary to improve the accuracy and affordability of assistive wheelchairs. Moreover, staircase wheelchair climbing capabilities have been proposed in the literature, but further research is required to enable commercial implementation.

Bibliography

Ahmed F. & Deb K. 2013. Multi-objective optimal path planning using elitist non-dominated sorting genetic algorithms. *Soft Computing*, 17(7):1283–1299.

Ahmed K.I. 1999. *Modeling Drivers ' Acceleration and Lane Changing Behavior*. Ph.D. thesis, Massachusetts Institute of Technology.

Allen R.W., Szostak H.T., & Rosenthal T.J. 1987. Analysis and Computer Simulation of Driver/Vehicle Interaction. Technical report, Society of Automotive Engineers (SAE International).

Ambike S. & Schmiedeler J.P. 2006. Modeling time invariance in human arm motion coordination. In J. Lennarčič & B. Roth, editors, *Advances in Robot Kinematics*, 177–184. Springer Netherlands, Dordrecht. ISBN 978-1-4020-4940-8.

Ando N. & Ueda S. 2000. Functional deterioration in adults with cerebral palsy. *Clinical Rehabilitation*, 14(3):300–306.

Apel A. & Mitschke M. 1997. Adjusting vehicle characteristics by means of driver models. *International Journal of Vehicle Design*, 18(6):583–596.

Astolfi A. 1996. Discontinuous control of nonholonomic systems. *Systems & Control Letters*, 27(1):37–45.

Barraquand J., Langlois B., & Latombe J.C. 1992. Numerical potential field techniques for robot path planning. *IEEE Transactions on Systems, Man, and Cybernetics*, 22(2):224–241.

Bauer A., Wollherr D., & Buss M. 2008. Human-robot collaboration: A survey. *International Journal of Humanoid Robotics*, 05(01):47–66.

Beard R. 2005. Satisficing approach to human-in-the-loop safeguarded control. In *Proceedings of the 2005, American Control Conference, 2005.*, 4985–4990. IEEE. ISBN 0-7803-9098-9.

Beare A.N. & Dorris R.E. 1983. A Simulator-Based Study of Human Errors in Nuclear Power Plant Control Room Tasks. *Proceedings of the Human Factors and Ergonomics Society Annual Meeting*, 27(2):170–174.

Berg-Yuen P.E., Mehta S.S., Pasiliao E.L., & Murphey R.A. 2012. Control of human-machine interaction for wide area search munitions in the presence of target uncertainty. In *Proceedings of the seventh annual ACM/IEEE international conference on Human-Robot Interaction - HRI '12*, 195. ACM Press, New York, New York, USA. ISBN 9781450310635.

Bidram A., Lewis F.L., & Davoudi A. 2014. Synchronization of nonlinear heterogeneous cooperative systems using inputoutput feedback linearization. *Automatica*, 50(10):2578–2585.

Bloch A. & McClamroch N. 1989. Control of mechanical systems with classical nonholonomic constraints. In *Proceedings of the 28th IEEE Conference on Decision and Control*, 201–205. IEEE.

Book W.J. 1984. Recursive Lagrangian Dynamics of Flexible Manipulator Arms. *The International Journal of Robotics Research*, 3(3):87–101.

Boril J., Jalovecky R., & Ali R. 2012. Human-machine interaction and simulation models used in aviation.

Bornard J.C., Sassman M., & Bellet T. 2016. Use of a computational simulation model of drivers' cognition to predict decision making and behaviour while driving. *Biologically Inspired Cognitive Architectures*, 15:41–50.

Bortoff S.A. 1997. Approximate state-feedback linearization using spline functions. *Automatica*, 33(8):1449–1458.

Bruemmer D., Few D., Boring R., Marble J., Walton M., & Nielsen C. 2005. Shared Understanding for Collaborative Control. *IEEE Transactions on Systems, Man, and Cybernetics - Part A: Systems and Humans*, 35(4):494–504.

Bryant R.L. 2006. Geometry of Manifolds with Special Holonomy: "100 Years of Holonomy". In G. Jensen & S. Krantz, editors, *150 Years of Mathematics at Washington University in St. Louis*, 29–38. American Mathematical Society, Providence, Rhode Island. ISBN 082183603X.

Byung-Ju Yi & Whee Kuk Kim 2000. The kinematics for redundantly actuated omnidirectional mobile robots. In *Proceedings 2000 ICRA. Millennium Conference. IEEE International Conference on Robotics and Automation. Symposia Proceedings*

(Cat. No.00CH37065), volume 3, 2485–2492. IEEE, San Francisco, CA. ISBN 0-7803-5886-4.

Cacciabue P.C. & Carsten O. 2010. A simple model of driver behaviour to sustain design and safety assessment of automated systems in automotive environments. *Applied ergonomics*, 41(2):187–97.

Campion G., D'Andrea-Novel B., & Bastin G. 1991. Controllability and state feedback stabilizability of non holonomic mechanical systems. In C. Canudas de Wit, editor, *Control of Robotic Systems with Nonholonomic Constraints: Advanced Robot Control*, volume 162 of *Lecture Notes in Control and Information Sciences*, 106–124. Springer Berlin Heidelberg, Berlin, Heidelberg. ISBN 978-3-540-54169-1.

Carlson T. & Demiris Y. 2008. Collaborative control in human wheelchair interaction reduces the need for dexterity in precise manoeuvres. In *Proceedings of "Robotic Helpers: User Interaction, Interfaces and Companions in Assistive and Therapy Robotics", a Workshop at ACM/IEEE HRI 2008*, 59–66. University of Hertfordshire.

Carlson T. & Demiris Y. 2012. Collaborative control for a robotic wheelchair: evaluation of performance, attention, and workload. *IEEE transactions on systems, man, and cybernetics. Part B, Cybernetics : a publication of the IEEE Systems, Man, and Cybernetics Society*, 42(3):876–88.

Chen I.M. & Yang G. 1998. Automatic Model Generation for Modular Reconfigurable Robot Dynamics. *Journal of Dynamic Systems, Measurement, and Control*, 120(3):346.

Chen L.K. & Ulsoy a.G. 2001. Identification of a Driver Steering Model, and Model Uncertainty, From Driving Simulator Data. *Journal of Dynamic Systems, Measurement, and Control*, 123(4):623.

Chen P.c. & Huang H.p. 2006. 3D Dynamical Analysis for a Caster Wheeled Mobile Robot Moving on the Frictional Surface. In *2006 IEEE/RSJ International Conference on Intelligent Robots and Systems*, 3056–3061. IEEE. ISBN 1-4244-0258-1.

Chen W. 2001. Dynamic modeling of multi-link flexible robotic manipulators. *Computers & Structures*, 79(2):183–195.

Cheng B. & Fujioka T. 1997. A hierarchical driver model. In *Proceedings of Conference on Intelligent Transportation Systems*, 960–965. IEEE. ISBN 0-7803-4269-0.

Chénier F., Bigras P., & Aissaoui R. 2011. A new dynamic model of the manual wheelchair for straight and curvilinear propulsion. *IEEE ... International Conference on Rehabilitation Robotics : [proceedings]*, 2011:5975357.

Chenier F., Bigras P., & Aissaoui R. 2011. An Orientation Estimator for the Wheelchair's Caster Wheels. *IEEE Transactions on Control Systems Technology*, 19(6):1317–1326.

Chénier F., Bigras P., & Aissaoui R. 2015. A new dynamic model of the wheelchair propulsion on straight and curvilinear level-ground paths. *Computer methods in biomechanics and biomedical engineering*, 18(10):1031–1043.

Chiang H.H.H., Wu S.J.J., Perng J.W.W., Wu B.F.F., & Lee T.T.T. 2010. The human-in-the-loop design approach to the longitudinal automation system for an intelligent vehicle. *IEEE Transactions on Systems, Man, and Cybernetics Part A:Systems and Humans*, 40(4):708–720.

Chrpa L., Pinto J., Ribeiro M.A., Py F., Sousa J., & Rajan K. 2015. On mixed-initiative planning and control for Autonomous underwater vehicles. In *2015 IEEE/RSJ International Conference on Intelligent Robots and Systems (IROS)*, 1685–1690. IEEE. ISBN 978-1-4799-9994-1.

Chua J.J., Fuss F.K., & Subic A. 2010. Rolling friction of a rugby wheelchair. *Procedia Engineering*, 2(2):3071–3076.

Codourey A. 1998. Dynamic Modeling of Parallel Robots for Computed-Torque Control Implementation. *The International Journal of Robotics Research*, 17(12):1325–1336.

Cooper R.a., Robertson R.N., Lawrence B., Heil T., Albright S.J., VanSickle D.P., & Gonzalez J. 1996. Life-cycle analysis of depot versus rehabilitation manual wheelchairs. *Journal of rehabilitation research and development*, 33(1):45–55.

Corno M., Giani P., Tanelli M., & Savaresi S.M. 2015. Human-in-the-Loop Bicycle Control via Active Heart Rate Regulation. *IEEE Transactions on Control Systems Technology*, 23(3):1029–1040.

Costa T.V., Fileti A.M.F., Oliveira-Lopes L.C., & Silva F.V. 2014. Experimental assessment and design of multiple model predictive control based on local model networks for industrial processes. *Evolving Systems*, 6(4):243–253.

Dabo M., Chafouk H., & Langlois N. 2009. Unconstrained NCGPC with a guaranteed closed-loop stability: Case of nonlinear SISO systems with the relative degree greater than four. In *Proceedings of the 48h IEEE Conference on Decision and Control (CDC) held jointly with 2009 28th Chinese Control Conference*, 1980–1985. IEEE. ISBN 978-1-4244-3871-6.

D'Andrea-Novel B., Bastin G., & Campion G. 1991. Modelling and control of non-holonomic wheeled mobile robots. In *Proceedings. 1991 IEEE International Conference on Robotics and Automation*, 1130–1135. IEEE Comput. Soc. Press. ISBN 0-8186-2163-X.

Dasgupta B. & Choudhury P. 1999. A general strategy based on the NewtonEuler approach for the dynamic formulation of parallel manipulators. *Mechanism and Machine Theory*, 34(6):801–824.

De La Cruz C., Bastos T.F., & Carelli R. 2011. Adaptive motion control law of a robotic wheelchair. *Control Engineering Practice*, 19(2):113–125.

De Luca A. 2000. Feedforward/feedback laws for the control of flexible robots. In *Proceedings 2000 ICRA. Millennium Conference. IEEE International Conference on Robotics and Automation. Symposia Proceedings (Cat. No.00CH37065)*, volume 1, 233–240. IEEE. ISBN 0-7803-5886-4.

De Luca A. & Ferrajoli L. 2009. A modified newton-euler method for dynamic computations in robot fault detection and control. In *2009 IEEE International Conference on Robotics and Automation*, 3359–3364. IEEE. ISBN 978-1-4244-2788-8.

de Waard D. 1996. *The measurement of drivers' mental workload*. Ph.D. thesis, University of Groningen.

DeFigueiredo R.J.P. & Chen G. 1993. *Nonlinear feedback control systems: an operator theory approach*. Academic Press. ISBN 0122086309.

Demeester E., Hüntemann A., Vanhooydonck D., Vanacker G., Degeest A., Van Brussel H., & Nuttin M. 2006. Bayesian estimation of wheelchair driver intents: Modeling intents as geometric paths tracked by the driver. In *IEEE International Conference on Intelligent Robots and Systems*, 5775–5780. ISBN 142440259X.

Demeester E., Nuttin M., Vanhooydonck D., & Van Brussel H. 2003a. A model-based, probabilistic framework for plan recognition in shared wheelchair control: experiments and evaluation. In *Proceedings 2003 IEEE/RSJ International Conference on Intelligent Robots and Systems (IROS 2003) (Cat. No.03CH37453)*, volume 2, 1456–1461. IEEE. ISBN 0-7803-7860-1.

Demeester E., Nuttin M., Vanhooydonck D., & Van Brussel H. 2003b. Fine motion planning for shared wheelchair control: Requirements and preliminary experiments. In *Proceedings of ICAR 2003 The 11th International Conference on Advanced Robotics Coimbra, Portugal, June 30 - July 3, 2003*, 1278–1283.

Demirciolu H. & Gawthrop P. 1991. Continuous-time generalized predictive control (CGPC). *Automatica*, 27(1):55–74.

Dennett D. 1989. *The intentional stance*. MIT Press, Cambridge Mass. ISBN 9780262540537.

DeSantis R.M. 2009. Modeling and path-tracking control of a mobile wheeled robot with a differential drive. *Robotica*, 13(04):401.

Dicianno B.E., Cooper R.a., & Coltellaro J. 2010. Joystick control for powered mobility: current state of technology and future directions. *Physical medicine and rehabilitation clinics of North America*, 21(1):79–86.

Diehm G., Maier S., Flad M., & Hohmann S. 2013. An identification method for individual driver steering behaviour modelled by switched affine systems. *Proceedings of the IEEE Conference on Decision and Control*, 3547–3553.

Ding D. & Cooper R. 2005. Electric powered wheelchairs. *IEEE Control Systems Magazine*, 25(2):22–34.

Do K. 2015. Global output-feedback path-following control of unicycle-type mobile robots: A level curve approach. *Robotics and Autonomous Systems*, 74:229–242.

Donges E. 1978. A Two-Level Model of Driver Steering Behavior. *Human Factors: The Journal of the Human Factors and Ergonomics Society*, 20(6):691–707.

Eboli L., Mazzulla G., & Pungillo G. 2016. Combining speed and acceleration to define car users' safe or unsafe driving behaviour. *Transportation Research Part C: Emerging Technologies*, 68:113–125.

Edelmann J., Plöchl M., Reinalter W., & Tieber W. 2007. A passenger car driver model for higher lateral accelerations. *Vehicle System Dynamics*, 45(12):1117–1129.

Eghtesad M. & Necsulescu D.S. 2004. Experimental study of the dynamic based feedback linearization of an autonomous wheeled ground vehicle. *Robotics and Autonomous Systems*, 47(1):47–63.

Eizmendi G., Azkoitia J.M., & Craddock G.M. 2007. *Challenges for Assistive Technology: AAATE 07*. IOS Press. ISBN 1586037919.

El-Shenawy A. 2010. *Motion Control of Holonomic Wheeled Mobile Robot with Modular Actuation*. Ph.D. thesis, The University of Mannheim Institute of Computer Engineering.

Emam H., Hamam Y., Monacelli E., & Djouani K. 2010. Power wheelchair driver behaviour modelling. In *7th International Multi-Conference on Systems, Signals and Devices*, 1–7. IEEE. ISBN 9781424475346.

Emam H., Hamam Y., Monacelli E., Mougharbel I., & Engineering E. 2007. Dynamic model of electrical wheelchair with slipping detection. In *Proc. EUROSIM 2007*, 1–6. EUROSIM / SLOSIM, Ljubljana, Slovenia. ISBN 9783901608322.

Enache N., Mammar S., Netto M., & Lusetti B. 2010. Driver Steering Assistance for Lane-Departure Avoidance Based on Hybrid Automata and Composite Lyapunov Function. *IEEE Transactions on Intelligent Transportation Systems*, 11(1):28–39.

Engström J. & Hollnagel E. 2007. A General Conceptual Framework for Modelling Behavioural Effects of Driver Support Functions. In *Modelling Driver Behaviour in Automotive Environments*, 61–84. Springer London. ISBN 978-1-84628-618-6.

Featherstone R. 1987. *Robot Dynamics Algorithms*. Kluwer Academic Publishers. ISBN 1475764375.

Fehr L., Langbein W.E., & Skaar S.B. 2000. Adequacy of power wheelchair control interfaces for persons with severe disabilities: a clinical survey. *Journal of rehabilitation research and development*, 37(3):353–60.

Feng L., Wiltsche C., Humphrey L., & Topcu U. 2016. Synthesis of Human-in-the-Loop Control Protocols for Autonomous Systems. *IEEE Transactions on Automation Science and Engineering*, 13(2):450–462.

Fierro R. & Lewis F.L. 1997. Control of a nonholomic mobile robot: Backstepping kinematics into dynamics. *Journal of Robotic Systems*, 14(3):149–163.

Finlayson M. & van Denend T. 2003. Experiencing the loss of mobility: perspectives of older adults with MS. *Disability and rehabilitation*, 25(20):1168–80.

Fiorentini L. & Serrani A. 2012. Adaptive restricted trajectory tracking for a non-minimum phase hypersonic vehicle model. *Automatica*, 48(7):1248–1261.

Fraichard T. 2007. A Short Paper about Motion Safety. In *Proceedings 2007 IEEE International Conference on Robotics and Automation*, 1140–1145. IEEE. ISBN 1-4244-0602-1.

Fuller R. 2005. Towards a general theory of driver behaviour. *Accident; analysis and prevention*, 37(3):461–72.

Gabay E. & Merhav S.J. 1977. Identification of a Parametric Model of the Human Operator in Closed-Loop Control Tasks. *IEEE Transactions on Systems, Man, and Cybernetics*, 7(4):284–292.

Galicki M. 2016. Real-time constrained trajectory generation of mobile manipulators. *Robotics and Autonomous Systems*, 78:49–62.

Gamarra C. & Guerrero J.M. 2015. Computational optimization techniques applied to microgrids planning: A review. *Renewable and Sustainable Energy Reviews*, 48:413–424.

Ge S. & Cui Y. 2002. Dynamic Motion Planning for Mobile Robots Using Potential Field Method. *Autonomous Robots*, 13(3):207–222.

Ge Z. & Song Z. 2008. Online monitoring of nonlinear multiple mode processes based on adaptive local model approach. *Control Engineering Practice*, 16(12):1427–1437.

Goodrich M.A. & Schultz A.C. 2007. Human-Robot Interaction: A Survey.

Gray A., Ali M., Gao Y., Hedrick J.K., & Borrelli F. 2013. A Unified Approach to Threat Assessment and Control for Automotive Active Safety. *IEEE Transactions on Intelligent Transportation Systems*, 14(3):1490–1499.

Guo H., Ji Y., Qu T., & Chen H. 2013. Understanding and Modeling the Human Driver Behavior Based on MPC. In *IFAC Proceedings Volumes*, volume 46, 133–138. ISBN 9783902823489.

Guo K., Ding H., Zhang J., Lu J., & Wang R. 2004. Development of a longitudinal and lateral driver model for autonomous vehicle control. *International Journal of Vehicle Design*, 36(1).

Hahn H. 2003. *Rigid Body Dynamics of Mechanisms 2: 2 Applications*. Springer Science & Business Media. ISBN 3540022376.

Hoc J.M. 2010. From human machine interaction to human machine cooperation. *Ergonomics*.

Hoffman M.D., Millet G.Y., Hoch A.Z., & Candau R.B. 2003. Assessment of wheelchair drag resistance using a coasting deceleration technique. *American journal of physical medicine & rehabilitation / Association of Academic Physiatrists*, 82(11):880–9; quiz 890–2.

Hollerbach J.M. 1980. A Recursive Lagrangian Formulation of Maniputator Dynamics and a Comparative Study of Dynamics Formulation Complexity. *IEEE Transactions on Systems, Man, and Cybernetics*, 10(11):730–736.

Holmberg R. & Khatib O. 2000. A Powered-Caster Holonomic Robotic Vehicle for Mobile Manipulation Tasks. In A. Morecki, G. Bianchi, & C. Rzymkowski, editors, *Romansy 13*, volume 422 of *CISM International Centre for Mechanical Sciences*, chapter Chapter II, 157–167. Springer Vienna, Vienna. ISBN 978-3-7091-2500-7.

Hori Y., Toyoda Y., & Tsuruoka Y. 1998. Traction Control of Electric Vehicle: Basic Experimental Results Using the Test EV UOT Electric March. *IEEE Transactions on Industry Applications*, 34(5):1131–1138.

How T.V., Wang R.H., & Mihailidis A. 2013. Evaluation of an intelligent wheelchair system for older adults with cognitive impairments. *Journal of neuroengineering and rehabilitation*, 10:90.

Hunt L.R., Meyer G., Su R., & Meyer G. 1983. Global transformations of nonlinear systems. *IEEE Transactions on Automatic Control*, 28(I):24–31.

Hüntemann A., Demeester E., Nuttin M., & Van Brussel H. 2008. Online user modeling with Gaussian Processes for Bayesian plan recognition during power-wheelchair steering. In *2008 IEEE/RSJ International Conference on Intelligent Robots and Systems, IROS*, 285–292. ISBN 9781424420582.

Isidori A. 1995. *Nonlinear Control Systems*. Springer Science & Business Media, third edition. ISBN 1846286158.

Isidori A. 1999. *Nonlinear Control Systems II*. Springer Science & Business Media. ISBN 1852331887.

Jaradat M.A.K., Garibeh M.H., & Feilat E.A. 2011. Autonomous mobile robot dynamic motion planning using hybrid fuzzy potential field. *Soft Computing*, 16(1):153–164.

Jaulin L. 2015. Feedback Linearization. In *Mobile Robotics*, chapter 2, 45–100. Elsevier. ISBN 9781785480485.

Jazar R.N. 2011. *Advanced Dynamics: Rigid Body, Multibody, and Aerospace Applications*. John Wiley & Sons. ISBN 0470398353.

Johansen T., Hunt K., Gawthrop P., & Fritz H. 1998. Off-equilibrium linearisation and design of gain-scheduled control with application to vehicle speed control. *Control Engineering Practice*, 6(2):167–180.

Johnson B.W. & Aylor J.H. 1985. Dynamic Modeling of an Electric Wheelchair. *IEEE Transactions on Industry Applications*, IA-21(5):1284–1293.

Ju J.S., Shin Y., & Kim E.Y. 2009. Vision based interface system for hands free control of an Intelligent Wheelchair. *Journal of neuroengineering and rehabilitation*, 6:33.

Kageyama I. & Owada Y. 1996. An Analysis of a Riding Control Algorithm for Two Wheeled Vehicles with a Neural Network Modeling. *Vehicle System Dynamics*, 25(sup1):317–326.

Kageyama I. & Pacejka H.B. 1992. On a new driver model with fuzzy control. *Vehicle System Dynamics*, 20(Supp 1):314–324.

Kahn M.E. & Roth B. 1971. The Near-Minimum-Time Control of Open-Loop Articulated Kinematic Chains. *Journal of Dynamic Systems, Measurement, and Control*, 93(3):164.

Kane T.R. & Levinson D.A. 1983. The Use of Kane's Dynamical Equations in Robotics. *The International Journal of Robotics Research*, 2(3):3–21.

Kane T.R., Ryan R., & Banerjee A.K. 2012. Dynamics of a cantilever beam attached to a moving base. *Journal of Guidance, Control, and Dynamics*.

Kanzawa T., Haruki M., & Yamanaka K. 2016. Steering Law of Control Moment Gyroscopes for Agile Attitude Maneuvers. *Journal of Guidance, Control, and Dynamics*, 1–11.

Katevas N. 2001. Mobile Robotics in Healthcare. In N. Katevas, editor, *Assistive Technology Research Series 7*, 380. IOS Press, Tokyo, Japan. ISBN 1586030795.

Katrakazas C., Quddus M., Chen W.H., & Deka L. 2015. Real-time motion planning methods for autonomous on-road driving: State-of-the-art and future research directions. *Transportation Research Part C: Emerging Technologies*, 60:416–442.

Katsura S. & Ohnishi K. 2004. Human Cooperative Wheelchair for Haptic Interaction Based on Dual Compliance Control. *IEEE Transactions on Industrial Electronics*, 51(1):221–228.

Keen S.D. & Cole D.J. 2012. Bias-free identification of a linear model-predictive steering controller from measured driver steering behavior. *IEEE transactions on systems, man, and cybernetics. Part B, Cybernetics : a publication of the IEEE Systems, Man, and Cybernetics Society*, 42(2):434–443.

Kelly A. & Seegmiller N. 2010. A Vector Algebra Formulation of Kinematics of Wheeled Mobile Robots. In K. Yoshida & S. Tadokoro, editors, *International conference on Field and Service Robotics*, 1–14. Springer-Verlag Berlin Heidelberg, Matsushima, Miyagi, Japan.

Kelly R., Davila V.S., & Perez J.A.L. 2006. *Control of Robot Manipulators in Joint Space*. Springer Science & Business Media. ISBN 1852339993.

Khalil W. 2011. Dynamic Modeling of Robots Using Newton-Euler Formulation. In J.A. Cetto, J.L. Ferrier, & J. Filipe, editors, *Informatics in Control, Automation and Robotics*, volume 89 of *Lecture Notes in Electrical Engineering*, 3–20. Springer Berlin Heidelberg, Berlin, Heidelberg. ISBN 978-3-642-19538-9.

Khalil W. & Ibrahim O. 2007. General Solution for the Dynamic Modeling of Parallel Robots. *Journal of Intelligent and Robotic Systems*, 49(1):19–37.

Khalil W. & Kleinfinger J.F. 1987. Minimum operations and minimum parameters of the dynamic models of tree structure robots. *IEEE Journal on Robotics and Automation*, 3(6):517–526.

Khatib O. 1985. Real-time obstacle avoidance for manipulators and mobile robots. *Proceedings. 1985 IEEE International Conference on Robotics and Automation*, 2:500–505.

Khondaker B. & Kattan L. 2015. Variable speed limit: A microscopic analysis in a connected vehicle environment. *Transportation Research Part C: Emerging Technologies*, 58:146–159.

Khosla P.K. & Kanade T. 1988. Experimental Evaluation of Nonlinear Feedback and Feedforward Control Schemes for Manipulators. *The International Journal of Robotics Research*, 7(1):18–28.

Kleinman D. & Perkins T. 1974. Modeling human performance in a time-varying anti-aircraft tracking loop. *IEEE Transactions on Automatic Control*, 19(4):297–306.

Kondo M. & Ajimine A. 1968. Driver's Sight Point and Dynamics of the Driver-Vehicle-System Related to It. Technical report, Society of Automotive Engineers.

Koon W.S. & Marsden J.E. 1997. The Hamiltonian and Lagrangian approaches to the dynamics of nonholonomic systems. *Reports on Mathematical Physics*, 40(1):21–62.

Korayem M. & Ghariblu H. 2003. Maximum allowable load on wheeled mobile manipulators imposing redundancy constraints. *Robotics and Autonomous Systems*, 44(2):151–159.

Korayem M. & Shafei A. 2009. Motion equations proper for forward dynamics of robotic manipulator with flexible links by using recursive Gibbs-Appell formulation. *Scientia Iranica*, 16(6):479–495.

Koren Y. & Borenstein J. 1991. Potential field methods and their inherent limitations for mobile robot navigation. *Proceedings of the IEEE Int. Conf. on Robotics and Automation*, 1398–1404.

Kozłowski K. & Pazderski D. 2004. Modeling and control of a 4-wheel skid-steering mobile robot. *International Journal of Applied Mathematics and Computer Science*, 14(4):477–496.

Kraiss K. & Kuttelwesch H. 1991. Identification and application of neural operator models in a car driving situation. In *IJCNN-91-Seattle International Joint Conference on Neural Networks*, volume ii, 917. IEEE. ISBN 0-7803-0164-1.

Krüger J., Lien T., & Verl A. 2009. Cooperation of human and machines in assembly lines. *CIRP Annals - Manufacturing Technology*, 58(2):628–646.

Kruse T., Pandey A.K., Alami R., & Kirsch A. 2013. Human-aware robot navigation: A survey. *Robotics and Autonomous Systems*, 61(12):1726–1743.

Kuriyagawa Y., Im H.E., Kageyama I., & Onishi S. 2002. A Research on Analytical Method of Driver-Vehicle-Environment System for Construction of Intelligent Driver Support System. *Vehicle System Dynamics*, 37(5):339–358.

Lam C.P. & Sastry S.S. 2014. A POMDP framework for human-in-the-loop system. In *53rd IEEE Conference on Decision and Control*, 6031–6036. IEEE. ISBN 978-1-4673-6090-6.

Latombe J.C. 1991. *Robot Motion Planning*. Kluwer Academic Publishers. ISBN 079239206X.

Lauffenburger J., Basset M., Coffin F., & Gissinger G. 2003. Driver-aid system using path-planning for lateral vehicle control. *Control Engineering Practice*, 11(2):217–231.

Lauffenburger J.P., Basset M., & Gissinger G.L. 2005. Design of a coupled longitudinal-lateral trajectographic driver model. In *Proceedings of the 16th IFAC World Congress*, volume 16 Part 1, 1893–1893. ISBN 978-3-902661-75-3.

Laumond J.P., editor 1998. *Robot Motion Planning and Control*, volume 229 of *Lecture Notes in Control and Information Sciences*. Springer Berlin Heidelberg, Berlin, Heidelberg. ISBN 978-3-540-76219-5.

Lee S. & Lee H. 1992. Teleoperator control system design with human in control loop and telemonitoring force feedback. In *[1992] Proceedings of the 31st IEEE Conference on Decision and Control*, 2674–2679. IEEE. ISBN 0-7803-0872-7.

Levine P.S., Bell A.D., Jaros A.L., Simpson C.R., Koren Y., & Borenstein J. 1999. The NavChair Assistive Wheelchair Navigation System. *IEEE Transactions on Rehabilitation Engineering*, 7(4):443–451.

Li Z. & Yang C. 2012. Neural-Adaptive Output Feedback Control of a Class of Transportation Vehicles Based on Wheeled Inverted Pendulum Models. *IEEE Transactions on Control Systems Technology*, 20(6):1583–1591.

Looney C. & Tacker E. 1990. Human-in-the-loop control with majority vote neural networks. In *1990 IEEE International Conference on Systems, Man, and Cybernetics Conference Proceedings*, 224–226. IEEE. ISBN 0-87942-597-0.

Luh J.Y.S., Walker M.W., & Paul R.P.C. 1980. On-Line Computational Scheme for Mechanical Manipulators. *Journal of Dynamic Systems, Measurement, and Control*, 102(2):69.

MacAdam C., Bareket Z., Fancher P., & Ervin R. 1998. Using neural networks to identify driving style and headway control behavior of drivers. *Vehicle System Dynamics*, 29(sup1):143–160.

MacAdam C.C. 1980. An Optimal Preview Control for Linear Systems. *Journal of Dynamic Systems, Measurement, and Control*, 102(3):188.

MacAdam C.C. 2003. Understanding and Modeling the Human Driver. *Vehicle System Dynamics*, 40(1-3):101–134.

Mano H., Kon K., Sato N., Ito M., Mizumoto H., Goto K., Chatterjee R., & Matsuno F. 2009. Treaded control system for rescue robots in indoor environment. In *2008 IEEE International Conference on Robotics and Biomimetics*, 1836–1843. IEEE. ISBN 978-1-4244-2678-2.

Mariappan M., Wee C.C., Vellian K., & Weng C.K. 2009. A navigation methodology of an holonomic mobile robot using optical tracking device (OTD). In *TENCON 2009 - 2009 IEEE Region 10 Conference*, 1–6. IEEE. ISBN 978-1-4244-4546-2.

Masehian E. & Sedighizadeh D. 2007. Classic and Heuristic Approaches in Robot Motion Planning A Chronological Review. *World Academy of Science, Engineering and Technology*, 29(5):101–106.

Matni N. 2008. Reachability-based abstraction for an aircraft landing under shared control. In *2008 American Control Conference*, 2278–2284. IEEE. ISBN 978-1-4244-2078-0.

Mayne D., Rawlings J., Rao C., & Scokaert P. 2000. Constrained model predictive control: Stability and optimality. *Automatica*, 36(6):789–814.

McRuer D. & Krendel E. 1962. The Man-Machine System Concept. *Proceedings of the IRE*, 50(5):1117–1123.

McRuer D.T., Allen R.W., Weir D.H., & Klein R.H. 1977. New Results in Driver Steering Control Models. *Human Factors: The Journal of the Human Factors and Ergonomics Society*, 19(4):381–397.

Mei J., Ren W., & Ma G. 2011. Distributed Coordinated Tracking With a Dynamic Leader for Multiple Euler-Lagrange Systems. *IEEE Transactions on Automatic Control*, 56(6):1415–1421.

Merlet J.P. 2007. Jacobian, Manipulability, Condition Number and Accuracy of Parallel Robots. In S. Thrun, R. Brooks, & H. Durrant-Whyte, editors, *Robotics*

Research, volume 28 of *Springer Tracts in Advanced Robotics*. Springer Berlin Heidelberg, Berlin, Heidelberg. ISBN 978-3-540-48110-2.

Michon J.A. 1985. A Critical View of Driver Behavior Models: What Do We Know, What Should We Do? In L. Evans & R.C. Schwing, editors, *Human Behavior and Traffic Safety*, chapter Human Beha, 485–524. Springer US. ISBN 978-1-4613-2173-6.

Miller K. 2004. Optimal Design and Modeling of Spatial Parallel Manipulators. *The International Journal of Robotics Research*, 23(2):127–140.

Mitchell I.M., Viswanathan P., Adhikari B., Rothfels E., & Mackworth A.K. 2014. Shared control policies for safe wheelchair navigation of elderly adults with cognitive and mobility impairments: Designing a wizard of oz study. In *2014 American Control Conference*, 4087–4094. IEEE. ISBN 978-1-4799-3274-0.

Mitschke M. 1993. Driver-Vehicle-Lateral dynamics under Regular Driving Conditions. *Vehicle System Dynamics*, 22(5-6):483–492.

Mohareri O., Dhaouadi R., & Rad A.B. 2012. Indirect adaptive tracking control of a nonholonomic mobile robot via neural networks. *Neurocomputing*, 88:54–66.

Montesano L., Díaz M., Bhaskar S., & Minguez J. 2010. Towards an intelligent wheelchair system for users with cerebral palsy. *IEEE transactions on neural systems and rehabilitation engineering : a publication of the IEEE Engineering in Medicine and Biology Society*, 18(2):193–202.

Montiel O., Orozco-Rosas U., & Sepúlveda R. 2015. Path planning for mobile robots using Bacterial Potential Field for avoiding static and dynamic obstacles. *Expert Systems with Applications*, 42(12):5177–5191.

Montiel O., Sepúlveda R., & Orozco-Rosas U. 2014. Optimal Path Planning Generation for Mobile Robots using Parallel Evolutionary Artificial Potential Field. *Journal of Intelligent & Robotic Systems*, 79(2):237–257.

Morales R. 2006. Kinematic Model of a New Staircase Climbing Wheelchair and its Experimental Validation. *The International Journal of Robotics Research*, 25(9):825–841.

Morris A., Donamukkala R., Kapuria A., Steinfeld A., Matthews J., Dunbar-Jacob J., & Thrun S. 2003. A robotic walker that provides guidance. In *2003 IEEE International Conference on Robotics and Automation (Cat. No.03CH37422)*, volume 1, 25–30. IEEE. ISBN 0-7803-7736-2.

Muir P.F. 1988. *Modeling and control of wheeled mobile robots*. Ph.D. thesis, Carnegie Mellon University.

Murphy R. 2004. HumanRobot Interaction in Rescue Robotics. *IEEE Transactions on Systems, Man and Cybernetics, Part C (Applications and Reviews)*, 34(2):138–153.

Murray-Smith R. & Johansen T. 1997. *Multiple Model Approaches To Nonlinear Modelling And Control*. Taylor & Francis. ISBN 074840595X, 9780748405954.

Nagai M., Onda M., & Katagiri T. 1997. Application of genetic algorithm to analysis of driver's behaviour in collision avoidance. *International Journal of Vehicle Design*, 18(6):626–638.

Nguyen N.T., Nguyen H.T., & Su S. 2007. Advanced robust tracking control of a powered wheelchair system. *Conference proceedings : ... Annual International Conference of the IEEE Engineering in Medicine and Biology Society. IEEE Engineering in Medicine and Biology Society. Annual Conference*, 2007:4767–70.

Niku S.B. 2001. *An Introduction to Robotics Analysis, Systems, Applications*. Prentice Hall, Upper Saddle River, New Jersey. ISBN 0130613096.

Okuda H., Guo X., Tazaki Y., Suzuki T., & Levedahl B. 2014. Model predictive driver assistance control for cooperative cruise based on hybrid system driver model. In *2014 American Control Conference*, 4630–4636. IEEE. ISBN 978-1-4799-3274-0.

Olson B., Shaw S., & Stépán G. 2003. Nonlinear Dynamics of Vehicle Traction. *Vehicle System Dynamics*, 40(6):377–399.

Onyango S., Hamam Y., Dabo M., Djouani K., & Qi G. 2009a. Dynamic control of an electrical wheelchair on an incline. In *AFRICON 2009*, 1–6. IEEE. ISBN 978-1-4244-3918-8.

Onyango S., Hamam Y., Djouani K., & Daachi B. 2015. Identification of wheelchair user steering behaviour within indoor environments. In *2015 IEEE International Conference on Robotics and Biomimetics (ROBIO),*, 2283–2288. IEEE, Zhuhai China.

Onyango S., Hamam Y., Djouani K., & Qi G. 2009b. Dynamic control of powered wheelchair with slip on an incline. In *2009 2nd International Conference on Adaptive Science & Technology (ICAST)*, 278–283. IEEE. ISBN 978-1-4244-3522-7.

Onyango S.O., Hamam Y., & Djouani K. 2011. Velocity and Orientation Control in an Electrical Wheelchair on an Inclined and Slippery Surface. In *Proceedings of the 8th International Conference on Informatics in Control, Automation and Robotics*, 112–119. ISBN 978-989-8425-74-4, 978-989-8425-75-1.

Onyango S.O., Hamam Y., Djouani K., & Daachi B. 2016. Modeling a powered wheelchair with slipping and gravitational disturbances on inclined and non-inclined surfaces. *SIMULATION*, 92(4):337–355.

Ortega R., Perez J.A.L., Nicklasson P.J., & Sira-Ramirez H. 2013. *Passivity-based Control of Euler-Lagrange Systems: Mechanical, Electrical and Electromechanical Applications*. Springer Science & Business Media. ISBN 1447136039.

Ostrovskaya S. 2000. Dynamics of a Mobile Robot with Three Ball-Wheels. *The International Journal of Robotics Research*, 19(4):383–393.

Oubbati M.O.M., Schanz M., & Levi P. 2005. Kinematic and dynamic adaptive control of a nonholonomic mobile robot using a RNN. In *International Symposium on Computational Intelligence in Robotics and Automation*, 27–33. ISBN 0-7803-9355-4.

Palli G., Melchiorri C., & De Luca A. 2008. On the feedback linearization of robots with variable joint stiffness. In *2008 IEEE International Conference on Robotics and Automation*, 1753–1759. IEEE. ISBN 978-1-4244-1646-2.

Panou M., Bekiaris E., & Papakostopoulos V. 2007. Modelling Driver Behaviour in European Union and International Projects. In P. Cacciabue, editor, *Modelling Driver Behaviour in Automotive Environments*, 3–25. Springer London. ISBN 978-1-84628-617-9.

Parasuraman R., Sheridan T., & Wickens C. 2000. A model for types and levels of human interaction with automation. *IEEE Transactions on Systems, Man, and Cybernetics - Part A: Systems and Humans*, 30(3):286–297.

Parikh S., Grassi V., Kumar V., & Okamoto J. 2004. Incorporating user inputs in motion planning for a smart wheelchair. In *IEEE International Conference on Robotics and Automation, 2004. Proceedings. ICRA '04. 2004*, volume 2, 2043–2048 Vol.2. ISBN 0-7803-8232-3.

Parikh S.P., Grassi Jr. V., Kumar V., & Okamoto Jr. J. 2007. Integrating Human Inputs with Autonomous Behaviors on an Intelligent Wheelchair Platform. *IEEE Intelligent Systems*, 22(2):33–41.

Pauwelussen J.P. 2015. *Essentials of Vehicle Dynamics*. Elsevier. ISBN 9780081000366.

Peinado G., Urdiales C., Peula J., Fdez-Carmona M., Annicchiarico R., Sandoval F., & Caltagirone C. 2011. Navigation skills based profiling for collaborative wheelchair control. In *2011 IEEE International Conference on Robotics and Automation*, 2229–2234. IEEE. ISBN 978-1-61284-386-5.

Pilutti T. & Galip Ulsoy a. 1999. Identification of driver state for lane-keeping tasks. *IEEE Transactions on Systems, Man, and Cybernetics Part A:Systems and Humans.*, 29(5):486–502.

Plöchl M. & Edelmann J. 2007. Driver models in automobile dynamics application. *Vehicle System Dynamics*, 45(7-8):699–741.

Plochl M. & Lugner P. 2000. A 3-level driver model and its application to driving simulations. In *The dynamics of vehicles on roads and on tracks - supplement to vehicle system dynamics, volume 33. Proceedings of the 16th IAVSD symposium held in Pretoria, South Africa, August 30 - September 3, 1999*, 71–82. Transportation Research Board of the National Academies, Pretoria, South Africa.

Prokop G. 2001. Modeling Human Vehicle Driving by Model Predictive Online Optimization. *Vehicle System Dynamics*, 35(1):19–53.

Qinan Li, Weidong Chen, & Jingchuan Wang 2011. Dynamic shared control for human-wheelchair cooperation. In *2011 IEEE International Conference on Robotics and Automation*, 4278–4283. IEEE. ISBN 978-1-61284-386-5.

Rahimi R., Abdollahi F., & Naqshi K. 2014. Time-varying formation control of a collaborative heterogeneous multi agent system. *Robotics and Autonomous Systems*, 62(12):1799–1805.

Raja R., Dutta A., & Venkatesh K. 2015. New potential field method for rough terrain path planning using genetic algorithm for a 6-wheel rover. *Robotics and Autonomous Systems*, 72:295–306.

Rani P., Sarkar N., & Adams J. 2007. Anxiety-based affective communication for implicit humanmachine interaction. *Advanced Engineering Informatics*, 21(3):323–334.

Rasmussen J. 1986. *Information processing and human-machine interaction: an approach to cognitive engineering*. North-Holland. ISBN 0444009876.

Riley V. 1989. A General Model of Mixed-Initiative Human-Machine Systems. *Proceedings of the Human Factors and Ergonomics Society Annual Meeting*, 33(2):124–128.

Rodgers M.M., Gayle G.W., Figoni S.F., Kobayashi M., Lieh J., & Glaser R.M. 1994. Biomechanics of wheelchair propulsion during fatigue. *Archives of physical medicine and rehabilitation*, 75(1):85–93.

Rofer T. & Lankenau A. 1999. Ensuring safe obstacle avoidance in a shared-control system. In *1999 7th IEEE International Conference on Emerging Technologies and Factory Automation. Proceedings ETFA '99 (Cat. No.99TH8467)*, volume 2, 1405–1414. IEEE. ISBN 0-7803-5670-5.

Rothrock L. & Narayanan S., editors 2011. *Human-in-the-Loop Simulations - Methods and Practice*. Springer-Verlag London, 1 edition. ISBN 978-0-85729-883-6.

Salvucci D. 2001. Predicting the effects of in-car interface use on driver performance: An integrated model approach. *International Journal of Human-Computer Studies*, 55(1):85–107.

Sarkar N. & Kumar V. 1994. Control of Mechanical Systems With Rolling Constraints: Application to Dynamic Control of Mobile Robots. *The International Journal of Robotics Research*, 13(1):55–69.

Schaal S., Ijspeert A., & Billard A. 2003. Computational approaches to motor learning by imitation. *Philosophical transactions of the Royal Society of London. Series B, Biological sciences*, 358(1431):537–47.

Schiehlen W. 1997. Multibody System Dynamics: Roots and Perspectives. *Multibody System Dynamics*, 1(2):149–188.

Schneider F. & Wildermuth D. 2005. Experimental Comparison of a Directed and a Non-Directed Potential Field Approach to Formation Navigation. In *2005 International Symposium on Computational Intelligence in Robotics and Automation*, 21–26. IEEE. ISBN 0-7803-9355-4.

Seppelt B.D. & Lee J.D. 2015. Modeling Driver Response to Imperfect Vehicle Control Automation. *Procedia Manufacturing*, 3:2621–2628.

Serrani A. 2013. Nested zero-dynamics redesign for a non-minimum phase longitudinal model of a hypersonic vehicle. In *52nd IEEE Conference on Decision and Control*, 4833–4838. IEEE. ISBN 978-1-4673-5717-3.

Sheridan T.B. & Verplank W.L. 1978. Human and Computer Control of Undersea Teleoperators. Technical report, Massachusetts Institute of Technology Cambridge, Man-Machine Systems Laboratory.

Sheth P.N. & Uicker J.J. 1971. A Generalized Symbolic Notation for Mechanisms. *Journal of Engineering for Industry*, 93(1):102.

Sidek N. & Sarkar N. 2008. Dynamic Modeling and Control of Nonholonomic Mobile Robot with Lateral Slip. In *Third International Conference on Systems (icons 2008)*, 35–40. IEEE. ISBN 978-0-7695-3105-2.

Siller-Alcalá I.I. 1998. *Nonlinear continuous-time generalised predictive control*. Ph.D. thesis, Glasgow University.

Silver W.M. 1982. On the Equivalence of Lagrangian and Newton-Euler Dynamics for Manipulators. *The International Journal of Robotics Research*, 1(2):60–70.

Simpson R.C. 2005. Smart wheelchairs: A literature review. *Journal of rehabilitation research and development*, 42(4):423–36.

Simpson R.C., LoPresti E.F., & Cooper R.a. 2008. How many people would benefit from a smart wheelchair? *Journal of rehabilitation research and development*, 45(1):53–71.

Singh Y. & Santhakumar M. 2016. Performance investigations on optimum mechanical design aspects of planar parallel manipulators. *Advanced Robotics*, 1–24.

Smith S. 2003. Humans in the loop: Human-computer interaction and security. *IEEE Security & Privacy Magazine*, 1(3):75–79.

Song B., Delorme D., & VanderWerf J. 2000. Cognitive and hybrid model of human driver. In *Proceedings of the IEEE Intelligent Vehicles Symposium 2000 (Cat. No.00TH8511)*, 1–6. IEEE. ISBN 0-7803-6363-9.

Sorrento G.U., Archambault P.S., Routhier F., Dessureault D., & Boissy P. 2011. Assessment of joystick control during the performance of powered wheelchair driving tasks. *Journal of neuroengineering and rehabilitation*, 8:31.

Spong M.W., Hutchinson S., & Vidyasagar M. 2006. *Robot modeling and control*. John Wiley & Sons, Hoboken, NJ. ISBN 0471649902 9780471649908.

Spong M.W. & Vidyasagar M. 2008. *Robot Dynamics And Control*. Wiley India Pvt. Limited. ISBN 8126517808.

Stanciu R. & Oh P.Y. 2007. Human-in-the-Loop Camera Control for a Mechatronic Broadcast Boom. *IEEE/ASME Transactions on Mechatronics*, 12(1):41–52.

Statistics South Africa & Lehohla P. 2014. Profile of persons with disability in South Africa. Technical report, Statistics South Africa.

Steyn N. 2014. *Virtual Reality Platform Modelling and Design for Versatile Electric Wheelchair Simulation in an Enabled Environment*. Ph.D. thesis, Tshwane University of Technology.

Steyn N., Monacelli E., & Hamam Y. 2013. Differential Driven Mobility Aid.

Stoelen M.F., Jardon A., Victores J.G., Balaguer C., & Bonsignorio F. 2010. Information Metrics for Assistive Human-In-The-Loop Cognitive Systems. In *Workshop on Good Experimental Methodology in Robotics and Replicable Robotics Research, Robotics Science and Systems (RSS)*, 1–6.

Stonier D., Cho S.H., Choi S.L., Kuppuswamy N.S., & Kim J.H. 2007. Nonlinear Slip Dynamics for an Omniwheel Mobile Robot Platform. In *Proceedings 2007 IEEE International Conference on Robotics and Automation*, 2367–2372. IEEE. ISBN 1-4244-0602-1.

Su R. 1982. On the linear equivalents of nonlinear systems. *Systems & Control Letters*, 2(1):48–52.

Subudhi B. & Morris A. 2002. Dynamic modelling, simulation and control of a manipulator with flexible links and joints. *Robotics and Autonomous Systems*, 41(4):257–270.

Summala H. 1988. Risk control is not risk adjustment: the zero-risk theory of driver behaviour and its implications. *ERGONOMICS*, 31(4):491–506.

Sun L., Li D., Gao Z., Yang Z., & Zhao S. 2016. Combined feedforward and model-assisted active disturbance rejection control for non-minimum phase system. *ISA transactions*.

Sunada W.H. & Dubowsky S. 1983. On the Dynamic Analysis and Behavior of Industrial Robotic Manipulators With Elastic Members. *Journal of Mechanisms Transmissions and Automation in Design*, 105(1):42.

Sundrum R., Logan S., Wallace A., & Spencer N. 2005. Cerebral palsy and socioeconomic status: a retrospective cohort study. *Archives of disease in childhood*, 90(1):15–8.

Taghirad H.D. 2013. *Parallel Robots: Mechanics and Control*. CRC Press. ISBN 1466555769.

Taha T., Miro J.V., & Dissanayake G. 2008. POMDP-based long-term user intention prediction for wheelchair navigation. In *2008 IEEE International Conference on Robotics and Automation*, 3920–3925. IEEE. ISBN 978-1-4244-1646-2.

Taha T., Miro J.V., Dissanayake G., Miró J.V., & Dissanayake G. 2007. Wheelchair Driver Assistance and Intention Prediction using POMDPs. In *Proceedings of the 2007 International Conference on Intelligent Sensors, Sensor Networks and Information Processing, ISSNIP*, 449–454. IEEE. ISBN 1424415020.

Tarokh M. & McDermott G.J. 2005. Kinematics modeling and analyses of articulated rovers. *IEEE Transactions on Robotics*, 21(4):539–553.

Tashiro S. & Murakami T. 2008. Step Passage Control of a Power-Assisted Wheelchair for a Caregiver. *IEEE Transactions on Industrial Electronics*, 55(4):1715–1721.

Taychouri F., Hamam Y., Monacelli E., & Chebbo N. 2007. Path planning for electrical wheelchair, accessibility and comfort. In *6th Conference Eurosim 2007, At Ljubljana, Slovenia*, 9–13. ISBN 978-3-901608-32-2.

Taylor D.H. 1964. Drivers' galvanic skin response and the risk of accident. *Ergonomics*, 7(4):439–451.

Tian Y., Shirinzadeh B., Zhang D., Liu X., & Chetwynd D. 2009. Design and forward kinematics of the compliant micro-manipulator with lever mechanisms. *Precision Engineering*, 33(4):466–475.

Treiber M., Hennecke A., & Helbing D. 2000. Congested traffic states in empirical observations and microscopic simulations. *Physical Review E*, 62(2):1805–1824.

Trujillo-León A. & Vidal-Verdú F. 2014. Driving Interface Based on Tactile Sensors for Electric Wheelchairs or Trolleys. *Sensors*, 14(2):2644–2662.

Tsui K.M., Behal A., Kontak D., & Yanco H.a. 2011. I Want That: Human-in-the-Loop Control of a Wheelchair-Mounted Robotic Arm. *Applied Bionics and Biomechanics*, 8(1):127–147.

Tzafestas S.G. & Tzafestas E.S. 2001. HumanMachine Interaction in Intelligent Robotic Systems: A Unifying Consideration with Implementation Examples. *Journal of Intelligent and Robotic Systems*, 32(2):119–141.

Uicker J.J. 1969. Dynamic Behavior of Spatial Linkages: Part 1Exact Equations of Motion, Part 2Small Oscillations About Equilibrium. *Journal of Engineering for Industry*, 91(1):251.

Ungoren A.Y. & Peng H. 2005. An adaptive lateral preview driver model. *Vehicle System Dynamics*, 43(4):245–259.

Urdiales C., Pérez E.J., Peinado G., Fdez-Carmona M., Peula J.M., Annicchiarico R., Sandoval F., & Caltagirone C. 2013. On the construction of a skill-based wheelchair navigation profile. *IEEE transactions on neural systems and rehabilitation engineering : a publication of the IEEE Engineering in Medicine and Biology Society*, 21(6):917–27.

Urdiales C., Peula J.M., Fdez-Carmona M., Barrué C., Pérez E.J., Sánchez-Tato I., del Toro J.C., Galluppi F., Cortés U., Annichiaricco R., Caltagirone C., & Sandoval F. 2010. A new multi-criteria optimization strategy for shared control in wheelchair assisted navigation. *Autonomous Robots*, 30(2):179–197.

Vadakkepat P., Tan K.C., & Ming-Liang W. 2000. Evolutionary artificial potential fields and their application in real time robot path planning. *Proceedings of the Congress on Evolutionary Computation*, 1:256–263.

Van-Overloop P., Maestre J., Sadowska A.D., Camacho E.F., & De Schutter B. 2015. Human-in-the-Loop Model Predictive Control of an Irrigation Canal [Applications of Control]. *IEEE Control Systems*, 35(4):19–29.

Vanacker G., Del R. Millán J., Lew E., Ferrez P.W., Moles F.G., Philips J., Van Brussel H., & Nuttin M. 2007. Context-based filtering for assisted brain-actuated wheelchair driving. *Computational Intelligence and Neuroscience*, 2007.

Vanacker G., Vanhooydonck D., Demeester E., Huntemann A., Degeest A., Brussel H., & Nuttin M. 2006. Adaptive filtering approach to improve wheelchair driving performance. In *ROMAN 2006 - The 15th IEEE International Symposium on Robot and Human Interactive Communication*, 527–532. IEEE. ISBN 1-4244-0564-5.

Vanhooydonck D., Demeester E., Hüntemann A., Philips J., Vanacker G., Van Brussel H., & Nuttin M. 2010. Adaptable navigational assistance for intelligent wheelchairs by means of an implicit personalized user model. *Robotics and Autonomous Systems*, 58(8):963–977.

Venture G., Ripert P.J., Khalil W., Gautier M., & Bodson P. 2006. Modeling and Identification of Passenger Car Dynamics Using Robotics Formalism. *IEEE Transactions on Intelligent Transportation Systems*, 7(3):349–359.

Viswanathan P., Little J.J., Mackworth A.K., & Mihailidis A. 2011. Navigation and obstacle avoidance help (NOAH) for older adults with cognitive impairment. In *The proceedings of the 13th international ACM SIGACCESS conference on Computers and accessibility - ASSETS '11*, 43. ACM Press, New York, New York, USA. ISBN 9781450309202.

Wang H., Salatin B., Grindle G.G., Ding D., & Cooper R.A. 2009. Real-time model based electrical powered wheelchair control. *Medical engineering & physics*, 31(10):1244–54.

Wang J., Li K., & Lu X.Y. 2014. *Advances in Intelligent Vehicles*. Elsevier. ISBN 9780123971999.

Wang R.H., Gorski S.M., Holliday P.J., & Fernie G.R. 2011. Evaluation of a Contact Sensor Skirt for an Anti-Collision Power Wheelchair for Older Adult Nursing Home Residents With Dementia: Safety and Mobility. *Assistive Technology*, 23(3):117–134.

Wei L., Hu H., & Zhang Y. 2011. Fusing EMG and visual data for hands-free control of an intelligent wheelchair. *International Journal of Humanoid Robotics*, 08(04):707–724.

Weiss C., Frohlich H., & Zell A. 2006. Vibration-based Terrain Classification Using Support Vector Machines. In *2006 IEEE/RSJ International Conference on Intelligent Robots and Systems*, 4429–4434. IEEE. ISBN 1-4244-0258-1.

Wells D. 1967. *Schaum's Outline of Lagrangian Dynamics*. McGraw Hill Professional. ISBN 0070692580.

Wickens C.D. 2002. Multiple resources and performance prediction. *Theoretical Issues in Ergonomics Science*, 3(2):159–177.

Wilde G.J.S. 1982. The Theory of Risk Homeostasis: Implications for Safety and Health. *Risk Analysis*, 2(4):209–225.

Williams R., Carter B., Gallina P., & Rosati G. 2002. Dynamic model with slip for wheeled omnidirectional robots. *IEEE Transactions on Robotics and Automation*, 18(3):285–293.

Wretstrand A., Petzäll J., & Ståhl A. 2004. Safety as perceived by wheelchair-seated passengers in special transportation services. *Accident Analysis & Prevention*, 36(1):3–11.

Wu W., Chen H., & Woo P.Y. 2000. Time optimal path planning for a wheeled mobile robot. *Journal of Robotic Systems*, 17(11):585–591.

Xiu C. & Chen H. 2010. A Behavior-Based Path Planning for Autonomous Vehicle. In H. Liu, H. Ding, Z. Xiong, & X. Zhu, editors, *Intelligent Robotics and Applications*, volume 6425 of *Lecture Notes in Computer Science*, 1–9. Springer Berlin Heidelberg, Berlin, Heidelberg. ISBN 978-3-642-16586-3.

Xu P. 2005. Mechatronics Design of a Mecanum Wheeled Mobile Robot. In V. Kordic, A. Lazinica, & M. Merdan, editors, *Cutting Edge Robotics*, July, chapter Mechatroni, 61–75. Pro Literatur Verlag, Germany. ISBN 3-86611-038-3.

Yang F. & Wang C. 2011. Adaptive tracking control for uncertain dynamic nonholonomic mobile robots based on visual servoing. *Journal of Control Theory and Applications*, 10(1):56–63.

Yang H., Jiang B., & Zhang H. 2012. Stabilization of non-minimum phase switched nonlinear systems with application to multi-agent systems. *Systems & Control Letters*, 61(10):1023–1031.

Yong Tao, Tianmiao Wang, Hongxing Wei, & Diansheng Chen 2009. A behavior control method based on hierarchical POMDP for intelligent wheelchair. In *2009 IEEE/ASME International Conference on Advanced Intelligent Mechatronics*, 893–898. IEEE. ISBN 978-1-4244-2852-6.

Yu H., Spenko M., & Dubowsky S. 2003. An Adaptive Shared Control System for an Intelligent Mobility Aid for the Elderly. *Autonomous Robots*, 15(1):53–66.

Yun X., Kumar V., Sarkar N., & Paljug E. 1992. Control of multiple arms with rolling constraints. In *Proceedings 1992 IEEE International Conference on Robotics and Automation*, 2193–2198. IEEE Comput. Soc. Press. ISBN 0-8186-2720-4.

Zaw M.T. 2003. *Kinematic and dynamic analysis of mobile robot.* Ph.D. thesis, National University of Singapore.

Zeng Q., Burdet E., & Teo C.L. 2009. Evaluation of a collaborative wheelchair system in cerebral palsy and traumatic brain injury users. *Neurorehabilitation and neural repair*, 23(5):494–504.

Zeng Q., Teo C.L., Rebsamen B., & Burdet E. 2008. A collaborative wheelchair system. *IEEE transactions on neural systems and rehabilitation engineering : a publication of the IEEE Engineering in Medicine and Biology Society*, 16(2):161–70.

Zeng Z., Lian L., Sammut K., He F., Tang Y., & Lammas A. 2015. A survey on path planning for persistent autonomy of autonomous underwater vehicles. *Ocean Engineering*, 110:303–313.

Zhang T. & Nakamura M. 2006. Neural Network-Based Hybrid Human-in-the-Loop Control for Meal Assistance Orthosis. *IEEE Transactions on Neural Systems and Rehabilitation Engineering*, 14(1):64–75.

Zhang Y., Liu H., & Wu X. 2009. Kinematics analysis of a novel parallel manipulator. *Mechanism and Machine Theory*, 44(9):1648–1657.

Zhu X., Dong G., Hu D., & Cai Z. 2006. Robust Tracking Control of Wheeled Mobile Robots Not Satisfying Nonholonomic Constraints. In *Sixth International Conference on Intelligent Systems Design and Applications*, volume 2, 643–648. IEEE. ISBN 0-7695-2528-8.

Appendix A

Derivation of Equations 3.17-3.19

Considering FIGURE 3.2 and its magnified extract in FIGURE A.1, $\mathbf{v_Y}$ in Equation (3.17) can be expressed from $\mathbf{v}_Y = (f + \bar{\bar{x}})\dot{\phi}_f$ as follows

$$\dot{\phi}_f = \frac{\mathbf{v}_Y}{(f + \bar{\bar{x}})} \tag{A.1}$$

But $\mathbf{v}_Y = \mathbf{v}\sin\beta$, denoting that,

$$\dot{\phi}_f = \frac{\mathbf{v}}{(f + \bar{\bar{x}})}\sin\beta \tag{A.2}$$

Also from FIGURE 3.2,

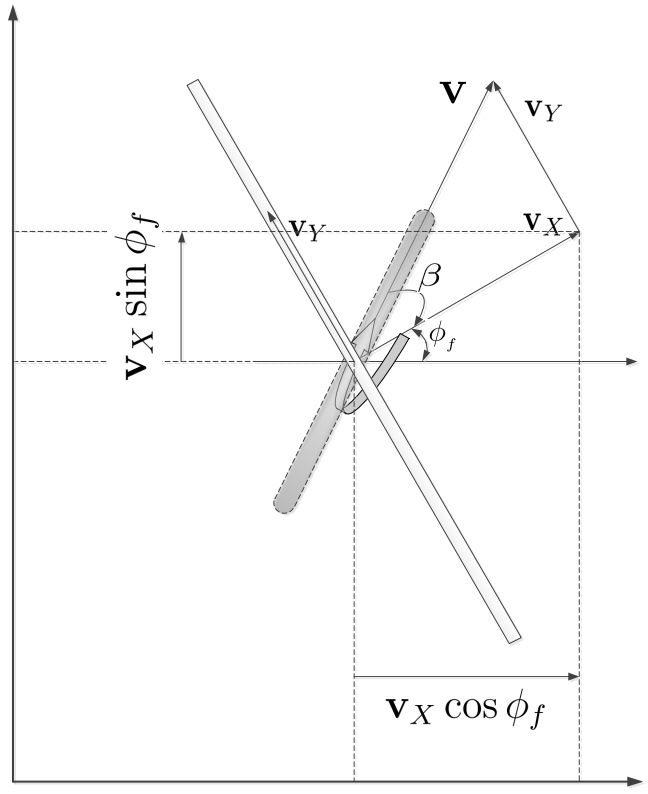

FIGURE A.1: A magnification from FIGURE 3.2

$$\tan\phi_f = \frac{\bar{\bar{x}}}{\rho + b} \tag{A.3}$$

$$\rho = \frac{\bar{\bar{x}}}{\tan\phi_f} - b = \frac{\bar{\bar{x}} - b\tan\phi_f}{\tan\phi_f} \tag{A.4}$$

Also,

$$\tan\beta = \frac{\bar{\bar{x}} + f}{\rho + b} = \frac{\bar{\bar{x}} + f}{\dfrac{\bar{\bar{x}} - b\tan\phi_f}{\tan\phi_f} + b} = \frac{(\bar{\bar{x}} + f)\tan\phi_f}{\bar{\bar{x}}} \tag{A.5}$$

From which,

$$\tan\phi_f = \frac{\bar{\bar{x}}}{\bar{\bar{x}} + f}\tan\beta \tag{A.6}$$

$$\phi_f = \arctan\left(\frac{\bar{\bar{x}}}{\bar{\bar{x}} + f}\tan\beta\right) \tag{A.7}$$

Also using Equation (A.4),

$$\tan\alpha_L = \frac{\bar{\bar{x}} + f}{\rho} = \frac{\bar{\bar{x}} + f}{\dfrac{\bar{\bar{x}} - b\tan\phi_f}{\tan\phi_f}} = \frac{(\bar{\bar{x}} + f)\tan\phi_f}{\bar{\bar{x}} - b\tan\phi_f} \tag{A.8}$$

$$\alpha_L = \arctan\left[\frac{(\bar{\bar{x}} + f)\tan\phi_f}{\bar{\bar{x}} - b\tan\phi_f}\right] \tag{A.9}$$

Making $\tan\phi_f$ in Equation (A.8) the subject,

$$\tan\phi_f = \frac{\bar{\bar{x}}\tan\alpha_L}{(\bar{\bar{x}} + f) + b\tan\alpha_L} \tag{A.10}$$

Similarly

$$\tan\alpha_R = \frac{\bar{\bar{x}} + f}{\rho + 2b} = \frac{\bar{\bar{x}} + f}{\dfrac{\bar{\bar{x}} - b\tan\phi_f}{\tan\phi_f} + 2b} = \frac{(\bar{\bar{x}} + f)\tan\phi_f}{\bar{\bar{x}} + b\tan\phi_f} \tag{A.11}$$

$$\alpha_R = \arctan\left[\frac{(\bar{\bar{x}} + f)\tan\phi_f}{\bar{\bar{x}} + b\tan\phi_f}\right] \tag{A.12}$$

Equation (3.19) may be computed by substituting Equation (A.10) in Equation (A.11)

$$\tan\alpha_R = \frac{(\bar{\bar{x}}+f)\,\dfrac{\bar{\bar{x}}\tan\alpha_L}{(\bar{\bar{x}}+f)+b\tan\alpha_L}}{\bar{\bar{x}}+b\left(\dfrac{\bar{\bar{x}}\tan\alpha_L}{(\bar{\bar{x}}+f)+b\tan\alpha_L}\right)} = \frac{(\bar{\bar{x}}+f)\tan\alpha_L}{(\bar{\bar{x}}+f+b\tan\alpha_L)+b\tan\alpha_L} \tag{A.13}$$

$$\tan\alpha_R = \frac{(\bar{\bar{x}}+f)\left[\dfrac{\sin\alpha_L}{\cos\alpha_L}\right]}{\left[\bar{\bar{x}}+f+b\dfrac{\sin\alpha_L}{\cos\alpha_L}\right]+b\left[\dfrac{\sin\alpha_L}{\cos\alpha_L}\right]} \tag{A.14}$$

$$\tan\alpha_R = \frac{(\bar{\bar{x}}+f)\sin\alpha_L}{(\bar{\bar{x}}+f)\cos\alpha_L+2b\sin\alpha_L} = \frac{\sin\alpha_L}{\cos\alpha_L+\dfrac{2b}{(\bar{\bar{x}}+f)}\sin\alpha_L} \tag{A.15}$$

In a similar manner,

$$\tan\alpha_L = \frac{\sin\alpha_R}{\cos\alpha_R-\dfrac{2b}{(\bar{\bar{x}}+f)}\sin\alpha_R} \tag{A.16}$$

Equation (3.18) may thus be expressed with consideration of Equation (A.5) and Equation (A.10) as follows

$$\tan\beta = \frac{\bar{\bar{x}}+f}{\bar{\bar{x}}}\left[\frac{\bar{\bar{x}}\tan\alpha_L}{(\bar{\bar{x}}+f)+b\tan\alpha_L}\right] = \frac{\tan\alpha_L}{1+\dfrac{b}{\bar{\bar{x}}+f}\tan\alpha_L} \tag{A.17}$$

$$\tan\beta = \frac{\sin\alpha_L}{\cos\alpha_L+\dfrac{b}{\bar{\bar{x}}+f}\sin\alpha_L} \tag{A.18}$$

Substituting Equation (A.18) into Equation (A.7),

$$\phi_f = \arctan\left[\frac{\bar{\bar{x}}}{\bar{\bar{x}}+f}\left(\frac{\sin\alpha_L}{\cos\alpha_L+\dfrac{b}{\bar{\bar{x}}+f}\sin\alpha_L}\right)\right] = \arctan\left[\frac{\bar{\bar{x}}\sin\alpha_L}{(\bar{\bar{x}}+f)\cos\alpha_L+b\sin\alpha_L}\right] \tag{A.19}$$

$$\phi_f = \arctan\left[\frac{\bar{\bar{x}}\sin\alpha_L}{(\bar{\bar{x}}+f)\cos\alpha_L+b\sin\alpha_L}\right] \tag{A.20}$$